



**PHASE TRANSITION KINETICS IN SYSTEMS
WITH LONG-RANGE INTERACTIONS**

KIPTON MARCOS BARROS

Dissertation submitted in partial fulfillment
of the requirements for the degree of
Doctor of Philosophy

**BOSTON
UNIVERSITY**

BOSTON UNIVERSITY
GRADUATE SCHOOL OF ARTS AND SCIENCES

Dissertation

**PHASE TRANSITION KINETICS IN SYSTEMS WITH
LONG-RANGE INTERACTIONS**

by

KIPTON MARCOS BARROS

B.S., Carnegie Mellon University, 2001

Submitted in partial fulfillment of the
requirements for the degree of
Doctor of Philosophy

2010

Approved by

First Reader

William Klein, Ph.D.
Professor of Physics

Second Reader

Karl Ludwig, Ph.D.
Professor of Physics

Acknowledgments

This work was made possible by many friends and collaborators. First among them is my advisor William Klein who not only introduced me to the subject of my dissertation research, but provided guidance and support in innumerable ways. A second close collaborator is Harvey Gould. Through their enthusiasm, patience, and kindness, Bill and Harvey nurtured my development as a researcher.

The wisdom provided by senior graduate students and postdocs has been invaluable; I would like to thank Louis Colonna-Romano, Jan Fiala, Natali Gulbahce, Aaron Santos, Aaron Schweiger, Hui Wang, and Junchao Xia.

It is a pleasure to recall the many stimulating discussions I've had with my friends and collaborators; I would like to thank Ronald Babich, Richard Brower, Ranjit Chacko, Claudio Chamon, Michael Clark, Rachele Dominguez, Jack Douglas, Paul Krapivsky, Claudio Rebbi, Sidney Redner, and Andrea Velenich, among many others.

I am grateful for steady support from Mirtha Cabello of the Department of Physics, and from Cheryl Endicott and Ilona Lappo of the Center for Computational Science – these wonderful people have created a “home away from home” for graduate students.

Finally, I would like to acknowledge the encouragement and enduring patience of my family – especially my wife, Mina Khanlarzadeh, to whom I dedicate this work.

into the metastable phase, near the spinodal. In the case of the fluid-to-solid transition in three dimensions and greater, the nucleating droplets are predicted to have a spherically symmetric onion structure, completely unlike the stable phase crystal symmetry. I also discuss nucleating droplets for solid-to-solid transitions in two dimensions.

Contents

1	Introduction	1
1.1	Motivation	1
1.2	The Ising model	7
1.2.1	Definition	7
1.2.2	The naïve mean-field approximation	8
1.2.3	The fully connected Ising model	9
1.3	Long-range Kac interactions	12
1.3.1	The Kac potential	12
1.3.2	Static coarse graining of the Ising model	13
1.3.3	Scaled lengths and the Kac mean-field limit	15
1.4	Ising Langevin dynamics	16
1.4.1	Summary of common dynamics	17
1.4.2	Scaled lengths and effectively small noise	18
1.5	Nucleation	19
1.5.1	Field theoretic formalism	20
1.5.2	Classical versus spinodal nucleation	23
1.6	The clump model	24
2	The long-range ferromagnet	27
2.1	Phase diagram	27
2.2	Spinodal nucleation	29
2.3	Dynamical coarse graining	31
2.3.1	Monte Carlo Ising dynamics	32
2.3.2	Langevin representation of spin-flip dynamics	33

2.3.3	Equilibrium analysis	37
2.3.4	Magnetization relaxation	39
2.3.5	Langevin representation of Kawasaki spin-exchange dynamics	40
2.4	Ordering dynamics following a critical quench	42
2.4.1	The CHC linear theory for spin-flip dynamics	44
2.4.2	Breakdown of the CHC linear theory	47
2.4.3	Expansion beyond the CHC linear theory	49
2.4.4	The CHC linear theory for Kawasaki spin-exchange dynamics	54
3	Long-range repulsive models and modulated phases	56
3.1	Model definition	56
3.1.1	The disordered phase and spinodal	58
3.1.2	The critical point	59
3.2	Two dimensions – the disordered, stripe, and clump phases	60
3.2.1	Equilibrium phase diagram	61
3.2.2	Spinodal instabilities	66
3.2.3	Nucleation	71
3.3	Nucleation from the disordered phase	74
3.3.1	Preliminaries	75
3.3.2	Lattice-structure droplets	77
3.3.3	Onion-structure droplets	80
3.3.4	Droplet free energy costs	83
3.3.5	Droplets categorized by spatial dimension	85
3.4	Spatial symmetry breaking and the emergent CHC theory	86
4	Closing remarks	95
4.1	Closing remarks	95
A	Mathematical tools	97
A.1	The Fourier transform	97

A.2	Functionals and functional derivatives	99
A.3	White Gaussian noise	102
A.4	Langevin equations	104
A.5	The radial step function	105
	References	108
	Curriculum Vitae	112

List of Tables

3.1	Stationary points of the free energy functional of the two-dimensional anti-ferromagnet near the critical point.	64
3.2	Coexistence and spinodal curves of the 2d antiferromagnet near the critical point.	66

List of Figures

1-1	Nucleation and the saddle point of the free energy functional.	22
2-1	Phase diagram of the long-range Ising ferromagnet near the critical point. . .	29
2-2	Relaxation in the ferromagnet: magnetization versus time.	40
2-3	Relaxation in the ferromagnet: dm/dt versus magnetization m	41
2-4	Ising continuous ordering measurements and comparison with the CHC theory.	47
2-5	SFG dynamics and $O(R^{-d})$ corrections to the CHC theory structure factor.	49
2-6	SFM dynamics and $O(R^{-d/2})$ corrections to the CHC theory structure factor.	50
2-7	Consecutive corrections to the CHC theory structure factor at $\vec{k} = 0$	52
2-8	First correction to the CHC theory structure factor at $t = 1.0$	53
2-9	Second correction to the CHC theory structure factor at $t = 1.6$	53
2-10	Ising spinodal decomposition measurements and comparison with the CHC theory.	54
3-1	The metastable stripe phase and the unstable “mixed” saddle point.	64
3-2	The metastable clump phase and the unstable “mixed” saddle point.	65
3-3	Phase diagram of the two-dimensional antiferromagnet near the critical point.	65
3-4	The unstable clump saddle point and its connection to both the disordered and clump metastable phases.	69
3-5	Depiction of spatial symmetry breaking and the emergent CHC theory.	91
3-6	The classical CHC theory and the fluid-to-stripe transition following a critical quench.	92
3-7	The emergent CHC theory and the fluid-to-clump transition following an off-critical quench.	93

List of Abbreviations

BCC	Body centered cubic (lattice symmetry)
CHC	Cahn-Hilliard-Cook (linear theory of ordering)
NGF	noisy gradient flow (Ising dynamics)
LS	lattice-structure (nucleating droplets)
MCS	Monte Carlo steps
OS	onion-structure (nucleating droplets)
SEG	spin-exchange Glauber (Ising dynamics)
SEM	spin-exchange Metropolis (Ising dynamics)
SFG	spin-flip Glauber (Ising dynamics)
SFM	spin-flip Metropolis (Ising dynamics)
UV	ultraviolet (high frequency cutoff)

Chapter 1

Introduction

1.1 Motivation

The subject of this dissertation is the kinetics of phase transitions. I will focus on two broad categories of phase transitions: continuous and first-order. A well known continuous phase transition occurs in the ferromagnet. Above the critical temperature T_c (also known as the Curie temperature) the ferromagnet is not magnetized in the absence of an external magnetic field. Below T_c the ferromagnet obtains a spontaneous *equilibrium* magnetization m (for simplicity, m is restricted to be a scalar, either positive or negative). An important *non-equilibrium* process is initiated when the ferromagnet is quenched from above T_c to below T_c . Following the quench, local domains of enhanced magnetization form and then coarsen. Despite extensive study, many details of this process are still not understood.

First-order phase transitions, unlike continuous phase transitions, allow for metastable phases. As mentioned, below T_c the ferromagnet in equilibrium adopts a nonzero magnetization m even in the absence of an external magnetic field h . If an external field $h \neq 0$ is applied, the equilibrium condition is that m is aligned with h . If the directions of m and h are opposite, the magnet is in a metastable phase. The mechanism by which a long-lived metastable phase eventually decays to equilibrium involves nucleation. A nucleation event occurs when (rare) fluctuations appear in the metastable phase that initiate a rapid decay process. In the classical theory of nucleation this process occurs through a compact object called the nucleating droplet. The droplet can be pictured as an “island” of the stable phase living in a “sea” of the metastable phase [1]. The classical theory of nucleation is valid when there is little free energy difference between the metastable and stable phases

(i.e., $h \approx 0$). For quenches deep into the metastable phase, the classical theory is no longer effective and an alternate description is necessary [2].

Another example of a first-order phase transition is the liquid-solid transition, e.g., freezing in water. Below 0°C the equilibrium phase of water is ice. Water can also be supercooled into a long lived metastable liquid phase. The decay of the metastable liquid phase occurs through nucleation. The nucleating droplet in this case takes the form of a crystal. In *simple models* of liquid-to-solid nucleation, and for deep quenches, the nucleating droplet often has a structure completely different than that of the stable phase crystal (see Section 3.3 and Refs. [3, 4]). The tendency to nucleate through an intermediate unstable phase is sometimes called the Ostwald step rule [5]. Understanding the mechanisms of nucleation is of significant theoretical and practical interest, with important applications to materials science and chemistry.

In this dissertation I will consider simple model systems with long-range interactions of the form given by Kac [6]. Systems with Kac interactions have convenient analytic properties allowing them to be studied within a non-trivial mean-field framework. “Kac mean-field theory” involves a particular order of limits: first the system volume is taken to infinity, second the interaction range is taken to infinity (while weakening the interaction strength). One appeal of working with mean-field systems is mathematical tractability. Another is universality: sometimes predictions can be made that are largely insensitive to system details. Universality offers hope that theoretical results, obtained from simple models, apply to real systems.

The mean-field assumption may seem drastic because the microscopic interactions in most real materials are of finite range due to screening. Still, mean-field theory may apply if the system has *effective* long-range interactions (i.e., long-range interactions that emerge in a coarse grained description). Polymer systems are a good example: mean-field theories of polymers, such as the Flory-Huggins theory, are effective due to large persistence lengths [7]. Metals may also admit accurate mean-field descriptions due to effective long-range elastic interactions [8].

Much of the work in this dissertation builds on the Ising model, a toy model of ferromagnetism, in which the spin degrees of freedom (each either *up* or *down*) are arranged on a lattice. In the usual Ising model all interactions are between nearest neighbor spins only. I will work with a generalized Ising model in which pairs of spins interact through a long-range Kac potential. One particularly simple Kac potential is the radial step function: pairs of spins, separated by a distance d , do not interact if $d > R$ and interact with a fixed strength that is proportional to R^{-d} if $d < R$. The interactions may be either ferromagnetic or antiferromagnetic (repulsive) depending on the choice of sign. Systems with ferromagnetic interactions, considered in Chapter 2, exhibit uniform spontaneous magnetization. Systems with antiferromagnetic interactions, considered in Chapter 3, have modulated, spatially nonuniform, phases at low temperatures [9].

In Section 1.3.2 it is demonstrated that for large interaction range R , the Ising model partition function may be represented as a functional integral over $\phi(\vec{x})$, the coarse grained (locally averaged) magnetization [6, 10]. The probability of a configuration $\phi(\vec{x})$ is given by the Boltzmann factor $e^{-\beta F}$, where the coarse grained free energy functional $F[\phi]$ (also known as the Landau-Ginzburg-Wilson effective Hamiltonian) can be derived from the microscopic Hamiltonian. A remarkable property of Kac interactions is that, upon scaling all lengths by R , the free energy functional can be expressed as $F = R^d \tilde{F}$, where \tilde{F} has no R dependence. Thus, large values of R serve to dampen statistical fluctuations. In the Kac mean-field limit, where $R \rightarrow \infty$, Laplace’s method enables the exact calculation of the partition function. Kac mean-field theory is analogous to quantum mechanics in the “classical” limit; R^d corresponds to \hbar^{-1} .

Systems with long-range interactions provide an excellent context with which to study metastable phases and nucleation. Metastable phases correspond to *local* minima of the free energy functional – they are stable to small fluctuations. Control parameters, such as the temperature and external magnetic field, affect the free energy functional and the stability of the metastable phase. The *spinodal curve* is the locus of control parameters at which the metastable phase has marginal stability; the spinodal is an inherently mean-field

object. Critical phenomena occur at the spinodal.

A metastable phase, although locally stable, will eventually decay to the stable phase if the interaction range R is finite. The decay process is initiated by the formation of a nucleating droplet. In Section 1.5.1 I introduce the mean-field theory of nucleation [1]. The rate of nucleation is proportional to $\exp(-\beta\Delta F)$, where $\Delta F \propto R^d$ is the free energy cost of the nucleating droplet (metastable equilibrium is valid when $R \gg 1$, which is assumed). The nucleating droplet is the configuration of minimum free energy that straddles the stable and metastable wells: a saddle point of the free energy functional. As the spinodal limit of metastability is approached, the free energy cost of the nucleating droplet typically decreases. Nucleation near the spinodal has a character different than that predicted by the classical theory [2], and is studied in Section 2.2 for the Ising ferromagnet.

Ising model dynamics is the subject of Section 2.3. Although the Ising model is usually introduced as a purely equilibrium model, it can be extended with many possible dynamics while preserving the Boltzmann equilibrium distribution. Most common are spin-flip Glauber (SFG) and Metropolis (SFM) Monte Carlo dynamics (Section 2.3.1). Effective Langevin equations for both SFG and SFM dynamics in the large R limit are derived in Section 2.3.2. Noisy gradient flow (NGF) dynamics is another possibility and is described in Section 1.4. Unlike SFG and SFM dynamics, NGF dynamics does not have a microscopic basis, being defined directly in terms of the coarse grained magnetization. Although these three dynamics are usually expected to have the same qualitative behavior, surprising differences are encountered in Sections 2.4.2 and 2.4.3.

The ferromagnetic ordering process following a quench from above to below the critical temperature is considered in Section 2.4. I focus on continuous ordering, in which the total magnetization is not conserved. The continuous ordering process occurs in several temporal stages. At the earliest stage the coarse grained magnetization, $\phi(x, t)$, is small and the dynamical equations can be linearized about $\phi(x) = 0$. The result is the Cahn-Hilliard-Cook (CHC) linear theory [11, 12]. The main prediction of the CHC linear theory is that the Fourier modes $\phi(k)$ grow exponentially at early times. Scaling arguments indicate that

$\phi \sim R^{-d/2}$, so the CHC theory lasts a time of order $\ln R$ before the condition $\phi \ll 1$ fails [7], which has been confirmed in Ising model simulations [13, 14]. After the CHC linear theory fails, there is a transient nonlinear stage, succeeded by an extended coarsening stage [15, 16].

The transient stage immediately following the breakdown of the CHC theory has been the subject of much study [17, 18, 19, 20, 21, 22]. Important progress was made when it was realized that the CHC prediction for the structure factor is just the leading order in an R^{-d} perturbation expansion. Higher orders in the expansion were calculated explicitly using a Landau-Ginzburg ϕ^4 field theory [23]. One difficulty encountered is that corrections to the CHC theory diverge with the ultraviolet (UV) cut-off Λ , a problem familiar from quantum field theory [24]. Regularization – an explicit choice of Λ – is possible but not satisfactory; the effectiveness of the Langevin equation depends on a decoupling from microscopic system details.

I will show in Section 2.4.3 that the R^{-d} expansion of the structure factor for the continuous ordering process is *free* of UV divergences for the special case of SFG dynamics. I will derive the first correction to the CHC theory analytically and demonstrate agreement with Ising simulation data. Similar attempts to develop an R^{-d} perturbation expansion for SFM dynamics are stymied by a non-analyticity at $\phi = 0$: namely, $|\phi|$ appears explicitly in the Langevin equation. This difficulty is actually a virtue: the first correction to the CHC theory enters at order $R^{d/2}$ rather than R^{-d} , and leads to the prediction that the CHC theory fails earlier for SFM dynamics than for SFG dynamics. In Section 2.4.2 I will show simulation results that are consistent with this prediction.

Models with long-range repulsive interactions may exhibit modulated (spatially nonuniform) phases [9]. A typical example is the long-range *antiferromagnetic* Ising model discussed in Section 3.1. At high temperatures this model exhibits a disordered phase, while at low temperatures spatial patterns form. In two dimensions there are three possible phases: the disordered phase, the stripe phase, and the clump phase (bubble regions of enhanced magnetization arranged in a hexagonal lattice structure). Similar phenomena have been observed in a variety of systems with effective long-range repulsive interactions

including “magnet garnet films modeled as a dipolar Ising ferromagnet, Langmuir monolayers, adsorbates on metal surfaces, two-component vesicles, and liquid crystal films of achiral molecules undergoing chiral symmetry breaking” [9].

In the mean-field limit the disordered phase terminates at a well defined spinodal limit of stability, as is discussed in Section 3.1.1. The spinodal can be universally characterized with only a few physical parameters and exhibits critical behavior, e.g., divergent fluctuations.¹

At zero external field, the disordered phase spinodal is a true critical point. In Section 3.2.1 the phase diagram in the vicinity of the critical point is analyzed. The result is illustrated in Fig. 3-3 and includes coexistence and spinodal curves separating disordered, clump, and stripe phases. The phase diagram is universal to a large class of models with long-range repulsive interactions. An investigation of nucleation near the critical point presented in Section 3.2.3.

By definition, the spinodal demarcates the limit of metastability – the point at which the Hessian of the free energy functional has modes with zero eigenvalue (cf. Section 3.2.2). A unique property of the disordered phase is that, at the spinodal, there is a *continuum* of unstable modes – all Fourier wave vectors with magnitude $|\vec{k}| = k_0$ become unstable. As a result, there are many interesting saddle points of the free energy functional near the disordered phase spinodal, as demonstrated in Section 3.3. The structure of the nucleating droplet (the saddle point with minimum free energy) is described in Section 3.3.5; in two dimensions the nucleating droplet has a hexagonal clump structure, while in three dimensions and above it has an onion structure.

If a system is quenched beyond the metastable phase, there is no nucleation barrier and the phase transition kinetics will be unstable growth. One example, continuous ordering of the ferromagnet, was already discussed. In Section 3.4 I consider unstable growth processes in models with long-range repulsive interactions. The transitions in these models exhibit *spatial symmetry breaking* (the initial phase contains a symmetry not present in the final

¹In mean-field theory all measurements, including measurements of fluctuations, are calculated from the neighborhood of the free energy functional minimum.

phase). I will demonstrate that transitions involving spatial symmetry breaking exhibit an emergent CHC-like linear theory even when the classical CHC theory does not apply. This emergent theory differs from the CHC theory in two interesting ways: exponential growth does not begin immediately following the quench, and the objects that grow exponentially are not necessarily Fourier modes.

The remainder of this chapter will introduce theoretical tools to be used in rest of the dissertation.

1.2 The Ising model

1.2.1 Definition

The Ising model is defined on a lattice of spins $\{s\} = \{s_1, s_2, \dots\}$, with each spin taking the value 1 or -1 . The energy of a spin configuration is

$$E\{s\} = -\frac{1}{2} \sum_{i,j} J_{i,j} s_i s_j - h \sum_i s_i. \quad (1.1)$$

Spins interact with each other through the coupling, $J_{i,j}$, and also interact with an external magnetic field h . The usual Ising model has only nearest neighbor (nn) couplings

$$J_{i,j}^{(\text{nn})} = \begin{cases} 1 & \text{if } (i, j) \in \text{nn} \\ 0 & \text{otherwise} \end{cases} \quad (1.2)$$

Consider an ensemble with fixed temperature T . The equilibrium properties of the Ising model derive from the equilibrium partition function

$$Z = \sum_{\{s\}} e^{-\beta E\{s\}}, \quad (1.3)$$

where $\beta = T^{-1}$ and the Boltzmann constant is chosen to be $k_B = 1$. At fixed temperature the probability of any particular spin configuration $\{s\}$ is given by

$$\mathcal{P}\{s\} = \frac{1}{Z} e^{-\beta E\{s\}}. \quad (1.4)$$

The free energy is defined as

$$F = -\beta^{-1} \ln Z. \quad (1.5)$$

Derivatives of the free energy give useful thermodynamic quantities such as the mean magnetization,

$$\begin{aligned} -\frac{\partial}{\partial h} F &= \beta^{-1} \frac{1}{Z} \frac{\partial}{\partial h} \sum_{\{s\}} e^{-\beta E\{s\}}, \\ &= \sum_{\{s\}} \left(\sum_i s_i \right) \mathcal{P}\{s\} \\ &= \langle M \rangle, \end{aligned} \quad (1.6)$$

and the susceptibility

$$\begin{aligned} -\frac{\partial^2}{\partial h^2} F &= \frac{\partial}{\partial h} \langle M \rangle \\ &= \langle M^2 \rangle - \langle M \rangle^2. \end{aligned} \quad (1.7)$$

The exact evaluation of the partition function Z is often difficult, if not impossible. (The two-dimensional Ising model has been solved exactly only when $h = 0$.) Most often it is necessary to make some sort of approximation.

1.2.2 The naïve mean-field approximation

Consider the mean magnetization at the k th lattice site,

$$\begin{aligned} \langle s_k \rangle &= \mathcal{P}[s_k = 1] - \mathcal{P}[s_k = -1] \\ &= \frac{1}{Z} \left(\sum_{\{s\}; s_k=1} e^{-\beta E\{s\}} - \sum_{\{s\}; s_k=-1} e^{-\beta E\{s\}} \right). \end{aligned} \quad (1.8)$$

Decompose the energy function as

$$E\{s\} = \mathcal{E}_1\{s'\} + s_k \mathcal{E}_2\{s'\}, \quad (1.9)$$

where $\{s'\}$ denotes the collection of spins $\{s\}$ excluding s_k , and where

$$\mathcal{E}_1\{s'\} = -\frac{1}{2} \sum_{i \neq k; j \neq k} J_{i,j} s_i s_j - \frac{1}{2} J_{k,k} - h \sum_{i \neq k} s_i \quad (1.10)$$

$$\mathcal{E}_2\{s'\} = -\sum_{i \neq k} J_{k,i} s_i - h. \quad (1.11)$$

Using this decomposition Eq. (1.8) becomes

$$\langle s_k \rangle = \frac{\sum_{\{s'\}} e^{-\beta \mathcal{E}_1\{s'\}} \left[e^{-\beta \mathcal{E}_2\{s'\}} - e^{+\beta \mathcal{E}_2\{s'\}} \right]}{\sum_{\{s'\}} e^{-\beta \mathcal{E}_1\{s'\}} \left[e^{-\beta \mathcal{E}_2\{s'\}} + e^{+\beta \mathcal{E}_2\{s'\}} \right]}. \quad (1.12)$$

In the *naïve mean-field* theory we make the uncontrolled approximation

$$\sum_j J_{kj} s_j \rightarrow J \langle s_k \rangle \quad (1.13)$$

where J is a constant that represents the overall interaction strength. Under this approximation \mathcal{E}_2 has no dependence on $\{s'\}$ and Eq. (1.12) reduces to

$$\langle s_k \rangle = \frac{e^{-\beta \mathcal{E}_2} - e^{+\beta \mathcal{E}_2}}{e^{-\beta \mathcal{E}_2} + e^{+\beta \mathcal{E}_2}} = \tanh(\beta J \langle s_k \rangle + h). \quad (1.14)$$

Because the system is constructed to be translationally invariant, $\langle s_k \rangle = m$ is the mean magnetization per spin and Eq. (1.14) can be written as

$$m = \tanh[\beta(Jm + h)]. \quad (1.15)$$

Equation (1.15) is the mean-field equation of state and can be solved numerically. For $h = 0$ it predicts a critical temperature of $\beta^{-1} = J$.

1.2.3 The fully connected Ising model

Naïve mean-field theory is exact for the fully connected Ising model, in which every pair of spins interacts. The fully connected Ising model is realized by choosing

$$J_{i,j}^{(\text{inf})} = \frac{J}{N}, \quad (1.16)$$

and has a well defined thermodynamic $N \rightarrow \infty$ limit.

The partition function, Eq. (1.3), can be written as

$$Z = \sum_M \sum_{\{s\}; \sum s_i = M} e^{-\beta E\{s\}}, \quad (1.17)$$

where the inner sum is over all spin configurations which have magnetization M . Because all pairs of spins interact equally, $E\{s\}$ is a function of M only. The partition function can be rewritten as

$$Z = \sum_M \exp[-\beta F(M)], \quad (1.18)$$

where

$$F(M) = E(M) - \beta^{-1} \ln \Omega(M) \quad (1.19)$$

and $\Omega(M)$ denotes the number of spin configurations $\{s\}$ that have magnetization M . It will become evident that the function $F(M)$ evaluated at its minimum is the system free energy.

The energy is simply

$$\begin{aligned} E(M) &= -\frac{1}{2} \sum_{i,j} J_{i,j}^{(\text{inf})} s_i s_j - h \sum_i s_i \\ &= -N \left[\frac{J}{2} m^2 + hm \right], \end{aligned} \quad (1.20)$$

where

$$m = M/N. \quad (1.21)$$

Now let us consider the calculation of $\Omega(M)$. For fixed M let n^+ and n^- denote the number of up spins and down spins, respectively. From the relations $n^+ + n^- = N$ and $n^+ - n^- = M$, we find

$$n^+ = \frac{N}{2}(1 + m). \quad (1.22)$$

The number of spin configurations $\{s\}$ that have magnetization M is then

$$\Omega(M) = \binom{N}{n^+} = \frac{N!}{\left(\frac{N}{2}(1+m)\right)\left(\frac{N}{2}(1-m)\right)!}. \quad (1.23)$$

Stirling's approximation, valid for large N , is

$$N! \approx N \ln N - N. \quad (1.24)$$

Application to Eq. (1.23) yields, to leading order,

$$\ln \Omega = \frac{N}{2} (2 \ln 2 - (1-m) \ln(1-m) - (1+m) \ln(1+m)). \quad (1.25)$$

Insert Eqs. (1.20) and (1.25) into Eq. (1.19) to obtain

$$F(M) = N \left[-\frac{J}{2} m^2 - hm + \frac{\beta^{-1}}{2} [(1-m) \ln(1-m) + (1+m) \ln(1+m)] \right], \quad (1.26)$$

up to an additive constant.

It is now possible to evaluate the partition function using Laplace's method. For large N there is nearly a continuum of magnetizations m between -1 and 1 . The sum of Eq. (1.18) is well approximated by an integral

$$Z = \int_{-1}^1 \frac{dm}{2/N} e^{-\beta F(M)}. \quad (1.27)$$

Because $F(M)$ is proportional to N , Laplace's method can be applied to obtain the leading order behavior of the partition function,

$$Z \propto e^{-\beta F}, \quad (1.28)$$

where F , the thermodynamic free energy, equals $F(M)$ evaluated at its minimum. The minimum of $F(M)$ is found by solving

$$\frac{dF}{dm} = 0. \quad (1.29)$$

Differentiation of Eq. (1.26) yields

$$N(-Jm - h + \beta^{-1} \operatorname{atanh}(m)) = 0. \quad (1.30)$$

By rearranging terms, it is found that the fully connected Ising model shares the mean-field equation of state, Eq. (1.15).

1.3 Long-range Kac interactions

Naïve mean-field theory, with only a single degree of freedom m , is often too drastic an approximation. In this section I will describe Kac mean-field theory, a more refined approach.

In the Kac mean-field limit the interaction range between particles, R , is taken to be infinitely large compared to the average inter-particle separation, yet infinitely small compared to the system size. Thus, local processes (including nucleation and ordering) can be modeled using Kac mean-field theory. Physical systems with effective long (but finite) range interactions are said to be *near-mean-field* and are approximately described by Kac mean-field theory.

1.3.1 The Kac potential

A Kac potential \mathcal{J}_R is parametrized by R and has the form [6]

$$\mathcal{J}_R(\vec{x}) = R^{-d} \mathcal{J}(\vec{x}/R). \quad (1.31)$$

It is assumed that $\mathcal{J}_R(\vec{x})$ goes to zero sufficiently fast as $\vec{x} \rightarrow \infty$. The parameter R represents the interaction range; each particle interacts with roughly R^d others.

A particularly simple choice for \mathcal{J}_R is the radial step function Θ_R described in Appendix A.5. Up to a choice of sign, the radial step function can represent either attractive or repulsive interactions.

The Kac mean-field limit is defined by taking the volume to infinity first and R to infinity second. In this limit, each spin interacts with infinitely many others in a local region, effectively damping fluctuations and simplifying the physical description.

1.3.2 Static coarse graining of the Ising model

Return to the Ising model, Eq. (1.1), and choose interactions $J_{i,j}$ to be of the Kac potential form

$$J_{i,j} = \mathcal{J}_R(\vec{x}(i) - \vec{x}(j)) = R^{-d} \mathcal{J}((\vec{x}(i) - \vec{x}(j))/R), \quad (1.32)$$

where $\vec{x}(i)$ is the position of the i th spin. In this section I will show that the Ising model partition function Z is considerably simplified in the Kac mean-field limit, where $V \rightarrow \infty$ first and $R \rightarrow \infty$ second.

Rather than working directly with the spins, I will work with the coarse grained magnetization $\phi(\vec{x})$ – a local average of spins. To define $\phi(\vec{x})$ precisely it is necessary to introduce some notation.

Choose the *coarse graining length* Δx to satisfy

$$1 \ll \Delta x \ll R, \quad (1.33)$$

which is possible for R sufficiently large. Note that all lengths are dimensionless, and are given in units of the lattice spacing.

The system volume is partitioned into a large number of *coarse graining cells*. Each cell is a hypercube that contains Δx^d spins, is indexed by i , and is centered at the position \vec{x}_i .

The coarse grained magnetization ϕ_i at the i^{th} cell is defined as the average of all spins s_α in that cell,

$$\phi_i = \phi(\vec{x}_i) = \frac{1}{\Delta x^d} \sum_{\alpha \in i} s_\alpha. \quad (1.34)$$

(Greek letters are adopted as spin indices to avoid confusion with cell indices.) By construction,

$$-1 \leq \phi_i \leq 1. \quad (1.35)$$

The Ising model partition function can be expressed as a functional integral over the

coarse grained magnetization,

$$Z = \int D\phi(x) e^{-\beta F[\phi]}, \quad (1.36)$$

where the free energy functional $F[\phi]$ is defined by

$$F[\phi] = E[\phi] - \beta^{-1} \ln \Omega[\phi], \quad (1.37)$$

$E[\phi]$ is the energy functional and $\Omega[\phi]$ is the degeneracy of spin configurations $\{s\}$ corresponding to the same coarse grained field ϕ . The free energy functional $F[\phi]$ is sometimes called the Landau-Ginzburg-Wilson Hamiltonian.

The significance of Eq. (1.36) is that, in the Kac mean-field limit, Laplace's method can be used to show that $F[\phi]$ is the thermodynamic free energy when it is evaluated at its minimum.

To determine the energy functional $E[\phi]$, consider two coarse graining cells centered at \vec{x}_i and \vec{x}_j . Because $\Delta x \ll R$, all spins in these two cells interact with the nearly constant strength $\mathcal{J}_{R;i,j} = \mathcal{J}_R(\vec{x}_i - \vec{x}_j)$. The sum of the interactions between the cells is therefore $-\frac{1}{2} \mathcal{J}_{R;i,j} (\Delta x^d \phi_i) (\Delta x^d \phi_j)$. The full Ising energy, Eq. (1.1), can be expressed as a sum over all pairs of coarse graining cells,

$$E[\phi] = - \sum_i \Delta x^d \left(\phi_i \sum_j \frac{1}{2} \Delta x^d \mathcal{J}_{R;i,j} \phi_j + h \phi_i \right). \quad (1.38)$$

Now turn to the coarse graining degeneracy $\Omega[\phi]$. The coarse grained magnetization ϕ_i represents an average of Δx^d spins where n^+ are up and n^- are down. Because $\Delta x^d \gg 1$, Stirling's approximation may be applied,

$$\begin{aligned} \ln \Omega[\phi] &= \sum_i \ln \binom{\Delta x^d}{n_i^\pm} \\ &= \sum_i \frac{\Delta x^d}{2} (2 \ln 2 - (1 - \phi_i) \ln(1 - \phi_i) - (1 + \phi_i) \ln(1 + \phi_i)). \end{aligned} \quad (1.39)$$

Both $E[\phi]$ and $\ln \Omega[\phi]$ (Eqs. (1.38), (1.39)) can be expressed in continuum notation. Up to

additive terms the result is

$$\begin{aligned} F[\phi] &= \int d\vec{x} (E[\phi] - \beta^{-1}\Omega[\phi]) \\ &= \int d\vec{x} \left(-\frac{1}{2}\phi(\mathcal{J}_R * \phi) + \frac{\beta^{-1}}{2}[(1 - \phi)\ln(1 - \phi) + (1 + \phi)\ln(1 + \phi)] - h\phi \right), \end{aligned} \quad (1.40)$$

where

$$(\mathcal{J}_R * \phi)(\vec{x}) = \int d\vec{x}' \mathcal{J}_R(\vec{x} - \vec{x}')\phi(\vec{x}'). \quad (1.41)$$

The coarse grained Ising free energy functional will be used throughout the dissertation.

1.3.3 Scaled lengths and the Kac mean-field limit

It is natural to measure all positions in units of the single remaining fundamental (non-statistical) length scale, R ,

$$\vec{r} = \vec{x}/R \quad (1.42)$$

$$u(\vec{r}) = \phi(\vec{x}). \quad (1.43)$$

In these units the free energy functional, Eq. (1.40), becomes

$$F[\phi(\vec{x})] = R^d \tilde{F}[u(\vec{r})], \quad (1.44)$$

where \tilde{F} has no R dependence,

$$\tilde{F}[u] = \int d\vec{r} \left(-\frac{1}{2}u(\mathcal{J} * u) + \frac{\beta^{-1}}{2}[(1 - u)\ln(1 - u) + (1 + u)\ln(1 + u)] - hu \right). \quad (1.45)$$

Note that

$$(\mathcal{J} * u)(\vec{r}) = \int d\vec{r}' \mathcal{J}(\vec{r} - \vec{r}')u(\vec{r}') \quad (1.46)$$

where $\mathcal{J}(\vec{r})$ is related to Kac potential $\mathcal{J}_R(\vec{x})$ through Eq. (1.31). The partition function can be expressed in scaled variables,

$$Z = \int D\phi(\vec{x}) e^{-\beta F[\phi]} \propto \int Du(\vec{r}) e^{-\beta R^d \tilde{F}[u]}. \quad (1.47)$$

When R is large, the equilibrium distribution is concentrated at the minimum of the free energy functional and large fluctuations are unlikely. In the limit $R \rightarrow \infty$ (Kac mean-field) Laplace's method becomes exact,

$$Z \propto e^{-\beta R^d \tilde{F}}, \quad (1.48)$$

where \tilde{F} represents the scaled free energy functional $\tilde{F}[u]$ at its minimum. Solutions to the Euler-Lagrange equation, $\frac{\delta \tilde{F}}{\delta u} = 0$,²

$$u(\vec{r}) = \tanh(\beta(\mathcal{J} * u)(\vec{r}) + \beta h), \quad (1.49)$$

give the minima of \tilde{F} , which correspond to the stable and metastable phases. The validity of Eq. (1.49) has been proved [25].

If $u(\vec{r})$ is taken to be uniform, setting $J = \int d\vec{x} \mathcal{J}(\vec{x})$ exactly reproduces the mean-field result, Eq. (1.15). Unlike the fully connected model, solutions to Eq. (1.49) may be spatially varying. Indeed, for systems with repulsive interactions the stable phase at low temperatures is often spatially modulated.

1.4 Ising Langevin dynamics

When a Kac-type long-range interaction is applied to the Ising model, its equilibrium behavior can be modeled using a coarse grained free energy functional $F[\phi]$, Eq. (1.40). Here I summarize various coarse grained *dynamics* that can be applied to the long-range Ising model. They will mostly take the form of a Langevin equation (see Appendix A.4),

$$\frac{\partial \phi(\vec{x}, t)}{\partial t} = \theta[\phi] + \sqrt{2B[\phi]} \eta(\vec{x}, t), \quad (1.50)$$

where $\eta(\vec{x}, t)$ is white Gaussian noise that is characterized by

$$\langle \eta(\vec{x}, t) \rangle = 0 \quad (1.51a)$$

$$\langle \eta(\vec{x}, t) \eta(\vec{x}', t') \rangle = \delta(\vec{x} - \vec{x}') \delta(t - t'); \quad (1.51b)$$

²See Appendix A.2 for a discussion of functional derivatives.

the notation $\langle \cdot \rangle$ denotes an ensemble average. The functionals $\theta[\phi]$ and $B[\phi]$ are yet to be specified.

The Fokker-Planck equation,

$$\frac{\partial \mathcal{P}[\phi]}{\partial t} = \int d\vec{x} \left[-\frac{\delta}{\delta \phi} \theta \mathcal{P} + \frac{\delta}{\delta \phi} B \frac{\delta}{\delta \phi} \mathcal{P} \right], \quad (1.52)$$

(see Appendix A.4) describes the evolution of the probability distribution $\mathcal{P}[\phi]$ under Langevin dynamics.

If the Langevin equation is to represent the Ising model, it must conform to the Boltzmann equilibrium distribution $\mathcal{P}_{\text{eq}}[\phi] \propto \exp[-\beta F]$ in the long time limit. That is,

$$\frac{\partial \mathcal{P}_{\text{eq}}[\phi]}{\partial t} = 0, \quad (1.53)$$

under Fokker-Planck evolution, Eq. (1.52).

1.4.1 Summary of common dynamics

Noise gradient flow dynamics

For an arbitrary free energy functional F , a common choice of Langevin dynamics is noisy gradient flow (NGF),³

$$\theta = -M \frac{\delta F}{\delta \phi(\vec{x})} \quad (1.54a)$$

$$B = \beta^{-1} M, \quad (1.54b)$$

where M is an arbitrary mobility constant. For the coarse grained Ising free energy functional, Eq. (1.40), we obtain

$$\frac{\delta F}{\delta \phi(\vec{x})} = -\mathcal{J}_R * \phi + \beta^{-1} \text{arctanh}(\phi) - h. \quad (1.55)$$

NGF dynamics is consistent with the Boltzmann distribution \mathcal{P}_{eq} : the Fokker-Planck evolution satisfies Eq. (1.53), which follows from the identity $\frac{\delta \mathcal{P}_{\text{eq}}}{\delta \phi} = \frac{\delta F}{\delta \phi} \mathcal{P}_{\text{eq}}$.

³NGF dynamics is also known as Model A in the Hohenberg-Halperin classification scheme [26].

Monte Carlo dynamics

It is desirable to define microscopic (spin based) Ising dynamics without reference to the coarse grained magnetization. To this end we interpret the Markov processes corresponding to Monte Carlo sampling of Ising spin configurations as a dynamical evolution (several variations are discussed in Section 2.3.1). By using a coarse graining procedure, I will derive Langevin equations representing spin-flip Glauber (SFG) dynamics,

$$\theta = \tanh(\beta(\mathcal{J}_R * \phi + h)) - \phi \quad (1.56a)$$

$$B = 1 - \frac{1}{2} \tanh^2(\beta(\mathcal{J}_R * \phi + h)) - \frac{1}{2} \phi^2, \quad (1.56b)$$

and spin-flip Metropolis (SFM) dynamics,

$$\theta = 2e^{-|\beta(\mathcal{J}_R * \phi + h)|} [\sinh(\beta(\mathcal{J}_R * \phi + h)) - \phi \cosh(\beta(\mathcal{J}_R * \phi + h))] \quad (1.57a)$$

$$B = 2 + O(|\phi|), \quad (1.57b)$$

in Section 2.3.2. The results are demonstrated to be consistent with the Boltzmann distribution in the limit $R \rightarrow \infty$ (Section 2.3.3).

Kawasaki spin-exchange is a Monte Carlo dynamics which locally conserves magnetization. Two variations are spin-exchange Glauber (SEG) and spin-exchange Metropolis (SEM) dynamics. In Section 2.3.5 the coarse grained description of SEG and SEM dynamics is discussed. In particular, the Langevin form, Eq. (1.50), is not applicable because the noise term exhibits spatial correlations.

1.4.2 Scaled lengths and effectively small noise

When lengths are scaled by R using Eqs. (1.42) and (1.43), the Langevin equation, Eq. (1.50), becomes

$$\frac{\partial u(\vec{r}, t)}{\partial t} = \tilde{\theta}[u] + R^{-d/2} \sqrt{2\tilde{B}[u]} \tilde{\eta}(\vec{r}, t), \quad (1.58)$$

where all the R dependence has been made explicit. The scaled and unscaled Langevin equations are equal (i.e., $\tilde{\theta}[u] = \theta[\phi]$ and $\tilde{B}[u] = B[\phi]$) and differ only in their functional

forms (i.e., $(u * \mathcal{J})(\vec{r})$ versus $(\phi * \mathcal{J}_R)(\vec{x})$).

The explicit R dependence comes from the scaling of the noise,

$$\eta(\vec{x}, t) = R^{-d/2} \tilde{\eta}(\vec{r}, t), \quad (1.59)$$

(readily verified in discretized form; see Appendix A.3) where $\tilde{\eta}$ is again white Gaussian noise with zero mean and the two-point correlation function

$$\langle \tilde{\eta}(\vec{r}, t) \tilde{\eta}(\vec{r}', t') \rangle = \delta(\vec{r} - \vec{r}') \delta(t - t'). \quad (1.60)$$

Equation (1.58) makes it apparent that a large interaction range R corresponds to effectively small fluctuations. This result is consistent with the fact that, in the mean-field limit, configurations in thermodynamic equilibrium are concentrated at the minimum of the free energy functional.

1.5 Nucleation

Systems with a first-order phase transition exhibit metastable phases. Metastability implies that the lifetime of the phase is long (compared to, e.g., the decorrelation time).

The metastable phase corresponds to a local, but not global, minimum of the free energy functional. In the ideal Kac mean-field ($R \rightarrow \infty$) limit the metastable phase is infinitely long lived.⁴ When R is finite, the metastable phase will eventually decay to the stable phase. This decay process begins with nucleation.

Homogeneous nucleation occurs through a localized thermal fluctuation called the nucleating droplet. The nucleating droplet is the object of least free energy cost, ΔF , that sits between the metastable and stable phases – it is a saddle point of the free energy functional. Nucleation occurs at a rate which is proportional to the Boltzmann factor, $\mathcal{P} \propto e^{-\beta \Delta F}$, when the metastable phase is long lived [11, 1].

⁴Strictly speaking, it is *only* in the mean-field limit that the metastable phase is well defined.

1.5.1 Field theoretic formalism

I will use NGF dynamics (Eqs. (1.50), (1.54)) and show directly that the rate of nucleation is proportional to $e^{-\beta\Delta F}$ in the mean-field limit. Consider all possible trajectories which begin in the metastable phase ϕ_m , and reach the stable phase ϕ_s after a long time t_1 ,

$$\phi(\vec{x}, 0) = \phi_m \quad (1.61)$$

$$\phi(\vec{x}, t_1) = \phi_s. \quad (1.62)$$

Each trajectory occurs with a probability proportional to $e^{-\frac{1}{2} \int d\vec{x} dt \eta^2}$, where $\eta(\vec{x}, t)$ is the dynamical noise. Thus, the probability to transition from ϕ_m to ϕ_s satisfies

$$\mathcal{P}_{m \rightarrow s} \propto \int D\eta e^{-\frac{1}{2} \int d\vec{x} dt \eta^2} \propto \int D\phi J e^{-S[\phi]}, \quad (1.63)$$

where J is the Jacobian associated with the change of variables,

$$J = \det \left| \frac{\delta \eta(\vec{x}, t)}{\delta \phi(\vec{x}', t')} \right|, \quad (1.64)$$

S is the action associated with the dynamics of Eq. (1.50),

$$S[\phi] = \frac{1}{2} \int d\vec{x} dt \eta^2 = \frac{\beta}{4M} \int d\vec{x} dt \left(\frac{\partial \phi}{\partial t} + M \frac{\delta F}{\delta \phi} \right)^2, \quad (1.65)$$

and the functional integral in Eq. (1.63) is over all configurations satisfying the boundary conditions, Eqs. (1.61) and (1.62). The Langevin equation is defined using forward time discretization (see Appendix A.4) so the Jacobian is 1 [27].

As before, the strategy is to switch to scaled variables (Eqs. (1.42), (1.43), and (1.44))

$$\mathcal{P}_{m \rightarrow s} \propto \int Du e^{-R^d \tilde{S}[u]} \quad (1.66)$$

$$S[\phi] = R^d \tilde{S}[u] = \frac{R^d \beta}{4M} \int d\vec{r} dt \left(\frac{\partial u}{\partial t} + M \frac{\delta \tilde{F}}{\delta u} \right)^2, \quad (1.67)$$

justifying the application of Laplace's method. The transition probability becomes

$$\mathcal{P}_{m \rightarrow s} \propto e^{-R^d \tilde{S}}, \quad (1.68)$$

where \tilde{S} minimizes $\tilde{S}[u]$,⁵

$$\frac{\delta \tilde{S}[u]}{\delta u(\vec{r}, t)} = 0, \quad (1.69)$$

and u satisfies appropriate boundary conditions.

Evaluate the functional derivative and integrate by parts to obtain the Euler-Lagrange equation for the minimal action,

$$\int d\vec{r}' \left(-\delta(\vec{r} - \vec{r}') \frac{\partial}{\partial t} + M \frac{\delta^2 \tilde{F}}{\delta u(\vec{r}) \delta u(\vec{r}')} \right) \left(\frac{\partial u}{\partial t} + M \frac{\delta \tilde{F}}{\delta u(\vec{r}')} \right) = 0. \quad (1.70)$$

Because

$$\frac{\partial}{\partial t} \frac{\delta \tilde{F}}{\delta u(\vec{r})} = \int d\vec{r}' \frac{\delta^2 \tilde{F}}{\delta u(\vec{r}) \delta u(\vec{r}')} \frac{\partial u(\vec{r}')}{\partial t} \quad (1.71)$$

the cross terms in Eq. (1.70) cancel, leaving

$$-\frac{\partial^2 u}{\partial t^2} + M^2 \int d\vec{r}' \frac{\delta^2 \tilde{F}}{\delta u(\vec{r}) \delta u(\vec{r}')} \frac{\delta \tilde{F}}{\delta u(\vec{r}')} = 0. \quad (1.72)$$

Two solutions of Eq. (1.72) are

$$\frac{\partial u_{\pm}}{\partial t} = \pm M \frac{\delta \tilde{F}}{\delta u_{\pm}}, \quad (1.73)$$

as can be verified by substitution and the use of Eq. (1.71). The action cost of these solutions is determined by insertion into Eq. (1.67),

$$\tilde{S}[u_-] = 0 \quad (1.74)$$

$$\begin{aligned} \tilde{S}[u_+] &= \beta \int d\vec{r} dt \frac{\delta \tilde{F}}{\delta u_+} \frac{\partial u_+}{\partial t} \\ &= \beta \int dt \frac{\partial \tilde{F}}{\partial t} \\ &= \beta \Delta \tilde{F}, \end{aligned} \quad (1.75)$$

⁵Note that the functional derivative operator $\delta/\delta u(\vec{r}, t)$ is distinct from $\delta/\delta u(\vec{r})$: the former measures the variation of a functional (e.g., $\tilde{S}[u]$) with respect to both the position (\vec{r}) and time (t) dependence of u . See Appendix A.2.

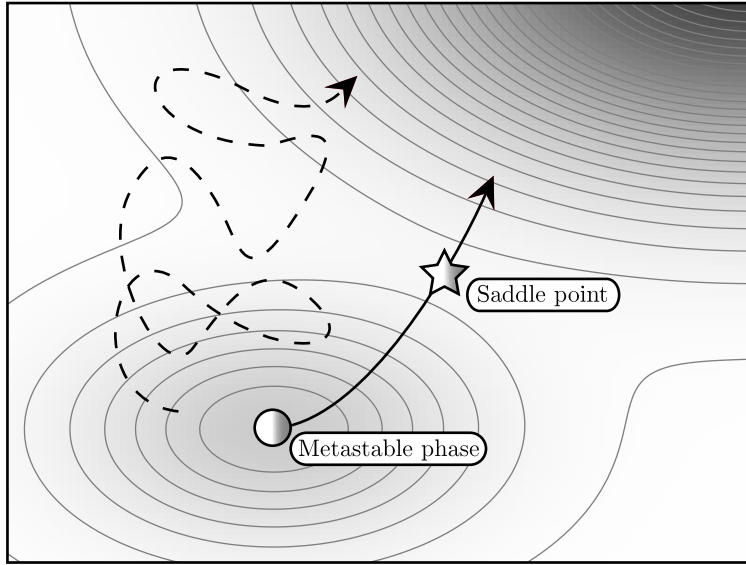


Figure 1.1: Nucleation is illustrated using a cartoon free energy landscape. When $R \rightarrow \infty$, the metastable phase corresponds to a local minimum of the free energy functional and the most likely decay trajectory (solid line) passes through the saddle point. For small nucleation barriers ($\beta\Delta F \sim 1$) metastability is ill-defined and it is difficult to identify a nucleation event (dashed line).

where $\Delta\tilde{F}$ is the free energy difference between the initial and final configurations of u .

The solution u_- corresponds to noiseless relaxation dynamics (i.e., $\eta = 0$). The solution u_+ is the time reversal of the trajectory u_- . We see that there is no action cost to decay from any configuration to the local free energy minimum, but the opposite trajectory has an action cost \tilde{S} proportional to $\beta\Delta\tilde{F}$. Analogous results hold for the unscaled variables,

$$S[\phi_-] = 0 \quad (1.76)$$

$$S[\phi_+] = \beta\Delta F. \quad (1.77)$$

The application to nucleation is direct. The metastable phase is a local minimum of the free energy. A trajectory that nucleates out of the metastable phase must go up in free energy before it goes down. For each trajectory $\phi(t)$ the free energy $F[\phi(t)]$ attains a maximum at some time $t_0 > 0$. The most likely nucleating trajectory is the one that minimizes $\Delta F = F[\phi(t_0)] - F[\phi(0)]$. This trajectory passes through a saddle point of

the free energy functional at time t_0 , as is illustrated in Fig. 1.1. The action cost of this trajectory is the action cost of reaching $\phi(t_0)$, namely $S = \beta\Delta F$ (there is no action cost for the relaxation dynamics beyond the saddle point). Therefore the probability of nucleation is

$$\mathcal{P} \propto e^{-S} = e^{-\beta\Delta F}, \quad (1.78)$$

where ΔF is again the free energy difference between the saddle point and metastable phase.

Langer derived a similar result by analytic continuation of the free energy functional [28], interpreting the jump discontinuities across the branch cut as the nucleation barrier. I prefer the derivation given in this section because it is direct (no analogies to simpler models are invoked) and because the mean-field assumption is explicit.

For a sufficiently large system the nucleating droplet is a localized object. Multiple nucleating droplets at different locations may form independently. Properly speaking, we should talk about the nucleation *rate* (the probability of nucleation per unit volume, per unit time) – the main result of this section is therefore that the nucleation rate is proportional to $e^{-\beta\Delta F}$.

1.5.2 Classical versus spinodal nucleation

The character of the nucleating droplets depends sensitively on the depth of the quench into the metastable phase.

The classical theory of nucleation applies near the coexistence curve where the free energy density difference between metastable and stable phases $f = (F_m - F_s)/V$ is small. The classical theory predicts an extended nucleating droplet with a well defined boundary separating the stable phase interior and the metastable phase exterior [29, 28, 15]. The free energy cost of such an object scales as

$$\Delta F \sim \sigma \ell^{d-1} - f \ell^d \quad (1.79)$$

where ℓ is the (large) characteristic radius of the droplet and σ is the surface tension at the droplet boundary. As discussed in Section 1.5.1, the nucleating droplet is a saddle point of the free energy functional. As a saddle point, the nucleating droplet has a length ℓ that maximizes the value of ΔF given in Eq. (1.79), and which thus scales as

$$\ell \sim \frac{\sigma}{f}. \quad (1.80)$$

The classical theory of nucleation is self-consistent near the coexistence curve: in the limit $f \rightarrow 0$ the droplet size diverges and the droplet boundary is well defined. Simulations of the Ising model in three dimensions are consistent with the classical theory [30].

For sufficiently deep quenches into the metastable phase the classical theory of nucleation fails. Near the spinodal limit of metastability (where ΔF is small) the nucleating droplet does not have a well defined boundary, and its interior does not resemble the stable phase [2, 3].

The nucleation rate is proportional to $e^{-\beta\Delta F}$, and we have seen that $\Delta F = O(R^d)$. Systems with long-range interactions are thus very unlikely to nucleate unless they are quenched near to the spinodal. The theory of nucleation near the spinodal, therefore, is the relevant one for systems with long-range interactions. Spinodal nucleation is discussed in Sections 2.2, 3.2.3, and 3.3. A word of caution: if the quench is so deep that ΔF is of the order 1, then metastable equilibrium and nucleation become ambiguous (in particular, the application of Laplace's method in Section 1.5.1 is questionable).

1.6 The clump model

The Ising model can be interpreted as a lattice gas model where up spins represent occupied sites. The coarse grained occupation density can be expressed in terms of the coarse grained magnetization,

$$\rho(\vec{x}) = \frac{1 + \phi(\vec{x})}{2}. \quad (1.81)$$

The Ising coarse grained free energy functional, Eq. (1.40), becomes

$$F = \int d\vec{x} \left(\frac{1}{2} \rho \Lambda_R * \rho + \beta^{-1} \rho \ln \rho + \beta^{-1} (1 - 2\rho) \ln(1 - 2\rho) - \mu \rho \right), \quad (1.82)$$

where the effective potential between particles is $\Lambda_R = -4\mathcal{J}_R$, the chemical potential μ is analogous the Ising external field h , and additive constants to the free energy have been dropped. Choose the Λ_R to be the radial step function Θ_R from Appendix A.5.

In the dilute gas limit, where $\rho \ll 1$, derivatives of the term $(1 - 2\rho) \ln(1 - 2\rho)$ are negligible compared to those of $\rho \ln \rho$. The former, therefore, do not influence thermodynamic behavior and can be neglected. The result,

$$F = \int d\vec{x} \left(\frac{1}{2} \rho \Lambda_R * \rho + \beta^{-1} \rho \ln \rho - \mu \rho \right), \quad (1.83)$$

is the *clump model*. Equilibrium stable and metastable phases correspond to the minima of the functional F and satisfy

$$0 = \frac{\delta F}{\delta \rho(\vec{x})} = \Lambda_R * \rho + \beta^{-1} \ln \rho - \mu, \quad (1.84)$$

where μ is the effective chemical potential. Equation (1.84) is called the Kirkwood-Monroe equation [31].

In this section the clump model free energy functional has been derived as the dilute limit of the antiferromagnetic Ising model, interpreted as a lattice gas. The Kirkwood-Monroe equation was originally derived for off-lattice particles, and is proven to be exact in the limit of large R [32, 32].

Interestingly, the phase diagram of the clump model can be characterized by a single physical control parameter. To appreciate this, it is convenient to work at fixed background density

$$\rho_0 = \frac{1}{V} \int d\vec{x} \rho \ll 1 \quad (1.85)$$

rather than chemical potential μ . The free energy becomes

$$F = \int d\vec{x} \left(\frac{1}{2} \psi \Lambda_R * \psi + \beta^{-1} (\rho_0 + \psi) \ln(\rho_0 + \psi) \right), \quad (1.86)$$

where

$$\rho = \rho_0 + \psi. \quad (1.87)$$

The free energy can be expressed in a simplified form

$$F = \int d\vec{r} \left(\frac{1}{2} \tilde{\psi} \Lambda_{\tilde{R}} * \tilde{\psi} + \tilde{\beta}^{-1} (1 + \tilde{\psi}) \ln(1 + \tilde{\psi}) \right) \quad (1.88)$$

using the scaled variables

$$\tilde{\psi}(\vec{r}) = \rho_0 \psi(\rho_0^{2/d} \vec{x}) \quad (1.89)$$

$$\tilde{\beta}^{-1} = \rho_0 \beta^{-1} \quad (1.90)$$

$$R = \rho_0^{-2/d} R. \quad (1.91)$$

In the mean-field limit the parameter R is infinite. The single remaining parameter in Eq. (1.88), $\tilde{\beta}^{-1}$, controls all the thermodynamics of the clump model.

Chapter 2

The long-range ferromagnet

The subject of this chapter is the Ising model with long-range ferromagnetic interactions described by the coarse grained free energy functional,

$$F = \int d\vec{x} \left(-\frac{1}{2} \phi (\mathcal{J}_R * \phi) + \frac{\beta^{-1}}{2} [(1 - \phi) \ln(1 - \phi) + (1 + \phi) \ln(1 + \phi)] - h\phi \right), \quad (2.1)$$

as in Section 1.3.2. The potential \mathcal{J}_R is ferromagnetic, i.e., its Fourier transform,

$$\hat{\mathcal{J}}_R(\vec{k}) = J_0 - J_2(kR)^2 + O((kR)^4), \quad (2.2)$$

has a maximum at $k = 0$ and satisfies $J_0, J_2 > 0$.

The mathematical development in this chapter is general, but a simple choice of the potential \mathcal{J}_R is the radial step function Θ_R (cf. Appendix A.5). With this choice each spin interacts uniformly with all other spins within a distance R ; the normalization is such that $\mathcal{J}_R * \phi$ represents a local average of $O(R^d)$ spins. For simplicity, all simulations reported in this chapter were performed using $d = 1$ and $\hat{\mathcal{J}}_R = \hat{\Theta}_R = \frac{\sin kR}{kR}$.

2.1 Phase diagram

For large R the stable and metastable phases correspond to minima of the free energy functional and thus satisfy the Euler-Lagrange equation

$$\beta \frac{\delta F}{\delta \phi} = -K * \phi + \operatorname{arctanh}(\phi) - H = 0, \quad (2.3)$$

where

$$K(\vec{x}) = \beta \mathcal{J}_R(\vec{x}) \quad (2.4)$$

$$H = \beta h. \quad (2.5)$$

Inspection of the free energy functional reveals that uniform solutions $\phi(\vec{x}) = m$ are favored in ferromagnetic systems; the Euler-Lagrange equation becomes an ordinary differential equation,

$$V\beta \frac{dF}{dm} = -K_0 m + \operatorname{arctanh}(m) - H = 0, \quad (2.6)$$

where

$$K_0 = \beta J_0 \quad (2.7a)$$

$$K_2 = \beta J_2 \quad (2.7b)$$

...

The coexistence curve $m_{\text{co}}(\beta)$ between phases of positive and negative spontaneous magnetization occurs at $h = 0$. An approximate solution to Eq. (2.6) at the coexistence curve

$$K_0^{-1} \approx 1 - \frac{1}{3} m_{\text{co}}^2, \quad (2.8)$$

is obtained by expanding $\frac{dF}{dm}(m)$ to $O(m^2)$; this approximation is valid near the critical temperature $K_0^{-1} = 1$.

Metastable phases are local (but not global) minima of the free energy; they satisfy the Euler-Lagrange equation dF/dm and the local stability condition $d^2F/dm^2 > 0$. The spinodal limit of metastability occurs when $d^2F/dm_{\text{sp}}^2 = 0$; this equation has the exact solution

$$K_0^{-1} = 1 - m_{\text{sp}}^2. \quad (2.9)$$

Equations (2.6) and (2.9) together specify H_{sp} , the value of H at which the instability occurs. The phase diagram of the ferromagnet, including the coexistence and spinodal

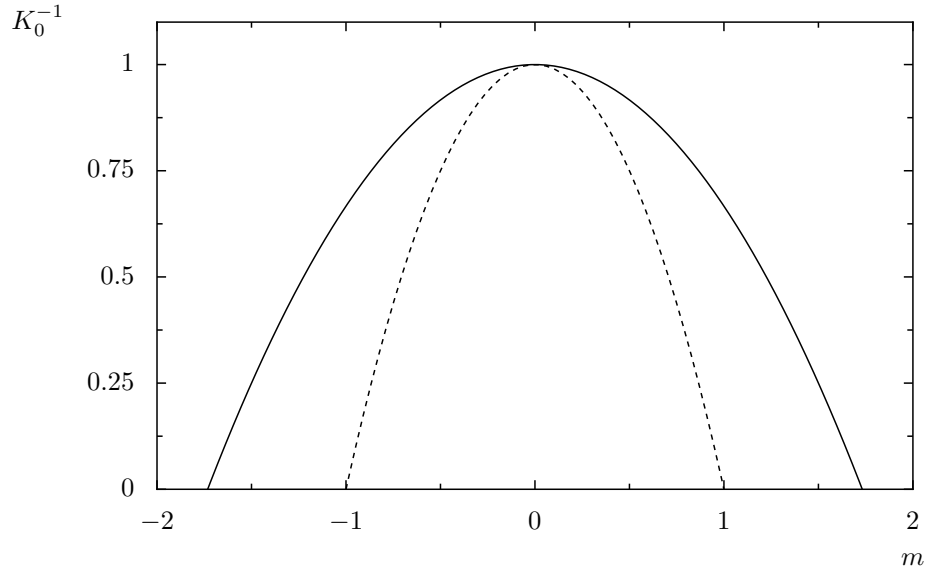


Figure 2.1: Phase diagram of the ferromagnet near the critical point $h = 0$, $K_0^{-1} = 1$. The solid line represents equilibrium coexistence between phases with positive and negative magnetization. The dashed line is the spinodal limit of metastability. The center region of the diagram, between the spinodal lines, is unstable.

curves (Eqs. (2.8) and (2.9)), is plotted in Fig. 2.1.

2.2 Spinodal nucleation

Nucleating droplets in the mean-field limit are saddle points of the free energy functional (cf. Section 1.5.1) and thus satisfy the Euler-Lagrange equation, Eq. (2.3). I will consider nucleation near the spinodal limit of metastability, which is relevant for systems with long-range interactions (cf. Section 1.5.2).

As the spinodal is approached, the metastable phase goes to $\phi(\vec{x}) = m_{\text{sp}}$ (cf. Eq. (2.9)) and satisfies the Euler-Lagrange equation

$$-K_0 m_{\text{sp}} + \text{arctanh}(m_{\text{sp}}) - H_{\text{sp}} = 0. \quad (2.10)$$

I work near the spinodal,

$$H_{\text{sp}} - H = \Delta H \ll 1, \quad (2.11)$$

and seek a nucleating droplet of the form

$$\phi_{\text{nuc}}(\vec{x}) = m_{\text{sp}} + \psi(\vec{x}). \quad (2.12)$$

Following Unger and Klein [2], I assume that $\psi(\vec{x})$ is small in magnitude, smooth, and slowly varying on length scales of order R – these conditions will be justified self-consistently. The expansion of the free energy cost of the droplet in powers of ψ yields

$$\begin{aligned} \beta\Delta F &= \beta(F[\phi_{\text{nuc}}] - F[m_{\text{sp}}]) \\ &\approx \int d\vec{x} \left[-\frac{1}{2}\psi(K * \psi) + \frac{1}{2}K_0\psi^2 + \frac{1}{3}K_0^2 m_{\text{sp}}\psi^3 + \Delta H\psi \right]; \end{aligned} \quad (2.13)$$

terms of the order $O(\psi^4)$ will be shown to be negligible. The Euler-Lagrange equation for the nucleating droplet saddle point is

$$\beta \frac{\delta\Delta F}{\delta\psi} = -K * \psi + K_0\psi + K_0^2 m_{\text{sp}}\psi^2 + \Delta H = 0. \quad (2.14)$$

Because ψ is slowly varying, the convolution can be expanded and truncated,

$$\begin{aligned} K * \psi &= \mathcal{F}^{-1}[\hat{K}\hat{\psi}] \\ &= \mathcal{F}^{-1}[(K_0 - K_2(kR)^2 + \dots)\hat{\psi}] \\ &\approx K_0\psi(\vec{x}) + K_2R^2\nabla^2\psi(\vec{x}), \end{aligned} \quad (2.15)$$

and the Euler-Lagrange equation becomes

$$K_2R^2\nabla^2\psi(\vec{x}) = \Delta H + K_0^2 m_{\text{sp}}\psi^2. \quad (2.16)$$

Up to this point I have not specified the direction of the spontaneous magnetization. With the choice $m_{\text{sp}} < 0$ (such that $H, \Delta H > 0$) the Euler-Lagrange equation can be written in scaled form as

$$\nabla^2 u = 1 - u^2, \quad (2.17)$$

where

$$\psi(\vec{x}) = au(\vec{x}/b) \quad (2.18a)$$

$$a = K_0|m_{\text{sp}}|^{-1/2}\Delta H^{1/2} \quad (2.18b)$$

$$b = \sqrt{\frac{K_2}{K_0}}|m_{\text{sp}}|^{-1/4}R\Delta H^{-1/4}. \quad (2.18c)$$

In one dimension Eq. (2.17) has the spherically symmetric solution

$$u(x) = 3 \operatorname{sech}^2\left(\frac{r-r_0}{\sqrt{2}}\right) - 1. \quad (2.19)$$

When solutions to Eq. (2.17) exist¹ the scaling form of Eq. (2.18) justifies our initial assumptions: when $\Delta H \rightarrow 0$, the solution ψ becomes both small in magnitude and slowly varying in space.

Equation (2.18) predicts that the droplet free energy cost scales as

$$\Delta F \sim R^d \Delta H^{3/2-d/2}, \quad (2.20)$$

which was first pointed out in Ref. [2]. The nucleation rate, which is proportional to $e^{-\beta\Delta F}$, substantially increases as the spinodal is approached

Note that, near the spinodal, the nucleating droplet represents a small deviation from the metastable phase, and thus is not affected by the structure of the stable phase. Nucleating droplets near the spinodal are substantially different than those predicted by the classical theory of nucleation (Section 1.5.2).

2.3 Dynamical coarse graining

Given a free energy functional $F[\phi]$ (such as that of the Ising ferromagnet, Eq. (1.40)) there are many Langevin dynamics of the form

$$\frac{\partial\phi}{\partial t} = \theta[\phi] + \sqrt{2B[\phi]}\eta \quad (2.21)$$

¹Solutions to Eq. (2.17) exist if and only if $d < 6$ [33, 34]. When $d = 6$ the nucleating droplets can be determined asymptotically near the spinodal; when $d > 6$ their form is non-universal [34].

(cf. Appendix A.4) that faithfully reproduce the Boltzmann distribution $\mathcal{P}_{\text{eq}}[\phi] \propto e^{-\beta F}$. One choice is the noisy gradient flow (NGF) dynamics considered in Section 1.4,

$$\theta = -M \frac{\delta F}{\delta \phi} = -\beta^{-1} M(-K * \phi + \text{arctanh}(\phi) - H) \quad (2.22)$$

$$B = \beta^{-1} M, \quad (2.23)$$

where K and H are given in Eqs. (2.4) and (2.5). Other choices of θ and B can also yield the correct equilibrium distribution, and it is not clear, a priori, which is the most representative of real systems.

In most studies of the kinetic Ising model some form of Monte Carlo dynamics, rather than NGF dynamics, is employed. I will review spin-flip Glauber (SFG) and Metropolis (SFM) dynamics, and show how they can be represented as Langevin equations in the long-range limit (Kac mean-field). The results, given in Eqs. (2.44) and (2.45), differ significantly from NGF dynamics; for example, in SFG and SFM dynamics the drift term θ never diverges and the noise term B remains finite at both zero and infinite temperature.

2.3.1 Monte Carlo Ising dynamics

Monte Carlo dynamics is defined as a set of transition probabilities between spin configurations. Let $W(s \rightarrow s')$ denote the probability that the system transitions between spin configurations $\{s\}$ and $\{s'\}$. If W satisfies the detailed balance condition

$$e^{-\beta E\{s\}} W(s \rightarrow s') = e^{-\beta E\{s'\}} W(s' \rightarrow s), \quad (2.24)$$

then the sequence of configurations generated samples the Boltzmann distribution $\mathcal{P}_{\text{eq}}\{s\} \propto e^{-\beta E\{s\}}$. (In fact, the weaker balance condition — the invariance of the Boltzmann distribution under stochastic evolution — is sufficient [35].)

At each update step of *spin-flip* Monte Carlo dynamics a random spin is chosen and is flipped with a probability W that depends on the energy cost ΔE of the spin-flip. Two

common choices of transition probabilities,

$$W_{\text{Glauber}}(\beta\Delta E) = \frac{e^{-\beta\Delta E/2}}{e^{-\beta\Delta E/2} + e^{\beta\Delta E/2}} \quad (2.25)$$

$$W_{\text{Metropolis}}(\beta\Delta E) = \min(1, e^{-\beta\Delta E}), \quad (2.26)$$

correspond to spin-flip Glauber (SFG) and spin-flip Metropolis (SFM) dynamics respectively.

In contrast, at each update step of *spin-exchange* (Kawasaki) Monte Carlo dynamics, two nearby spins are randomly selected and are exchanged with probability W .² The transition probabilities listed in Eqs. (2.25) and (2.26) correspond to spin-exchange Glauber (SEG) and spin-exchange Metropolis (SEM) dynamics respectively. By construction, spin-exchange dynamics locally conserves magnetization.

In both spin-flip and spin-exchange dynamics the unit of time is the Monte Carlo step (MCS). One MCS denotes N individual update steps, where N is the number of spins.

2.3.2 Langevin representation of spin-flip dynamics

In this section I will derive Langevin equations representing the spin-flip Monte Carlo dynamics (SFG and SFM) of the long-range Ising model. The central limit theorem plays a key role in the derivation – from it, the noise term arises naturally.

The *dynamic* coarse graining procedure is similar to the static coarse graining that was employed in Section 1.3.2 to derive the free energy functional. As before, assume that the Ising model interactions are of the Kac form, \mathcal{J}_R , with R large. Partition the system volume into a large number of coarse graining cells; each cell is indexed by i , is centered at \vec{x}_i , and contains Δx^d spins. The coarse graining length Δx is chosen to satisfy

$$1 \ll \Delta x \ll R \quad (2.27)$$

(which is possible for sufficiently large interaction range R). The coarse grained magneti-

²Typically, spins are exchanged only if they are separated by a distance less than the interaction range, but the discussion in this Chapter is general.

zation $\phi_i = \phi(\vec{x}_i)$ represents the average of all Δx^d spins in the i th coarse graining cell.

The energy cost to flip an arbitrary spin in the i th cell from down (-) to up (+),

$$\varepsilon_i = \Delta E(- \rightarrow +) = -\Delta E(+ \rightarrow -), \quad (2.28)$$

can be expressed as a sum over coarse grained magnetization cells,³

$$\begin{aligned} \beta\varepsilon_i &= -2 \sum_j \beta \mathcal{J}_R(\vec{x}_i - \vec{x}_j) \phi_j - 2\beta h \\ &= -2(K * \phi_i + H). \end{aligned} \quad (2.29)$$

where K and H are given in Eqs. (2.4) and (2.5).

Because $\Delta x \ll R$, the spins within the i th coarse graining cell are nearly independent, and each is up/down with probability

$$P\{\pm\} = \frac{n^\pm}{n^+ + n^-} = \frac{1}{2}(1 \pm \phi_i). \quad (2.30)$$

I have used the fact that n^\pm , the numbers of up/down spins in the coarse graining cell, satisfy

$$n^+ - n^- = \Delta x^d \phi_i \quad (2.31a)$$

$$n^+ + n^- = \Delta x^d. \quad (2.31b)$$

At each Monte Carlo update step a spin (up/down) is selected at random and subsequently flipped with probability

$$P\{\pm \rightarrow \mp\} = W(\mp\beta\varepsilon_i), \quad (2.32)$$

where $W(\beta\Delta E)$ is the Glauber or Metropolis transition probability (Eqs. (2.25) and (2.26)). Define a random variable $d\phi_i$ to represent the change in the coarse grained field ϕ_i after such a trial spin-flip. There are two possible outcomes, $d\phi_i = \pm 2/\Delta x^d$, corresponding to a

³Note that ε_i is proportional to the functional derivative of the coarse grained energy functional, Eq. (1.38).

spin flipping up/down. As a random variable, $d\phi_i$ has a mean

$$\begin{aligned}\langle d\phi_i \rangle &= \frac{2}{\Delta x^d} P\{-\}P\{- \rightarrow +\} - \frac{2}{\Delta x^d} P\{+\}P\{+ \rightarrow -\} \\ &= \frac{1}{\Delta x^d} [(1 - \phi_i)W(\beta\varepsilon_i) - (1 + \phi_i)W(-\beta\varepsilon_i)],\end{aligned}\tag{2.33}$$

a mean squared value

$$\begin{aligned}\langle d\phi_i^2 \rangle &= \left(\frac{2}{\Delta x^d}\right)^2 P\{-\}P\{- \rightarrow +\} + \left(\frac{-2}{\Delta x^d}\right)^2 P\{+\}P\{+ \rightarrow -\} \\ &= \frac{2}{\Delta x^{2d}} [(1 - \phi_i)W(\beta\varepsilon_i) + (1 + \phi_i)W(-\beta\varepsilon_i)],\end{aligned}\tag{2.34}$$

and a variance

$$\text{Var}[d\phi_i] = \langle (d\phi_i - \langle d\phi_i \rangle)^2 \rangle = \langle d\phi_i^2 \rangle - \langle d\phi_i \rangle^2.\tag{2.35}$$

Let Δt denote the temporal coarse graining period (because time is measured in units of MCS, the expected number of spin-flip trials per spin is Δt). Choose Δt to satisfy

$$(\Delta x^d)^{-1} \ll \Delta t \ll 1,\tag{2.36}$$

which is possible for Δx sufficiently large.

Of primary interest is the total change $\Delta\phi_i$ of the field ϕ_i after the small time Δt passes:

$$\Delta\phi_i(t) = \phi_i(t + \Delta t) - \phi_i(t).\tag{2.37}$$

Because $\Delta t \ll 1$, at most a small fraction of the Δx^d spins contributing to ϕ_i flip in this time interval. Nevertheless, the expected number of spin-flip trials within the coarse graining cell is large, $\Delta t \Delta x^d \gg 1$. The random change $\Delta\phi_i$ to the field ϕ_i is well approximated by the sum of $\Delta t \Delta x^d$ random variables, each distributed like $d\phi_i$:

$$\Delta\phi_i(t) = (d\phi_i)_1 + (d\phi_i)_2 + \dots + (d\phi_i)_{\Delta x^d \Delta t}.\tag{2.38}$$

By the central limit theorem, $\Delta\phi_i(t)$ is well approximated by

$$\phi_i(t + \Delta t) - \phi_i(t) = \Delta t \Delta x^d \langle d\phi_i(t) \rangle + \sqrt{\Delta t \Delta x^d \text{Var}[d\phi_i(t)]} \xi(x_i, t), \quad (2.39)$$

where $\xi(x, t)$ is a Gaussian random variable with zero mean and unit variance.

Comparison with the discretized Langevin equation, Eq. (A.50), reveals the identifications

$$\theta[\phi] = \Delta x^d \langle d\phi \rangle \quad (2.40)$$

$$\sqrt{2B[\phi]} = \Delta x^d \sqrt{\text{Var}[d\phi_i]}. \quad (2.41)$$

To proceed, the mean and variance of $d\phi_i$ must be evaluated from Eqs. (2.33) and (2.35) using the acceptance probability $W(\beta\Delta E)$.

For SFG dynamics, Eq. (2.25), the application of Eqs. (2.29), (2.33), and (2.35) and straightforward algebra yields

$$\langle d\phi_i \rangle = \frac{1}{\Delta x^d} (\tanh(K * \phi_i + H) - \phi_i) \quad (2.42)$$

$$\text{Var}[d\phi_i] = \frac{1}{\Delta x^{2d}} (2 - \tanh^2(K * \phi_i + H) - \phi_i^2). \quad (2.43)$$

The Langevin equation, Eq. (2.21), that represents SFG dynamics is thus

$$\theta = \tanh(K * \phi + H) - \phi \quad (2.44a)$$

$$B = 1 - \frac{1}{2} \tanh^2(K * \phi + H) - \frac{1}{2} \phi^2. \quad (2.44b)$$

For SFM dynamics, Eq. (2.26), similar algebra leads to

$$\theta = 2e^{-|K*\phi+H|} [\sinh(K * \phi + H) - \phi \cosh(K * \phi + H)] \quad (2.45a)$$

$$\begin{aligned} B &= 2e^{-|K*\phi+H|} [\cosh(K * \phi + H) - \phi \sinh(K * \phi + H)] - \frac{\theta^2}{2} \\ &= 2 + O(|\phi|). \end{aligned} \quad (2.45b)$$

Equations (2.44) and (2.45) are the main results of this section. The correctness of the

former has been proved [25, 36]. Although the condition $\Delta x \gg 1$ was required to derive these Langevin equations, the coarse graining length Δx and period Δt *do not appear* in the final results, as is required for consistency (after all, Δx and Δt are essentially arbitrary). It is thus natural to interpret the Langevin equation in the continuum limit: $\Delta t \rightarrow 0$ first, $\Delta x \rightarrow 0$ second.⁴

2.3.3 Equilibrium analysis

In this section I will establish the consistency of the Langevin equations, Eqs. (2.44) and (2.45), with the coarse grained free energy functional $F[\phi]$ of the long-range Ising model, Eq. (1.40).

By using the Fokker-Plank equation from Appendix A.4,

$$\frac{\partial \mathcal{P}}{\partial t} = \int d^d x \left[-\frac{\delta}{\delta \phi} \theta \mathcal{P} + \frac{\delta}{\delta \phi} B \frac{\delta}{\delta \phi} \mathcal{P} \right], \quad (2.46)$$

it is straightforward to show that the equilibrium distribution of the Langevin equation is

$$\mathcal{P}_{\text{eq}} \propto e^{-\beta G} \quad (2.47)$$

where $G[\phi]$ satisfies

$$\frac{\delta G}{\delta \phi} = -\beta^{-1} \frac{\theta}{B}. \quad (2.48)$$

Consistency requires that the dynamical equilibrium distribution $e^{-\beta G}$ agrees with the Boltzmann distribution, $e^{-\beta F}$. If we choose $\theta[\phi]$ and $B[\phi]$ derived for SFG and SFM dynamics (Eqs. (2.44) and (2.45)) we find the discouraging result $\delta G/\delta \phi \neq \delta F/\delta \phi$, and thus $G \neq F$. Nonetheless, when $R \gg 1$, the dynamical equilibrium distribution $e^{-\beta G}$ converges to the Boltzmann distribution $e^{-\beta F}$, even though the functional G does not converge to F .

To appreciate this, note that the Boltzmann distribution is a sharply peaked Gaussian centered on the free energy minimum when $R \gg 1$ (see Section 1.3.3). Thus, consistency

⁴This order of limits is standard (cf. Appendix A.4). The condition $\Delta t \ll \Delta x$ is also a requirement for the consistency of the coarse graining procedure – it is a direct consequence of Eqs. (2.27) and (2.36).

with the Boltzmann distribution requires only that F and G have identical stationary solutions ϕ_0 ,

$$\frac{\delta F}{\delta \phi}[\phi_0] = 0 \Leftrightarrow \frac{\delta G}{\delta \phi}[\phi_0] = 0, \quad (2.49)$$

and also identical second derivatives when evaluated at ϕ_0 ,

$$\frac{\delta^2 F}{\delta \phi^2}[\phi_0] = \frac{\delta^2 G}{\delta \phi^2}[\phi_0]. \quad (2.50)$$

Consider θ and B corresponding to SFG dynamics (Eq. (2.44)) and to SFM dynamics (Eq. (2.45)). To verify the first condition, Eq. (2.49), notice that the two equations

$$-\beta \frac{\delta F}{\delta \phi} = K * \phi + H - \operatorname{arctanh} \phi = 0 \quad (2.51)$$

$$-\beta \frac{\delta G}{\delta \phi} = \frac{\theta}{B} = 0 \quad (2.52)$$

share the same solutions,

$$\phi_0 = \tanh(K * \phi_0 + H). \quad (2.53)$$

To verify the second condition, Eq. (2.50), we evaluate the second functional derivatives and observe agreement:

$$-\beta \frac{\delta^2 F}{\delta \phi^2}[\phi_0] = K * \phi' - \frac{\phi'}{(1 - \phi^2)} \quad (2.54)$$

$$-\beta \frac{\delta^2 G}{\delta \phi^2}[\phi_0] = \frac{\theta'}{B} = K * \phi' - \frac{\phi'}{1 - \phi^2}. \quad (2.55)$$

The prime notation indicates functional differentiation, evaluation at $\phi = \phi_0$ is implicit, and $\theta[\phi_0] = 0$ by construction.

Together, the two conditions of Eqs. (2.49) and (2.50) establish that the coarse grained SFG and SFM dynamics agree with the Boltzmann distribution in the Kac mean-field limit, $R \rightarrow \infty$.

2.3.4 Magnetization relaxation

To test the effective Langevin equations for spin-flip Glauber and Metropolis dynamics, I will consider the process in which the magnetization $\phi(\vec{x})$ relaxes to equilibrium following a quench of the external field h . As in Section 1.4.2, express SFG and SFM dynamics (Eqs. (2.44) and (2.45)) using scaled lengths (Eqs. (1.42), (1.43), and (1.44)),

$$\frac{\partial u(\vec{r}, t)}{\partial t} = \tanh(\tilde{K} * u + H) - u + O(R^{-d/2}) \quad (2.56)$$

$$\frac{\partial u(\vec{r}, t)}{\partial t} = 2e^{-|\tilde{K}*u+H|}[\sinh(\tilde{K} * u + H) - \phi \cosh(\tilde{K} * u + H)] + O(R^{-d/2}), \quad (2.57)$$

where

$$\tilde{K}(\vec{r}) = \beta \mathcal{J}(\vec{r}), \quad (2.58)$$

and \mathcal{J} is the scaled Kac potential, Eq. (1.31). Choose, for simplicity, the normalization $J_0 = \int d\vec{r} \mathcal{J}(\vec{r}) = 1$.

For sufficiently large R the noise term (at $O(R^{-d/2})$) is negligible and the magnetization $u(\vec{r}, t) = m(t)$ is nearly uniform. The dynamics becomes

$$\frac{\partial m}{\partial t} = \tanh(\beta m + \beta h) - \phi \quad (2.59)$$

$$\frac{\partial m}{\partial t} = 2e^{-|\beta m + \beta h|}[\sinh(\beta m + \beta h) - \phi \cosh(\beta m + \beta h)]. \quad (2.60)$$

These equations can be integrated numerically to give $m(t)$ for arbitrary initial conditions $m(0)$. They are identical to results derived for the fully connected Ising model using a master equation approach [37].

Equations (2.59) and (2.60) are compared to one-dimensional Ising simulations in Figs. 2·2 and 2·3. The system is quenched from an (artificial) initial configuration with uniform magnetization to $\beta^{-1} = 3/4$ and $h = 0$. The system size is 2^{20} spins, and the interaction range $R = 2^{16}$. The potential $\mathcal{J}_R(\vec{x})$ is chosen to be the radial step function (cf. Appendix A.5). Two initial conditions are considered: $m(0) = 0.05$ and 1. Following the quench the magnetization relaxes to its equilibrium value $m \approx 0.78$. Figure 2·2 shows the curve $m(t)$ obtained

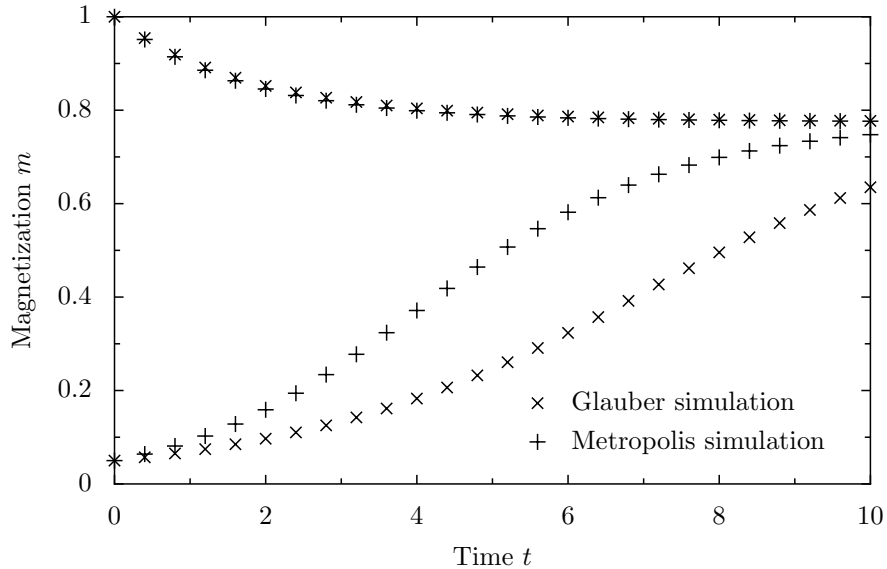


Figure 2-2: Ising simulations of the relaxation of the magnetization with $\beta = 4/3$ and $h = 0$. Both SFG and SFM dynamics are employed. The system size is 2^{20} spins and the interaction range $R = 2^{16}$.

by averaging 250 independent runs. In Fig. 2-3 the slope dm/dt is plotted versus m , and is found to agree with the theory.

A difference in character between spin-flip dynamics and NGF dynamics is apparent in Fig. 2-3 – the slope dm/dt at $m = 1$ would be infinite for NGF dynamics.

2.3.5 Langevin representation of Kawasaki spin-exchange dynamics

Kawasaki spin-exchange dynamics is an alternative to spin-flip dynamics. At each update step two spins are chosen at random: the first is selected with uniform probability and the second (at a distance r from the first) is selected with probability $\Gamma(r)$. The pair of spins is exchanged with either the Glauber or Metropolis transition probability. Spin-exchange dynamics conserves the total magnetization and is unaffected by the external magnetic field h .

In this section I will derive a Langevin equation representing coarse grained spin-exchange dynamics. It is assumed that both the potential \mathcal{J}_R and the pair selection probability Γ have the Kac form with the characteristic length R . The Langevin equation to be

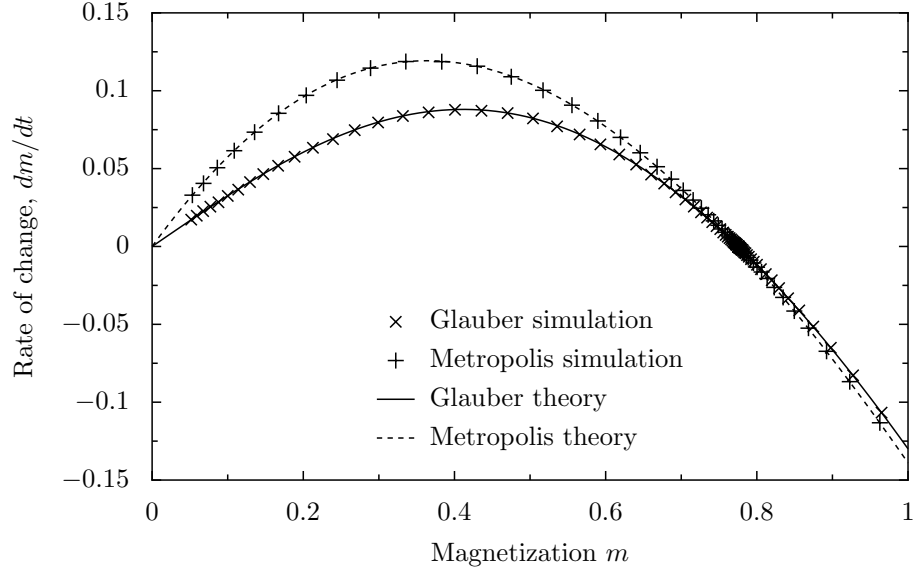


Figure 2.3: Ising simulations of the relaxation of the magnetization with $\beta = 4/3$ and $h = 0$, as in Fig. 2.2. The graph of dm/dt versus m is in agreement with the theory, Eqs. (2.59) and (2.60).

derived is valid in the $R \rightarrow \infty$ limit (Kac mean-field).

Because spin-exchange dynamics is significantly more complicated than spin-flip dynamics, I will assume that ϕ is small and work only at $O(\phi)$. Define $\langle d\phi_i \rangle$ to be the mean change in ϕ_i (the coarse grained magnetization, an average of Δx^d spins) after one spin-exchange trial. The result is calculated to be

$$\langle d\phi_i \rangle = \frac{M}{\Delta x^d} (-\phi_i + K * \phi_i + \Gamma * \phi_i - K * \Gamma * \phi_i) + O(\phi_i^2), \quad (2.61)$$

where M is 1 or 2 for Glauber or Metropolis acceptance probabilities, respectively.

The correlation between $d\phi$ at two coarse graining cells is calculated to be

$$\langle d\phi_i d\phi_j \rangle = \frac{\sqrt{M}}{\Delta x} (\delta_{i,j} - \Gamma_{i,j}) + O(\phi^2), \quad (2.62)$$

where $\delta_{i,j}$ is the Kronecker delta and $\Gamma_{i,j} = \Gamma(|\vec{x}_i - \vec{x}_j|)$.

Equation (2.62) suggests that the noise term η has spatial correlations,

$$\langle \eta(\vec{x}, t) \eta(\vec{x}', t') \rangle = C(\vec{x} - \vec{x}') \delta(t - t'), \quad (2.63)$$

where $C(\vec{x})$ is a function to be determined from Eqs. (2.61) and (2.62). Proceed by discretization. The integral of $\eta(\vec{x}, t)$ over a space-time region of size $\Delta x^d \Delta t$ (at position \vec{x}_i) corresponds to the sum of $\Delta x^d \Delta t$ random variables $d\phi_{i,\alpha}$ (labeled by α) minus their expected drift

$$\Delta\eta_i = \int_{\Delta x^d} d\vec{x} \int_{\Delta t} dt \eta(\vec{x}, t) = \sum_{\alpha=1}^{\Delta x^d \Delta t} (d\phi_{i,\alpha} - \langle d\phi_i \rangle). \quad (2.64)$$

From the central limit theorem it follows that

$$\begin{aligned} \langle \Delta\eta_i \Delta\eta_j \rangle &= \sum_{\alpha,\beta=1}^{\Delta x^d \Delta t} \langle (d\phi_{i,\alpha} - \langle d\phi_i \rangle) (d\phi_{j,\beta} - \langle d\phi_j \rangle) \rangle \\ &= \Delta x^d \Delta t M (\langle d\phi_i d\phi_j \rangle - \langle d\phi_i \rangle \langle d\phi_j \rangle). \end{aligned} \quad (2.65)$$

Equations (2.61), (2.62), and (2.65) together yield the dynamics

$$\frac{\partial}{\partial t} \phi(\vec{x}, t) = M (-\phi + K * \phi + \Gamma * \phi - K * \Gamma * \phi) + \eta + O(\phi^2) \quad (2.66)$$

$$\langle \eta(\vec{x}, t) \rangle = 0 \quad (2.67)$$

$$\langle \eta(\vec{x}, t) \eta(\vec{x}', t') \rangle = 2M (\delta(\vec{x} - \vec{x}') - \Gamma(\vec{x} - \vec{x}')) \delta(t - t'). \quad (2.68)$$

In Fourier space the convolution operations disappear,

$$\frac{\partial}{\partial t} \phi(\vec{k}, t) = M (-1 + K + \Gamma - K\Gamma) \phi + \eta + O(\phi^2) \quad (2.69)$$

$$\langle \eta(\vec{k}, t) \rangle = 0 \quad (2.70)$$

$$\langle \eta(\vec{k}, t) \eta(\vec{k}', t') \rangle = 2M (1 - \Gamma) \delta(\vec{k} - \vec{k}') \delta(t - t'). \quad (2.71)$$

In Section 2.4.4 these results will be applied to spinodal decomposition and compared to Monte Carlo simulations.

2.4 Ordering dynamics following a critical quench

An interesting process occurs when a ferromagnet is quenched from above to below the critical temperature with zero external field h . The coarse grained magnetization $\phi(\vec{x})$,

which is initially small, develops local domains of enhanced magnetization. The process is called *continuous ordering* or *spinodal decomposition* if $\phi(x)$ is conserved or non-conserved, respectively.

For simplicity, assume that the temperature is infinite before the quench, so that all spin configurations are equally likely (each spin is independently up with probability 1/2). Coarse graining these spins yields a local magnetization $\phi(\vec{x}, t = 0) = \zeta(\vec{x})$ that can be represented as white Gaussian noise

$$\langle \zeta \rangle = 0 \tag{2.72}$$

$$\langle \zeta(\vec{x}) \zeta(\vec{x}') \rangle = \delta(\vec{x} - \vec{x}'). \tag{2.73}$$

For systems with Kac-type interactions it is natural to work with scaled variables $u(\vec{x}/R, t) = \phi(\vec{x}, t)$. We find that the scaled initial condition becomes $u(\vec{r}, t = 0) = R^{-d/2} \tilde{\zeta}(\vec{r})$, where $\tilde{\zeta}(\vec{r})$ is again white Gaussian noise. This small initial condition suggests expanding the Langevin equation in powers of the magnetization ϕ , keeping only $O(\phi)$ terms. The result is called the Cahn-Hilliard-Cook (CHC) linear theory [11, 12] which predicts early time exponential growth of Fourier modes $\phi(\vec{k})$. The CHC prediction can be tested by scattering measurements of the time dependent static structure factor

$$S(\vec{k}, t) = \frac{1}{V} \langle |\phi(\vec{k}, t)|^2 \rangle, \tag{2.74}$$

where V is the system volume.

I will show that the CHC linear theory is identical (up to a time scale constant) for continuous ordering in NGF, SFG, and SFM dynamics (Eqs. (2.22), (2.44), and (2.45)).

Going beyond the CHC linear theory, however, is tricky. The problem is that a naive perturbation expansion of $S(\vec{k}, t)$ is ultraviolet (UV) divergent! Specifically, corrections to the CHC theory have an explicit dependence on the ill-defined cutoff, Δx^{-1} . (Note that Δx , the *arbitrary* coarse graining length, is not a physical quantity.) Furthermore, because all powers of ϕ appear in the Langevin dynamics, the UV divergence cannot be directly

resolved by the standard field theory renormalization procedure [38, 24].

Despite issues of renormalization, numerical evidence will be presented indicating that corrections to the CHC theory structure factor are $O(R^{-d/2})$ and $O(R^{-d})$ for SFM and SFG dynamics, respectively. Because SFM and SFG dynamics are generally expected to qualitatively agree, this observed difference is remarkable.

For the special case of SFG dynamics it is possible to avoid the UV divergence in the analytical expansion of $S(\vec{k}, t)$ in powers of R^{-d} . I will derive the exact leading order correction to the CHC theory. Numerical results for higher order corrections are also obtained.

All of the analytical results of this section will be compared with Monte Carlo simulations. Although the mathematics is general, the simulations are performed in one dimension using the radial step function potential $\mathcal{J}_R = \Theta_R$ (in Fourier space $\Theta_R(k) = \frac{\sin(kR)}{kR}$). Each system has 2^{20} spins and a large interaction range R . Ordering dynamics is simulated following a temperature quench from $\beta^{-1} = \infty$ to $4/9$. The process is either continuous ordering or spinodal decomposition, depending on whether spin-flip or spin-exchange dynamics are used.

2.4.1 The CHC linear theory for spin-flip dynamics

Begin with the Langevin equation

$$\frac{\partial \phi}{\partial t} = \theta[\phi] + \sqrt{2B[\phi]}\eta \quad (2.75)$$

where θ and B correspond to NGF dynamics (Eq. (2.22)), SFG dynamics (Eq. (2.44)), or SFM dynamics (Eq. (2.45)). Both $\eta(\vec{x}, t)$ and the initial condition $\phi(\vec{x}, t=0) = \zeta(\vec{x})$ are white Gaussian noise. Upon scaling lengths by R (see Section 1.4.2) the Langevin equation becomes

$$\frac{\partial u}{\partial t} = \tilde{\theta}[u] + R^{-d/2} \sqrt{2\tilde{B}[u]}\tilde{\eta}, \quad (2.76)$$

where $\tilde{\eta}(\vec{r}, t)$ is again white Gaussian noise that is characterized by

$$\langle \tilde{\eta}(\vec{r}, t) \rangle = 0 \quad (2.77a)$$

$$\langle \tilde{\eta}(\vec{r}, t) \tilde{\eta}(\vec{r}', t') \rangle = \delta(\vec{r} - \vec{r}') \delta(t - t'); \quad (2.77b)$$

and $\tilde{\theta}[u] = \theta[\phi]$ and $\tilde{B}[u] = B[\phi]$ have no R dependence.

From Eqs. (2.72) and (2.73) the scaled initial condition is

$$u(\vec{r}, t = 0) = R^{-d/2} \tilde{\zeta}(\vec{r}), \quad (2.78)$$

where $\tilde{\zeta}(\vec{r})$ is white Gaussian noise that is characterized by

$$\langle \tilde{\zeta}(\vec{r}) \rangle = 0 \quad (2.79a)$$

$$\langle \tilde{\zeta}(\vec{r}) \tilde{\zeta}(\vec{r}') \rangle = \delta(\vec{r} - \vec{r}'), \quad (2.79b)$$

and is uncorrelated with the dynamical noise,

$$\langle f[\tilde{\eta}] g[\tilde{\zeta}] \rangle = \langle f[\tilde{\eta}] \rangle \langle g[\tilde{\zeta}] \rangle. \quad (2.80)$$

Remarkably, at leading order in the (initially) small variable $u(\vec{r}, t)$, the NGF, SFG, and SFM dynamics all have the same form,

$$\frac{\partial u(\vec{r}, t)}{\partial t} = M(\tilde{K} * u - u) + R^{-d/2} \sqrt{2M} \tilde{\eta} + O(u^2), \quad (2.81)$$

where

$$M = \begin{cases} \beta & \text{(NGF dynamics)} \\ 1 & \text{(SFG dynamics)} \\ 2 & \text{(SFM dynamics)} \end{cases} . \quad (2.82)$$

We see that there is *universality* in the linearized dynamics.

Define the scaled Fourier transform of $u(\vec{r}, t)$ to be

$$\begin{aligned} u(\vec{q}, t) &= \int d\vec{r} e^{i\vec{q}\cdot\vec{r}} u(\vec{r}, t) = R^{-d} \int d\vec{x} e^{i\vec{k}\cdot\vec{r}} \phi(\vec{x}, t) \\ &= R^{-d} \phi(\vec{k}), \end{aligned} \quad (2.83)$$

where

$$\vec{q} = \vec{k}R \quad (2.84)$$

is dimensionless. The Fourier transform of Eq. (2.81) yields

$$\frac{\partial u(\vec{q}, t)}{\partial t} = \tilde{D}Mu + R^{-d/2} \sqrt{2M} \tilde{\eta} + O(u^2), \quad (2.85)$$

where

$$\tilde{D}(\vec{q}) = \tilde{K}(\vec{q}) - 1. \quad (2.86)$$

Analytic solution is possible at leading order,

$$u(\vec{q}, t) = R^{-d/2} \left[\tilde{\zeta} e^{\tilde{D}Mt} + \sqrt{2M} \int_0^t dt' e^{\tilde{D}M(t-t')} \tilde{\eta} \right] + O(R^{-d}). \quad (2.87)$$

Application of the white Gaussian noise identities, Eqs. (2.77), (2.79), and (2.80), yields

$$\frac{1}{\delta(\vec{q}=0)} \langle |u(\vec{q}, t)|^2 \rangle = R^{-d} \left[e^{2\tilde{D}Mt} (1 + \tilde{D}^{-1}) - \tilde{D}^{-1} \right] + O(R^{-3d/2}) \quad (2.88)$$

where $\delta(\vec{q}=0) = R^d/V$. The full structure factor, Eq. (2.74), is

$$S(\vec{k}, t) = S_l(k, t) + O(R^{-d/2}) \quad (2.89)$$

where

$$S_l(\vec{k}, t) = e^{2\tilde{D}Mt} (1 + \tilde{D}^{-1}) - \tilde{D}^{-1}. \quad (2.90)$$

For large R the CHC linear theory prediction, $S \approx S_l$, is a good approximation at early times. Due to exponential growth, the CHC theory fails at a time $t \sim \ln R$ [7].

The CHC prediction, Eq. (2.90), can be tested by direct simulation of the Ising model

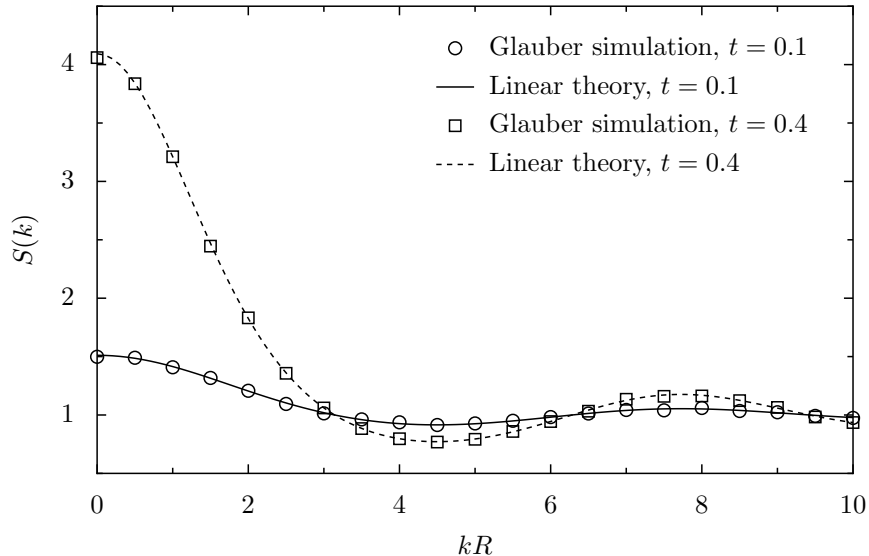


Figure 2.4: Structure factor measurements for continuous ordering using SFG dynamics. The system size is 2^{20} spins and the interaction range is $R = 2^{16}$. At the early times shown ($t = 0.1$ and $t = 0.4$) the structure factor is in agreement with the CHC prediction, Eq. (2.90).

using SFG dynamics. Figure 2.4 shows structure factor measurements of the continuous ordering process. A one-dimensional system of 2^{20} spins, with interaction range $R = 2^{16}$, is simulated following a quench from $\beta^{-1} = \infty$ to $4/9$. At early times ($t = 0.1$ and $t = 0.4$) the structure factor measurements agree well with Eq. (2.90).

2.4.2 Breakdown of the CHC linear theory

In the previous section I reviewed the CHC structure factor prediction, Eq. (2.90). The CHC linear theory is valid when R is large and t is sufficiently small (i.e., $t \ll \ln R$). It is natural to ask what happens when the linear theory breaks down.

Let's first take a step back and consider the Langevin equation in scaled form, Eq. (2.76). The noise term is $O(R^{-d/2})$ and would be negligible were it not for the fact that the initial condition $u(t = 0)$ is also $O(R^{-d/2})$. This balance led to the conclusion in Eq. (2.87) that $u = O(R^{-d/2})$ at early times ($t \ll \ln R$). At later times, when $t \sim \ln R$, exponential growth yields $u = O(1)$, nonlinear powers of u become relevant, and the linear theory fails. Notice from Eq. (2.76) that when $u = O(1)$ the noise term (which is $O(R^{-d/2})$) is negligible.

Thus, nonlinear powers of u in $\tilde{B}[u]$ are irrelevant, and the breakdown of the linear theory is entirely determined by $\tilde{\theta}[u]$.

Expansion of the relevant terms of SFG and SFM dynamics (Eqs. (2.44) and (2.45)) yields

$$\frac{\partial v}{\partial t} = \left(\tilde{K} * v - v + \sqrt{2}\tilde{\eta} \right) - \frac{1}{3} \left(\tilde{K} * v \right)^3 R^{-d} + O\left(R^{-2d}\right) \quad (2.91)$$

$$\frac{\partial v}{\partial t} = 2 \left(\tilde{K} * v - v + \tilde{\eta} \right) - 2|\tilde{K} * v| \left(\tilde{K} * v - v \right) R^{-d/2} + O\left(R^{-d}\right) \quad (2.92)$$

for SFG and SFM dynamics respectively, where

$$v(\vec{r}, t) = R^{-d/2}u(\vec{r}, t) = R^{-d/2}\phi(\vec{x}, t). \quad (2.93)$$

The initial condition,

$$v(\vec{r}, t = 0) = \tilde{\zeta}(\vec{r}), \quad (2.94)$$

is white Gaussian noise with no R dependence. The structure factor, Eq. (2.74), is

$$S(\vec{k}, t) = \frac{1}{\delta(\vec{q} = 0)} \langle |v(\vec{q}, t)| \rangle. \quad (2.95)$$

Strikingly, Eqs. (2.91) and (2.92) predict that corrections to the linear theory structure factor,

$$\delta S(\vec{k}, t) = S(\vec{k}, t) - S_l(\vec{k}, t), \quad (2.96)$$

are $O(R^{-d})$ for SFG dynamics and $O(R^{-d/2})$ for SFM dynamics:

$$\lim_{R \rightarrow \infty} \delta S(\vec{k}, t) R^{d/2} = \begin{cases} 0 & \text{(SFG dynamics)} \\ \text{finite} & \text{(SFM dynamics)} \end{cases}. \quad (2.97)$$

This prediction is tested by Monte Carlo using an increasing sequence of R values. A one-dimensional Ising model is simulated with 2^{20} spins and $R = \{2^8, 2^{10}, 2^{12}\}$. The corrections δS to the CHC linear theory at time $Mt = 1.4$ are plotted in Fig. 2.5 (SFG dynamics) and Fig. 2.6 (SFM dynamics). The structure factor is measured as an ensemble average

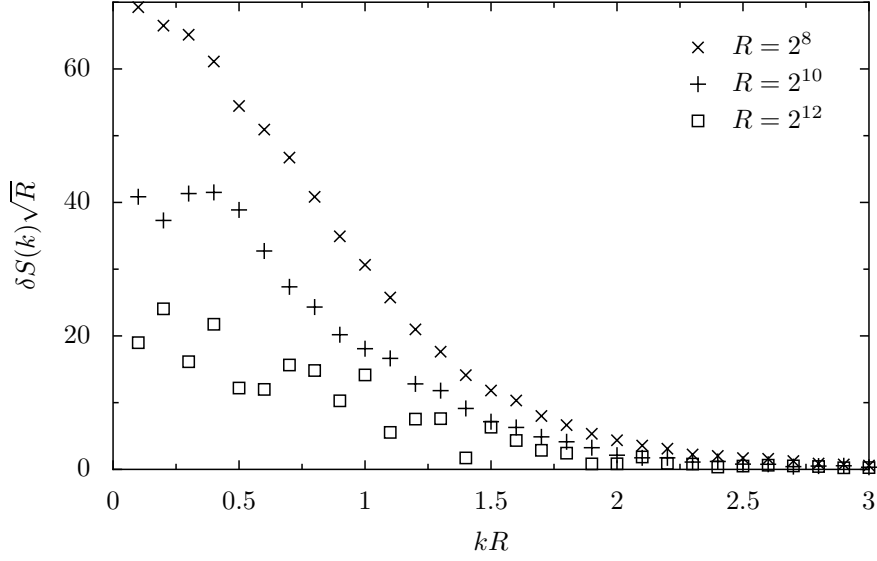


Figure 2.5: Corrections to the CHC linear theory structure factor. A one-dimensional Ising model with 2^{20} spins is simulated using SFG dynamics and increasing values of R . The results are consistent with $\delta S \sqrt{R} \rightarrow 0$ as $R \rightarrow 0$, supporting the prediction that $\delta S = O(R^{-d})$ for SFG dynamics.

of 2×10^4 quenches, each with different initial conditions. The results are consistent with Eq. (2.97), establishing a substantial difference between SFG and SFM dynamics.

2.4.3 Expansion beyond the CHC linear theory

In the case of SFG dynamics there exists a well behaved, analytical expansion in powers of R^{-d} for the structure factor. I will derive the first correction to the CHC theory analytically and present numerical results for the second-order correction.

A Fourier transform of the SFG dynamics, Eq. (2.91), yields

$$\frac{\partial v(\vec{q}, t)}{\partial t} = \tilde{D}v + \sqrt{2}\tilde{\eta} - \frac{(2\pi)^{-2d}}{3} (\tilde{K}v)^{3*} R^{-d} + O(R^{-2d}) \quad (2.98)$$

(see Appendix A.1), which can be reformulated as an integral equation,

$$v(\vec{q}, t) = e^{\tilde{D}t} \tilde{\zeta} + \int_0^t dt' e^{\tilde{D}(t-t')} \left(\sqrt{2}\tilde{\eta} - \frac{(2\pi)^{-2d}}{3} (\tilde{K}v)^{3*} R^{-d} + O(R^{-2d}) \right). \quad (2.99)$$

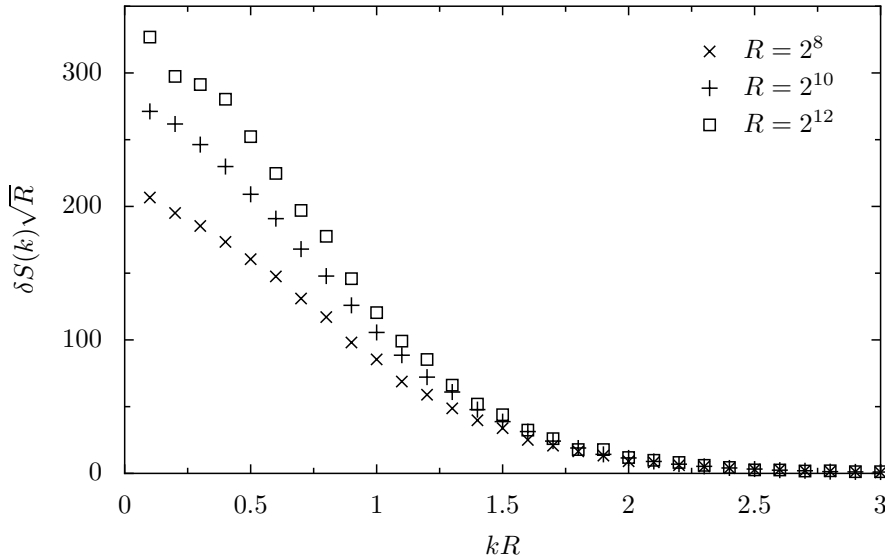


Figure 2.6: Corrections to the CHC linear theory structure factor. A one-dimensional Ising model with 2^{20} spins is simulated using SFM dynamics and increasing values of R . The results are consistent with $\delta S\sqrt{R} \rightarrow (\text{const})$ as $R \rightarrow 0$, supporting the prediction that $\delta S = O(R^{-d/2})$ for SFM dynamics.

It is straightforward to develop a perturbation expansion of the structure factor

$$S(\vec{k}, t) = \frac{1}{\delta(\vec{q}=0)} \langle |v(\vec{q})|^2 \rangle \quad (2.100)$$

in powers of R^{-d} . The steps are the following: (1) insert two factors of v from Eq. (2.99), (2) separate terms at each order of R^{-d} , (3) apply ensemble averages to the white Gaussian noise functions, $\tilde{\zeta}$ and $\tilde{\eta}$, to obtain δ -functions,⁵ (4) perform the trivial integrals over δ functions, and (5) perform the remaining non-trivial integrals.

Although straightforward in principle, the procedure is tedious. Steps (1–4) can be organized using diagrammatic notation [39, 40, 23, 27]. The diagrams are analogous to Feynman diagrams [38], but are complicated by a non-trivial t dependence. The number of loops in the diagram corresponds to the power of R^{-d} .

A rough description of the diagrammatic notation follows. Each diagram has two external legs corresponding to the two factors of v appearing in the structure factor. The legs

⁵For this step, the relevant identities are Eqs. (2.77), (2.79), and (2.80), and Wick’s theorem, which is described in Appendix A.3

have an “incoming time” t_1 of 0. Each leg may either (1) terminate, picking up the weight

$$e^{\tilde{D}t_1}\tilde{\zeta} + \sqrt{2} \int_0^{t_1} dt_2 e^{\tilde{D}(t_1-t_2)}\tilde{\eta}, \quad (2.101)$$

or (2) pick up the factor

$$\frac{R^{-d}}{3} \int_0^{t_1} dt_2 e^{\tilde{D}(t_1-t_2)} \quad (2.102)$$

and split into three new internal lines, each of which carries the weight \tilde{K} and has an “incoming time” t_2 . The newly created internal lines may again either terminate or split further. At $O(R^{-nd})$ there are exactly n split vertices in the diagram. To evaluate the structure factor we sum over all diagrams, connecting together the terminating lines in all possible ways (but $\tilde{\zeta}$ and $\tilde{\eta}$ don’t connect because they are uncorrelated random variables). Finally, we integrate over all internal “loop momenta” (a dummy \vec{q}' variable).

The structure factor, at one-loop order, is calculated to be

$$S(\vec{k}, t) = S^{(0)} + S^{(1)}R^{-d} + O(R^{-2d}) \quad (2.103a)$$

$$S^{(0)} = S_l \quad (2.103b)$$

$$S^{(1)} = 2 \int \frac{d\vec{q}'}{2\pi} \tilde{K}(\vec{q})\tilde{K}(\vec{q}')^2 \int_0^t da e^{\tilde{D}(\vec{q})(t-a)} BC, \quad (2.103c)$$

where

$$S_l = e^{2\tilde{D}(\vec{q})t} + 2 \int_0^t dt' e^{2\tilde{D}(\vec{q})(t-t')} \quad (2.104a)$$

$$B = e^{2\tilde{D}(\vec{q}')a} + 2 \int_0^a db e^{2\tilde{D}(\vec{q}')(a-b)} \quad (2.104b)$$

$$C = e^{2\tilde{D}(\vec{q})(a+t)} + 2 \int_0^a dc e^{2\tilde{D}(\vec{q})(a-c)}. \quad (2.104c)$$

Remarkably, the first correction to the linear theory, $S^{(1)}$, is well behaved: the momentum integral over \vec{q}' is damped by the factor $\tilde{K}(\vec{q}')^2$, and no UV divergence occurs. Higher

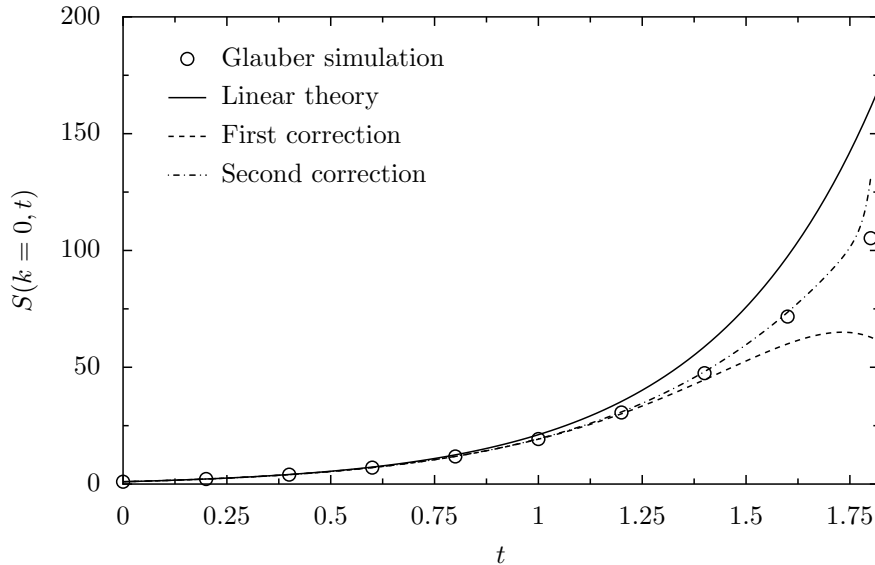


Figure 2-7: Structure factor measurements at $\vec{k} = 0$. A one-dimensional system of 2^{20} spins is simulated with the interaction range $R = 2^{16}$ and SFG dynamics. At increasing times following the quench an increasing number of corrections to the CHC linear theory is required to match the data.

order corrections are similarly protected.

It appears that SFG dynamics is special. If a perturbative calculation of the structure factor is attempted for NGF dynamics (Eq. (2.22)), the loop momentum integral over \vec{q}' would be missing the crucial factor $\tilde{K}(\vec{q}')^2$ (cf. Eq. (2.103)) and would be UV divergent. The perturbative expansion for SFM dynamics appears to be even more intractable than that of NGF because of an absolute value singularity at $\phi = 0$.

The corrections to the CHC linear theory can be compared to SFG Monte Carlo simulations. Figures 2-7–2-9 show simulation results of a one-dimensional system with 2^{20} spins and $R = 512$. In Fig. 2-7 the measured structure factor peak, $S(\vec{k} = 0, t)$, is compared with the CHC linear theory, the first correction (obtained analytically in Eq. (2.103)), and the second correction (obtained numerically). At early times the first correction to the CHC linear theory is in agreement with the simulation data over a range of k magnitudes, as shown in Fig. 2-8. At later times higher order corrections are required to describe the data, Fig. 2-9.

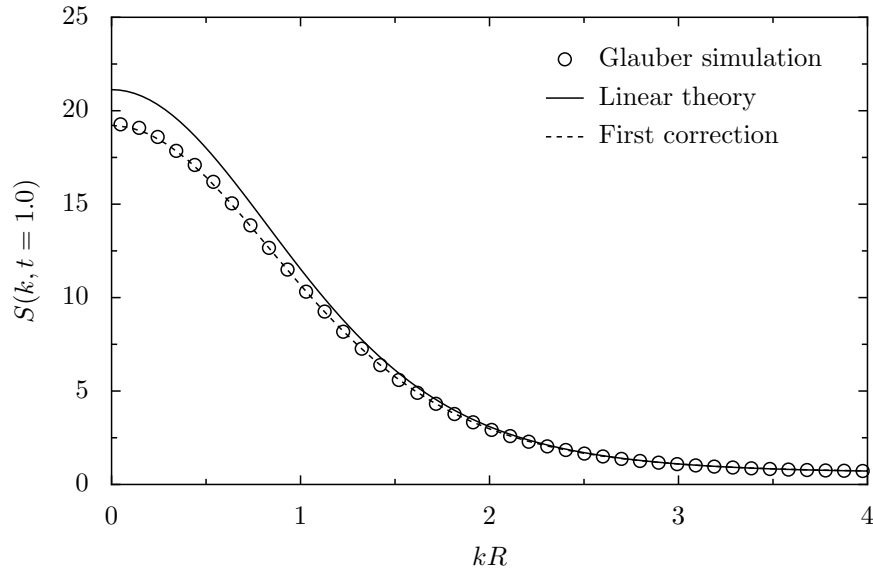


Figure 2-8: Structure factor measurements at time $t = 1.0$ following the quench. A one-dimensional system of 2^{20} spins is simulated with interaction range $R = 2^{16}$ and SFG dynamics. The first correction to the CHC linear theory (given analytically in Eq. (2.103)) agrees well with the simulation data.

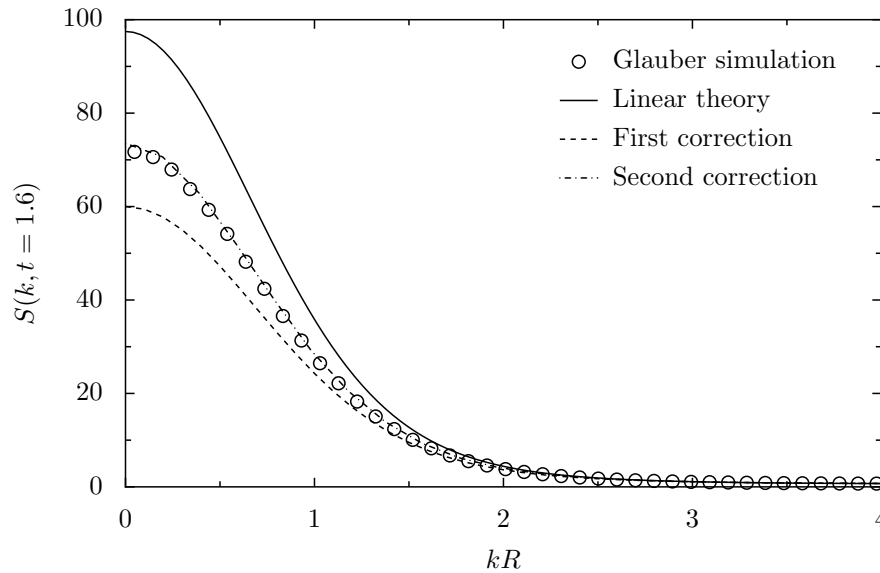


Figure 2-9: Structure factor measurements at time $t = 1.6$ following the quench. A one-dimensional system of 2^{20} spins is simulated with interaction range $R = 2^{16}$ and SFG dynamics. The second correction to the CHC linear theory (obtained numerically, of the order R^{-2d}) agrees well with the simulation data.

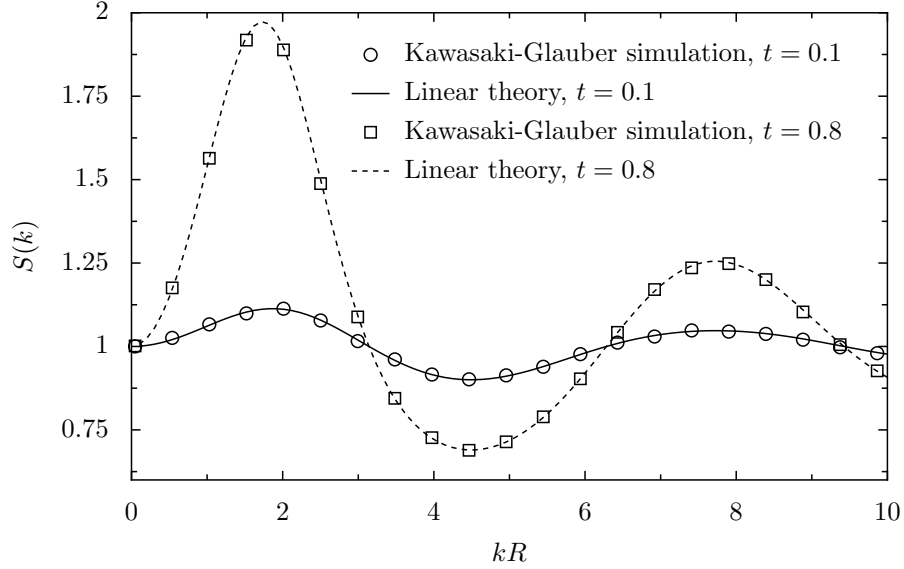


Figure 2-10: Structure factor measurements for spinodal decomposition using SEG dynamics. The system size is 2^{20} spins and the interaction range $R = 512$. At the early times shown ($t = 0.1$ and $t = 0.8$) the structure factor is in agreement with the linear theory, Eq. (2.105).

2.4.4 The CHC linear theory for Kawasaki spin-exchange dynamics

Kawasaki spin-exchange dynamics locally conserves magnetization. The ordering process following a quench is thus spinodal decomposition. By using Eqs. (2.69), (2.70), and (2.71) it is straightforward to calculate the linear theory structure factor,

$$S(\vec{k}, t) = e^{C(\vec{k})Mt} \left(1 + \frac{1 - \Gamma(\vec{k})}{C(\vec{k})} \right) - \frac{1 - \Gamma(\vec{k})}{C(\vec{k})}, \quad (2.105)$$

where

$$C(\vec{k}) = -1 + \Gamma(\vec{k}) + K(\vec{k}) - K(\vec{k})\Gamma(\vec{k}), \quad (2.106)$$

which can be compared to spin-flip case, Eq. (2.90). The prediction for $S(\vec{k}, t)$ can be tested by simulation of the Ising model using SFG dynamics. Figure 2-10 shows structure factor measurements of the spinodal decomposition process. A one-dimensional system of 2^{20} , with interaction range $R = 512$, is simulated following a quench from $\beta^{-1} = \infty$ to $4/9$. Spins within the distance R are selected with a uniformly random probability, so

that $\Gamma(\vec{k}) = \mathcal{J}_R(\vec{k}) = \frac{\sin(kR)}{kR}$. At early times ($t = 0.1$ and $t = 0.8$) the structure factor measurements agree well with Eq. (2.105).

Spin-exchange dynamics is much more complicated than spin-flip dynamics; I do not address the breakdown of the CHC linear theory as it applies to spinodal decomposition.

Chapter 3

Long-range repulsive models and modulated phases

In this chapter I will consider phase transitions in systems with long-range repulsive interactions (e.g., the long-range antiferromagnetic Ising model). Such systems are of interest because, unlike ferromagnets, they exhibit a wide range of modulated (spatially nonuniform) phases at low temperatures. The kinetics of transitions between these phases is particularly rich due to the associated changes in spatial symmetry.

3.1 Model definition

The starting point is the generic free energy functional

$$F = \int d\vec{x} \left[\frac{1}{2} \phi(\Lambda_R * \phi) + \beta^{-1} f(\phi) - h\phi \right] \quad (3.1)$$

where the entropy term $\beta^{-1} f(\phi)$ is an arbitrary convex function (i.e., $f''(\phi) > 0$), and the Kac potential,

$$\Lambda_R(\vec{x}) = R^{-d} \Lambda(\vec{x}/R), \quad (3.2)$$

is spherically symmetric and repulsive. This free energy functional can be used to represent both the long-range Ising and clump models (Sections 1.3.3, 1.6).

As in Section 1.3.3, the free energy functional can be expressed in scaled lengths,

$$F = R^d \int d\vec{r} \left[\frac{1}{2} u(\Lambda * u) + \beta^{-1} f(u) - hu \right], \quad (3.3)$$

where $u(\vec{r}) = u(\vec{x}/R) = \phi(\vec{x})$. In the limit $R \rightarrow \infty$ (Kac mean-field), the minima of the

free energy functional correspond to thermodynamic stable and metastable phases.

As a repulsive potential, $\Lambda(\vec{r})$ satisfies certain conditions. Its Fourier transform $\Lambda(\vec{q})$, considered as a function of the wave vector magnitude $q = |\vec{q}|$, is minimized at

$$0 < q_0 < \infty, \quad (3.4)$$

and is negative at its minimum,

$$\Lambda(q_0) < 0. \quad (3.5)$$

Expansion about the minimum yields

$$\Lambda(\vec{q}) = \Lambda(q_0) + \frac{1}{2}\Lambda''(q_0)(|\vec{q}| - q_0)^2 + \dots \quad (3.6)$$

A satisfactory choice for $\Lambda(\vec{r})$ is the radial step function $\Theta(\vec{r})$ described in Appendix A.5. The repulsive Gaussian potential e^{-r^2} , however, is not acceptable because the minimum of its Fourier transform is $\Lambda(|\vec{q}| = \infty) = 0$.

It is convenient to work in an ensemble with fixed mean magnetization

$$m = \frac{1}{V} \int d\vec{r} u(\vec{r}) \quad (3.7)$$

rather than fixed h ; the two ensembles are equivalent in the thermodynamic limit. I express the order parameter as

$$u(\vec{r}) = m + \psi(\vec{r}), \quad (3.8)$$

where ψ has been constructed to satisfy

$$\int d\vec{r} \psi(\vec{r}) = 0. \quad (3.9)$$

In anticipation that $\psi(\vec{r})$ will be small, I expand the free energy in a power series,

$$F = R^d \int d\vec{r} \left[\frac{1}{2} \psi(A * \psi) + \beta^{-1} \left[\frac{1}{3!} f^{(3)}(m) \psi^3 + \frac{1}{4!} f^{(4)}(m) \psi^4 + \dots \right] \right], \quad (3.10)$$

where

$$A(\vec{r}) = \Lambda(\vec{r}) + \delta(\vec{r})\beta^{-1}f^{(2)}(m) \quad (3.11)$$

and $f^{(i)}$ is the i th derivative of f .

3.1.1 The disordered phase and spinodal

At high temperatures β^{-1} the disordered solution $\psi = 0$ is the stable phase (i.e., the free energy minimum) because

1. the mean of ψ is zero by construction (Eq. (3.9));
2. the entropic term $\beta^{-1}f(u)$ becomes the dominant contribution to F (Eq. (3.3));
3. the convexity of $f(u)$ implies the stable phase is uniform.

Consider a system in the high temperature disordered phase, $\psi = 0$. For $R \gg 1$ the fluctuations are small and the free energy is well approximated by

$$F \approx \frac{R^d}{2} \int d\vec{r} \psi(\vec{r})(A * \psi)(\vec{r}) = \frac{R^d}{2(2\pi)^{-d}} \int d\vec{q} A(\vec{q}) |\psi(\vec{q})|^2, \quad (3.12)$$

where the second step follows from Parseval's theorem. The stability condition

$$\delta^2 F / \delta \psi^2 > 0 \quad (3.13)$$

fails if $A(\vec{q}) < 0$ for any \vec{q} . The spinodal limit of metastability occurs when $A(\vec{q})$, evaluated at its minimum $|\vec{q}| = q_0$, is zero,

$$A(q_0) = \Lambda(q_0) + \beta_{\text{sp}}^{-1} f^{(2)}(m) = 0. \quad (3.14)$$

Note that the spinodal temperature β_{sp}^{-1} has an m dependence.

3.1.2 The critical point

I will demonstrate that there is a critical point at $m = 0$ and $\beta^{-1} = \beta_{\text{sp}}^{-1}|_{m=0}$ when f is an even function. I begin by expanding $f(u)$ in a power series about $u = 0$,

$$f = \frac{1}{2!}f^{(2)}(0)u^2 + \frac{1}{4!}f^{(4)}(0)u^4 + \dots \quad (3.15)$$

Take m to be small and assume that $\psi = O(m)$, which will be justified self-consistently. Therefore the insertion of $u = m + \psi$ into $f(u)$ yields only a few relevant terms,

$$\beta^{-1}f(u) \approx \tilde{\beta}^{-1} \left[\frac{1}{2} (a + 3m^2) \psi^2 + m\psi^3 + \frac{1}{4}\psi^4 \right], \quad (3.16)$$

where

$$\tilde{\beta}^{-1} = \beta^{-1} \frac{f^{(4)}(0)}{6} \quad (3.17)$$

$$a = \frac{6f^{(2)}(0)}{f^{(4)}(0)}. \quad (3.18)$$

Using this approximation, the free energy functional, Eq. (3.3), becomes

$$F \approx \tilde{R}^d \int d\vec{r} \left[\frac{1}{2} \psi(\tilde{A} * \psi) + m\psi^3 + \frac{1}{4}\psi^4 \right], \quad (3.19)$$

with

$$\tilde{A}(\vec{q}) \approx t + 3m^2 + \tilde{\sigma}^2(|\vec{q}| - q_0)^2, \quad (3.20)$$

and

$$t = \tilde{\beta} \left(\Lambda(q_0) + \beta^{-1}f^{(2)}(0) \right) \quad (3.21)$$

$$\tilde{R}^d = \tilde{\beta}^{-1}R^d \quad (3.22)$$

$$\tilde{\sigma}^2 = \tilde{\beta}\sigma^2 = \tilde{\beta} \frac{\Lambda''(q_0)}{2}. \quad (3.23)$$

Note that t is the reduced temperature (i.e., the $m = 0$ disordered phase spinodal occurs at $t = 0$).

Stable and metastable phases correspond to minima of the free energy functional and satisfy the approximate Euler-Lagrange equation

$$\tilde{R}^{-d} \frac{\delta F}{\delta \psi(\vec{r})} = \tilde{A} * \psi + 3m\psi^2 + \psi^3 = 0, \quad (3.24)$$

which is valid near $m = t = 0$ (the critical point). When $t \sim m^2$, the Euler-Lagrange equation predicts nontrivial solutions which scale as $\psi(\vec{q}) \sim m$; these solutions are concentrated at $|\vec{q}| = q_0$ and have a characteristic width which scales as $(|\vec{q}| - q_0) \sim m/\tilde{\sigma}$. The existence of scaling solutions justifies the truncations made in Eqs. (3.16) and (3.20).

The assumption that $f(u)$ is an even function is crucial to the existence of a critical point at $m = t = 0$. If $f(u)$ were not an even function, the ψ^3 term appearing in the free energy functional would not contain an m prefactor and would therefore dominate the ψ^4 term for small ψ ; the non-zero stationary points of the resulting ψ^3 field theory (i.e., solutions to $\delta F/\delta \psi = 0$) would be unstable [41], resulting in a unique stable phase near $m = t = 0$.

The free energy functional near the critical point, Eq. (3.19), has only a few physically relevant parameters, viz.,

- The large interaction range \tilde{R} , which enables the mean-field approximation.
- The characteristic nucleating droplet envelope width, $\tilde{\sigma}$.
- The characteristic angular frequency of spatial modulations, q_0 .
- The reduced temperature t and the magnetization m .

Near the critical point the phase diagram predicted by the free energy functional, Eq. (3.3), is parametrized by t and m alone.

3.2 Two dimensions – the disordered, stripe, and clump phases

I will study two-dimensional systems near the critical point using the free energy functional, Eq. (3.19). A main result of this section is the phase diagram illustrated in Fig. 3-3, which

is valid near the critical point. There are three phases: disordered, clump, and stripe. The coexistence curves between these phases are derived in Section 3.2.1, reproducing prior work [42, 43]. In Section 3.2.2 I will derive the complete set of spinodal curves which, to my knowledge, are new. Nucleation near the spinodal curves is the subject of Section 3.2.3.

3.2.1 Equilibrium phase diagram

A first step toward the determination of the phase diagram is to identify solutions $\psi(\vec{r})$ of the Euler-Lagrange equation, Eq. (3.24), which represent stationary points of the free energy functional. The relatively small free energy cost of fluctuations in Fourier modes $\psi(\vec{q})$ with $|\vec{q}| \approx q_0$ motivates us to consider ψ peaked about this point. The ansatz,

$$\psi(\vec{r}) = b \sum_{\vec{e} \in \mathcal{Q}_b} \cos(q_0 \vec{e} \cdot \vec{r}) + c \sum_{\vec{e} \in \mathcal{Q}_c} \cos(q_0 \vec{e} \cdot \vec{r}), \quad (3.25)$$

has two real parameters b , c , and involves the unit reciprocal lattice vectors

$$\mathcal{Q}_b = \left\{ \begin{array}{l} \langle +1, 0 \rangle \\ \langle -1, 0 \rangle \end{array} \right\}, \quad (3.26)$$

and

$$\mathcal{Q}_c = \left\{ \begin{array}{l} \left\langle +\frac{1}{2}, +\frac{\sqrt{3}}{2} \right\rangle \\ \left\langle -\frac{1}{2}, +\frac{\sqrt{3}}{2} \right\rangle \\ \left\langle -\frac{1}{2}, -\frac{\sqrt{3}}{2} \right\rangle \\ \left\langle +\frac{1}{2}, -\frac{\sqrt{3}}{2} \right\rangle \end{array} \right\}. \quad (3.27)$$

The Fourier transform of Eq. (3.25) yields

$$\psi(\vec{q}) = (2\pi)^d \left[b \sum_{\vec{e} \in \mathcal{Q}_b} \delta(\vec{q} - q_0 \vec{e}) + c \sum_{\vec{e} \in \mathcal{Q}_c} \delta(\vec{q} - q_0 \vec{e}) \right]. \quad (3.28)$$

Note that the ansatz $\psi(\vec{q})$ fixes an angular orientation. Rotational invariance is added “by hand”: if $\psi(\vec{q})$ is a solution to Eq. (3.24), then so is $\psi(\mathcal{R}[\vec{q}])$, where \mathcal{R} is an arbitrary rotation.

I will now apply the ansatz to the free energy $F[\psi]$ yielding an ordinary function $F(b, c)$. The first step is to convert the free energy functional, Eq. (3.19), to its Fourier representation. This is achieved through the identity

$$\int d\vec{r}(\psi(\vec{r}))^n = \frac{1}{(2\pi)^{nd}} \int [d\vec{q}_1 \dots d\vec{q}_n] [\psi(\vec{q}_1) \dots \psi(\vec{q}_n)] (2\pi)^d \delta(\vec{q}_1 + \dots + \vec{q}_n) \quad (3.29)$$

(see Appendix A.1). The ansatz, Eq. (3.28), leads to considerable simplification: n -fold products such as $[\psi(\vec{q}_1) \dots \psi(\vec{q}_n)]$ contribute to $F[\psi]$ only when the vector sum $(\vec{q}_1 + \dots + \vec{q}_n)$ is nonzero. The free energy functional, Eq. (3.19), becomes

$$F[\psi] \rightarrow F(b, c) = R^d V \left[(t + 3m^2)(2c^2 + b^2) + 12mbc^2 + \left(\frac{3}{2}b^4 + 12b^2c^2 + 9c^4 \right) \right], \quad (3.30)$$

where $V = (2\pi)^d \delta(\vec{q} = 0)$ is the system volume. Each of the terms on the right-hand side of Eq. (3.30) is obtained by summing vectors, drawn from the sets \mathcal{Q}_b and \mathcal{Q}_c , that add to zero. For example, $\int d\vec{r} \psi^3 = 12bc^2$ because there are exactly 12 unique ordered triplets $(\vec{e}_1, \vec{e}_2, \vec{e}_3) \in (\mathcal{Q}_b \cup \mathcal{Q}_c)^3$ that satisfy $\vec{e}_1 + \vec{e}_2 + \vec{e}_3 = 0$. In each triplet, one vector is contained in \mathcal{Q}_b and two vectors are contained in \mathcal{Q}_c .

When the ansatz of Eq. (3.28) is applied, the Euler-Lagrange equation becomes,

$$\frac{\partial F(b, c)}{\partial b} = 2R^d V [(t + 3m^2)b + 6mc^2 + 3b^3 + 12bc^2] = 0 \quad (3.31a)$$

$$\frac{\partial F(b, c)}{\partial c} = 4R^d V [(t + 3m^2)c + 6mbc + 6b^2c + 9c^3] = 0, \quad (3.31b)$$

and has several solutions. The *disordered* phase solution is

$$b = b_d = 0 \quad (3.32a)$$

$$c = c_d = 0. \quad (3.32b)$$

There is one other solution with $c = 0$, the *stripe* phase,

$$b = b_s = -\sqrt{-\frac{1}{3}t - m^2} \quad (3.33a)$$

$$c = c_s = 0, \quad (3.33b)$$

which is unique up to the sign of b . The exchange of sign ($b \rightarrow -b$) corresponds to the simple translation $\psi(\vec{r}) \rightarrow \psi\left(\vec{r} + \left\langle \frac{\pi}{q_0}, 0 \right\rangle\right)$ and yields no new physics (cf. Eq. (3.25)).

Next consider the case $c \neq 0$; Eq. (3.31b) reduces to

$$c^2 = -\frac{1}{9}(t + 3m^2 + 6mb + 6b^2). \quad (3.34)$$

Insertion into Eq. (3.31a) yields

$$(t + 3m^2)b + 3b^3 + -\frac{1}{9}(6m + 12b)(t + 3m^2 + 6mb + 6b^2) = 0. \quad (3.35)$$

Equation (3.35) is cubic and has three solutions for b ; once b is known, Eq. (3.34) gives c . The first two solutions are the stable *clump* phase and unstable clump solution,

$$b_{c\mp} = \frac{1}{5} \left(-m \mp \sqrt{-\frac{5}{3}t - 4m^2} \right) \quad (3.36a)$$

$$c_{c\mp} = b_{c\mp}. \quad (3.36b)$$

The third solution is *mixed* – it is somewhat between stripes and clumps:

$$b_m = -2m \quad (3.37a)$$

$$c_m = -\frac{1}{3}\sqrt{-t - 15m^2}. \quad (3.37b)$$

The solutions given in Eqs. (3.36), (3.37) are unique up to the sign of c . The exchange of sign ($c \rightarrow -c$) corresponds to the translation $\psi(\vec{r}) \rightarrow \psi\left(\vec{r} + \left\langle 0, \frac{2\pi}{\sqrt{3}q_0} \right\rangle\right)$, yielding no new physics (cf. Eq. (3.25)).

Equations (3.32), (3.33), (3.36), and (3.37) represent the complete set of solutions to the Euler-Lagrange equation and are listed in Table 3.1. The solutions are graphically depicted in Figs. 3·1 and 3·2.

For given values of t and m the free energy, Eq. (3.30), can be evaluated for each of the solutions listed in Table 3.1. The stable phase is the solution with the minimum free energy. The resulting phase diagram shown in Fig. 3·3 reproduces prior work [42, 43]. Notice that the disordered, clump, and stripe solutions are each the stable phase in some region of

Disordered phase	$b_s = 0$ $c_s = 0$
Stripe phase	$b_s = -\sqrt{-\frac{1}{3}t - m^2}$ $c_s = 0$
Clump phase/clump saddle point	$b_{c\mp} = \frac{1}{5} \left(-m \mp \sqrt{-\frac{5}{3}t - 4m^2} \right)$ $c_{c\mp} = b_{c\mp}$
“Mixed” saddle point	$b_m = -2m$ $c_m = -\frac{1}{3}\sqrt{-t - 15m^2}$

Table 3.1: The four stationary points ψ of the free energy functional that are consistent with the ansatz of Eq. (3.25). Each has a physical interpretation as either a stable phase, metastable phase, or unstable saddle point.

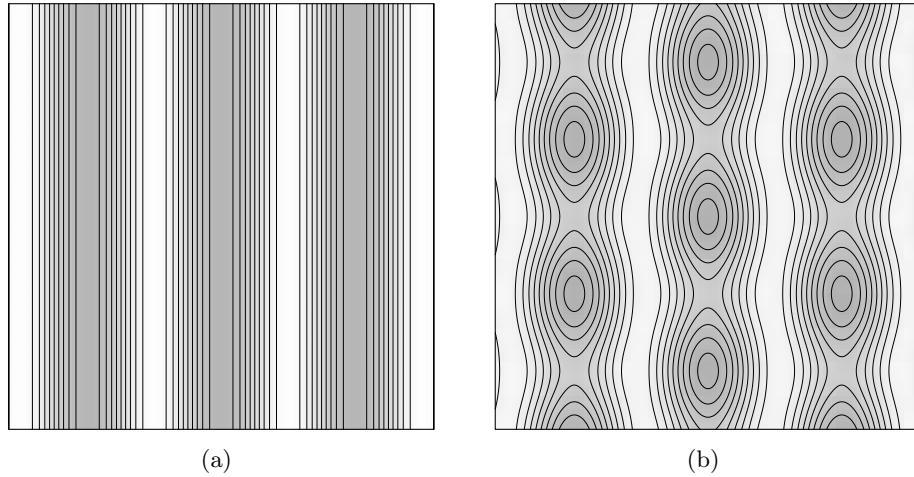


Figure 3.1: The metastable stripe phase (a) and the unstable “mixed” saddle point (b) at $t = -17.5m^2$. Both configurations are stationary points of the free energy functional. The two solutions merge at the $t = -15m^2$ spinodal.

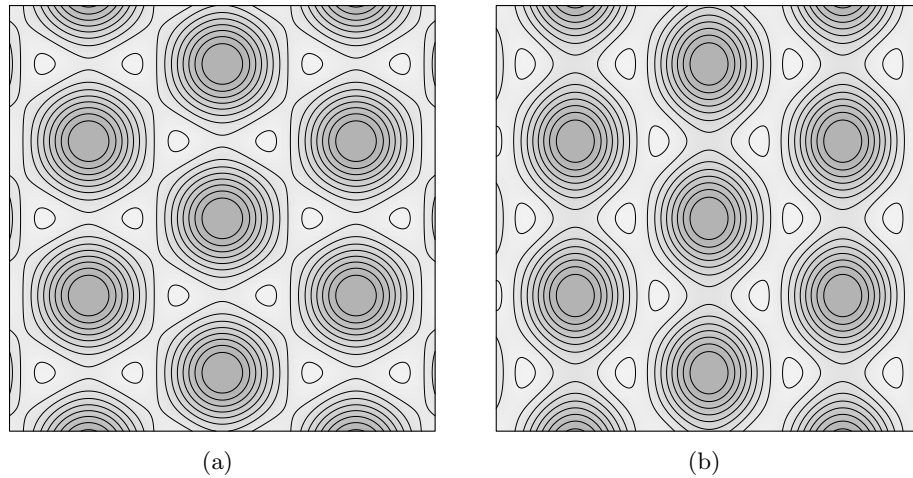


Figure 3-2: (a) The metastable clump phase and (b) the unstable “mixed” saddle point at $t = -35m^2$. Both configurations are stationary points of the free energy functional. The two solutions merge at the $t = -51m^2$ spinodal.

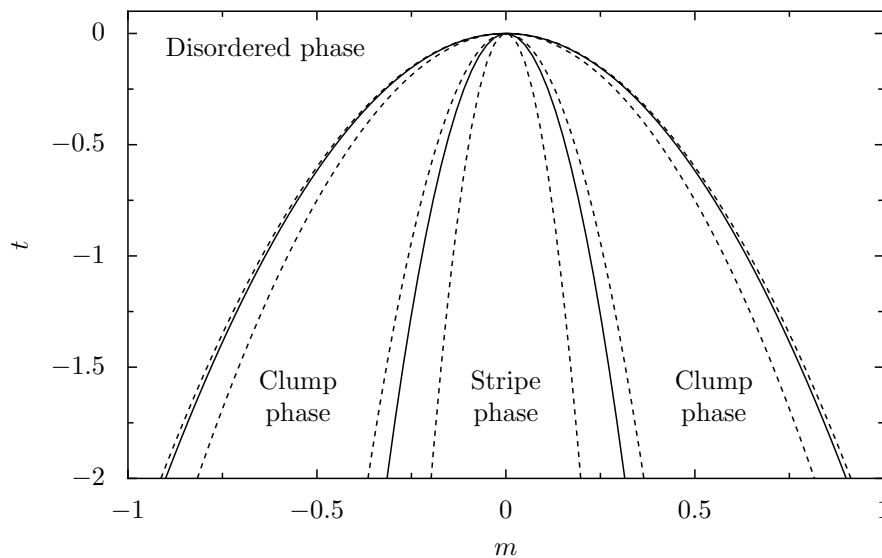


Figure 3-3: Phase diagram showing the disordered, clump, and stripe phases meeting at the critical point $t = m = 0$. The solid lines are coexistence curves between phases and the dashed lines are spinodal curves. The exact functions are given in Table 3.2.

Disordered-clump coexistence curve	$t = -\frac{37}{15}m^2$
Clump-stripe coexistence curve	$t = -\frac{3}{5}(19 + 6\sqrt{6})m^2$
Clump \rightarrow disordered spinodal curve	$t = -\frac{12}{5}m^2$
Disordered \rightarrow clump spinodal curve	$t = -3m^2$
Stripe \rightarrow clump spinodal curve	$t = -15m^2$
Clump \rightarrow stripe spinodal curve	$t = -51m^2$

Table 3.2: Coexistence and spinodal curves between disordered, stripe, and clump phases.

the (t, m) parameter space. The exact coexistence curves for the disordered-clump and clump-stripe transitions are listed in Table 3.2. Note that the mixed solution, Eqs. (3.37), is nowhere a stable phase; in the next section it is seen that the mixed solution is a saddle point of the free energy functional and plays an important role in nucleation between stripes and clumps.

One might wonder whether Table 3.1 lists *all* relevant solutions to the original Euler-Lagrange equation, Eq. (3.24) – might the ansatz, Eq. (3.25), have been too restrictive? A numerical solution of the original Euler-Lagrange equation indicates that the phase diagram in Fig. 3-3 is correct [43].

3.2.2 Spinodal instabilities

Now that the equilibrium phase diagram is understood, I will turn my attention to metastability and the kinetics of phase transitions near the critical point. The disordered-stripe transition is a special case: it occurs at the critical point $t = m = 0$, and is continuous in the mean-field limit (although fluctuations may induce a weak first-order transition [44, 45]).

There are also two first-order transitions: disordered-clump and clump-stripe.¹ Associated with first-order phase transitions are metastability and nucleation. For systems with long-range interactions nucleation is most relevant near the spinodal limit of metastability (cf. Section 1.5.2). The initial concern, therefore, is the determination of the spinodal curves.

There are four spinodal curves near the critical point: two are associated with the disordered-clump transition (one for each direction) and two more for the clump-stripe transition. Choose ψ to represent the disordered, clump, or stripe phase (see Table 3.1). By definition, ψ is stable if

$$F[\psi + \Delta\psi] > F[\psi] \quad (3.38)$$

for all infinitesimal perturbations $\Delta\psi$. A functional Taylor series gives (cf. Appendix A.2)

$$F[\psi + \Delta\psi] = F[\psi] + \int d\vec{r} \frac{\delta F[\psi]}{\delta\psi(\vec{r})} \Delta\psi(\vec{r}) + \frac{1}{2} \int d\vec{r} d\vec{r}' \frac{\delta^2 F[\psi]}{\delta\psi(\vec{r})\delta\psi(\vec{r}')} \Delta\psi(\vec{r})\Delta\psi(\vec{r}') + \dots \quad (3.39)$$

Because ψ is a stationary point of the free energy functional, it satisfies $\delta F/\delta\psi = 0$. The stability condition of Eq. (3.38) becomes

$$\int d\vec{r} d\vec{r}' \frac{\delta^2 F[\psi]}{\delta\psi(\vec{r})\delta\psi(\vec{r}')} \Delta\psi(\vec{r})\Delta\psi(\vec{r}') > 0. \quad (3.40)$$

The elements of the Hessian operator,

$$H_{r,r'} = \frac{\delta^2 F[\psi]}{\delta\psi(\vec{r})\delta\psi(\vec{r}')}, \quad (3.41)$$

are symmetric ($H_{r,r'} = H_{r',r}$). We choose to work in the eigenbasis of H . An arbitrary $\Delta\psi$ can be expressed as a linear combination of eigenvectors with real eigenvalues. The onset of a spinodal instability is indicated by the existence of a zero eigenvalue.

The strategy for determining the spinodals in the disordered-clump and clump-stripe transitions is to (a) guess where the spinodal curve is and (b) show that the guess is correct by finding an eigenvector $\Delta\psi$ of H with zero eigenvalue. The eigenvector $\Delta\psi$

¹The first-order nature of these transitions is predicted by the Landau rules [46], and has been numerically verified [43].

can be interpreted physically as a mode which becomes unstable at the spinodal limit of metastability.

We search for eigenvectors $\Delta\psi(\vec{r})$ using the same ansatz as we used for $\psi(\vec{r})$ in Eq. (3.25). With this restriction, the Hessian operator of Eq. (3.41) becomes a 2×2 Hessian matrix and the stability condition of Eq. (3.41) becomes

$$\begin{pmatrix} \Delta\psi_1 & \Delta\psi_2 \end{pmatrix} \begin{pmatrix} \partial_a^2 F & \partial_a \partial_b F \\ \partial_a \partial_b F & \partial_b^2 F \end{pmatrix} \begin{pmatrix} \Delta\psi_1 \\ \Delta\psi_2 \end{pmatrix} > 0. \quad (3.42)$$

The 2×2 Hessian matrix is easily diagonalized.

Disordered-clump transition

The coexistence between the disordered and clump phases occurs at $t = -\frac{37}{15}m^2$. There is a metastable clump region for $t > -\frac{37}{15}m^2$ and a metastable disordered region for $t < -\frac{37}{15}m^2$. The metastable phases terminate at the spinodal curves, which are to be determined.

To find the spinodal curves, consider the *unstable* clump solution which lies between the disordered and clump phases. For positive m the disordered and clump phases are given by (b_d, c_d) and (b_{c-}, c_{c-}) . The unstable clump solution, (b_{c+}, c_{c+}) , is a saddle point between these two. These three solutions are given in Table 3.1. Note that in all three cases, $b = c$.

Figure 3.4 indicates that for fixed t there is a specific value of m where the unstable clump solution matches the disordered phase (and another for the clump phase). I will now demonstrate that these matching points (listed in Table 3.2) are exactly the spinodals being sought.

The Hessian matrix evaluated at the disordered phase, $b_d = c_d = 0$, is

$$H = \begin{pmatrix} \partial_a^2 F & \partial_a \partial_b F \\ \partial_a \partial_b F & \partial_b^2 F \end{pmatrix} \propto \begin{pmatrix} t + 3m^2 & 0 \\ 0 & 2(t + 3m^2) \end{pmatrix}. \quad (3.43)$$

The unstable clump solution matches the disordered phase when $b_{c+} = 0$, which occurs at

$$t = -3m^2. \quad (3.44)$$

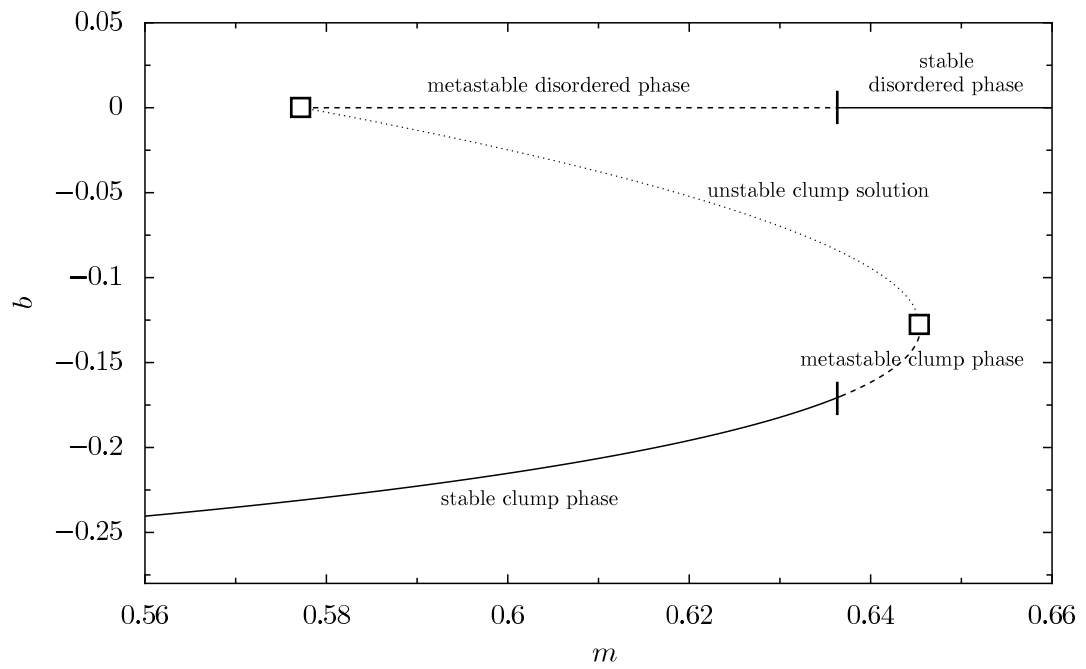


Figure 3-4: The disordered and clump phases. The amplitude of modulations ($b = c$) is plotted against m for $t = -1$. Solid lines represent stable phases, dashed lines represent metastable phases, and the dotted line represents unstable saddle points. The two squares represent spinodal limits of metastability.

Inserting this value into the Hessian matrix yields $H = 0$; the instability of the disordered phase confirms our guess that $t = -3m^2$ is the spinodal curve. In fact, the location of this spinodal had already been deduced in Section 3.1.1.

The disordered phase spinodal is unique in that multiple modes become unstable. In Section 3.1.1 it was shown that the disordered phase is unstable to *all* Fourier modes with $|\vec{q}| = q_0$. This fact leads to surprising nucleating droplet structures, as will be demonstrated in Section 3.3.

Now consider the metastable clump phase. The candidate spinodal (where $b_{c+} = b_{c-}$) is

$$t = -\frac{12}{5}m^2. \quad (3.45)$$

The Hessian matrix evaluated at the candidate spinodal is

$$H \propto \begin{pmatrix} 1 & -1 \\ -1 & 1 \end{pmatrix}. \quad (3.46)$$

The Hessian matrix has an eigenvector, $(1, 1)$, with eigenvalue zero. This eigenvector demonstrates an instability to fluctuations with $\Delta b = \Delta c$, and establishes that Eq. (3.45) identifies the spinodal. Interestingly, the clump-to-disordered spinodal coincides with a branch point of the metastable phase – a situation unique to this transition.

Clump-stripe transition

The unstable mixed solution (b_m, c_m in Eqs. (3.37)) plays the same role in the clump-stripe transition as the unstable clump solution (b_{c+}, c_{c+} in Eqs. (3.36)) plays in the disordered-clump transition. Specifically, the mixed solution interpolates between clump and stripe phases in a manner analogous to that shown in Fig. 3-4. We are led to investigate the points in which the mixed solution matches the clump or stripe phases.

For the metastable clump phase the candidate spinodal (where $b_m = b_c, c_m = c_c$) is

$$t = -51m^2. \quad (3.47)$$

Evaluation of the clump phase Hessian matrix at the candidate spinodal yields

$$H \propto \begin{pmatrix} 1 & 2 \\ 2 & 4 \end{pmatrix}. \quad (3.48)$$

The eigenvector $(2, -1)$ has zero eigenvalue, establishing that Eq. (3.47) identifies the spinodal of the clump-to-stripe transition.

Going in the other direction, the candidate spinodal (where $b_m = b_s$, $c_m = c_s$) is

$$t = -15m^2, \quad (3.49)$$

and the corresponding Hessian matrix is

$$H \propto \begin{pmatrix} 1 & 0 \\ 0 & 0 \end{pmatrix}. \quad (3.50)$$

The eigenvector $(1, 0)$ has zero eigenvalue, establishing that Eq. (3.47) identifies the spinodal of the clump-to-stripe transition.

This concludes our investigation of spinodals. The results, Eqs. (3.44), (3.45), (3.47), and (3.49), are collected in Table 3.2 and plotted in Fig. 3-3.

3.2.3 Nucleation

In this section I will discuss nucleation — the initial decay of the metastable phase — near the spinodal limits of metastability that were derived in Section 3.2.2. A general introduction to nucleation in systems with long-range interactions is given in Section 1.5.

The nucleating droplet is a saddle point of the free energy functional that sits between the metastable and stable phases. Among all such saddle points, the nucleating droplet is the one with minimum free energy cost (Section 1.5.1). Saddle points are unstable solutions of the Euler-Lagrange equation, Eq. (3.24). We have already met some saddle points, viz., b_{c+} , c_{c+} (when $m > 0$) and b_m, c_m from Eqs. (3.36) and (3.37) (see Figs. 3-1 and 3-2); these saddle points extend over the entire system volume and have an extensive

free energy cost. For sufficiently large systems (in particular, systems much larger than R^d) the nucleating droplet is an alternate saddle point – it has a non-extensive free energy cost and its deviations from the metastable phase are localized.

To determine the nucleating droplets near the metastable clump and stripe phase spinodals, consider configurations of the form

$$\psi(\vec{r}) = \psi_0(\vec{r}) + \xi(\vec{r}), \quad (3.51)$$

where ξ represents a small perturbation about the disordered, clump, or stripe metastable phase $\psi_0(\vec{r})$ (cf. Table 3.1). Expand the free energy of Eq. (3.19),

$$\begin{aligned} F[\psi] &= F[\psi_0] + \int d\vec{r} \frac{\delta F}{\delta \psi_0(\vec{r})} \xi(\vec{r}) + \frac{1}{2} \int d\vec{r} d\vec{r}' \frac{\delta^2 F}{\delta \psi_0(\vec{r}) \delta \psi_0(\vec{r}')} \xi(\vec{r}) \xi(\vec{r}') + \dots \quad (3.52) \\ &= f_0 + f_1 + f_2 + f_3 + O(\xi^4), \end{aligned}$$

where

$$f_0 = F[\psi_0] \quad (3.53a)$$

$$f_1 = 0 \quad (3.53b)$$

$$f_2 = \int d\vec{r} \frac{1}{2} (A * \xi) \xi + (3m\psi_0 + \frac{3}{2}\psi_0^2) \xi^2 \quad (3.53c)$$

$$f_3 = \int d\vec{r} (m + \psi_0) \xi^3, \quad (3.53d)$$

and terms higher order in ξ are negligible near the spinodal. The Euler-Lagrange equation, Eq. (3.24), becomes

$$\frac{\delta F}{\delta \xi(\vec{r})} = A * \xi + (6m\psi_0 + 3\psi_0^2) \xi + 3(m + \psi_0) \xi^2 = 0. \quad (3.54)$$

The Fourier transform of Eq. (3.54) gives

$$\begin{aligned} 0 &= A(\vec{q}) \xi(\vec{q}) + 6m \frac{(\psi_0 * \xi)(\vec{q})}{(2\pi)^d} + 3 \frac{(\psi_0 * \psi_0 * \xi)(\vec{q})}{(2\pi)^{2d}} \\ &\quad + 3m \frac{(\xi * \xi)(\vec{q})}{(2\pi)^d} + 3 \frac{(\psi_0 * \xi * \xi)(\vec{q})}{(2\pi)^{2d}}. \end{aligned} \quad (3.55)$$

We seek solutions $\xi(\vec{r})$ that represent localized saddle points of the free energy functional.

Nucleation from the disordered phase is special – Eq. (3.55) simplifies considerably when $\psi_0 = 0$, and a continuum of Fourier modes $\xi(\vec{q})$ become unstable at the spinodal (viz., those with $|\vec{q}| = q_0$). Section 3.3 is devoted to nucleation near the disordered phase spinodal where, surprisingly, the nucleating droplets have an onion-like structure in dimensions $d \geq 3$.

In the remainder of this section I will discuss clump-to-disordered nucleation when the distance from the spinodal,

$$\varepsilon = t + \frac{12}{5}m^2 \ll 1, \quad (3.56)$$

is small (cf. Eq. (3.45)). Although not discussed, spinodal-aided nucleation in the clump-to-stripe and stripe-to-clump transitions is analogous to that of the clump-to-disordered transition.

The metastable clump phase is

$$\psi_0(\vec{q}) = b(2\pi)^d \sum_{\vec{e} \in \mathcal{Q}_b \cup \mathcal{Q}_c} \delta(\vec{q} - q_0\vec{e}), \quad (3.57)$$

where $\mathcal{Q}_b \cup \mathcal{Q}_c$ is the set of six vectors from Eqs. (3.26) and (3.27), and where

$$b = -\frac{m}{5} + O(\varepsilon), \quad (3.58)$$

which follows from Eqs. (3.36), (3.56). Seek solutions to Eq. (3.54) of the form

$$\xi(\vec{q}) = \frac{\varepsilon}{3m}(2\pi)^d \sum_{\vec{e} \in \mathcal{Q}_b \cup \mathcal{Q}_c} \left(\frac{\sigma}{\varepsilon^{1/2}}\right)^d f_{\vec{e}}\left(\frac{\sigma}{\varepsilon^{1/2}}(\vec{q} - q_0\vec{e})\right), \quad (3.59)$$

where the six envelope functions $f_{\vec{e}}$ are, as yet, unknown and where $\tilde{\sigma}$ is given in Eq. (3.22). This scaling form is self consistent in the limit that $\varepsilon \rightarrow 0$: the function ξ becomes the sum of six δ function peaks and indeed satisfies Eq. (3.54).

To make further progress I will assume that the six envelope functions $f_{\vec{e}}$ are identical.

Inserting Eq. (3.59) into Eq. (3.55) gives, after some algebra,

$$(1 + (\vec{v} \cdot \vec{e})^2)f(\vec{v}) - (f * f)(\vec{v}) = 0, \quad (3.60)$$

where

$$\vec{v} = \frac{\sigma}{\varepsilon^{1/2}} \vec{q}. \quad (3.61)$$

This equation must be simultaneously satisfied for all vectors $\vec{e} \in \mathcal{Q}_b \cup \mathcal{Q}_c$. The convolution $(f * f)$ is with respect to the variable \vec{v} .

Interestingly, there is a strong resemblance between Eq. (3.60) and the equation for the nucleating droplet in the ferromagnet (cf. Section 2.2 and Ref. [2]). If one makes the uncontrolled approximation

$$(\vec{v} \cdot \vec{e})^2 f \rightarrow \vec{v}^2 f \quad (3.62)$$

then the identification would be exact [3], and spherically symmetric solutions $f(\vec{v})$ would exist for $d < 6$ [34].

If solutions to Eq. (3.60) exist (besides the δ -function solution) then the scaling form Eq. (3.59) implies that nucleating droplets have a radius of the order $\varepsilon^{-1/2}$ and an amplitude of the order ε . Unfortunately, the symmetry breaking appearance of $\vec{v} \cdot \vec{e}$ in Eq. (3.60) makes it doubtful that solutions exist! Thus, the assumption that each of the $f_{\vec{e}}(\vec{v})$, indexed by \vec{e} , are identical is most likely incorrect.

Despite its flaws, this argument is suggestive of an appealing connection between anti-ferromagnetic and ferromagnetic nucleation near the respective spinodals (e.g., with respect to the scaling of the reduced temperature ε). Numerical solution of the full Euler-Lagrange equation, Eq. (3.54), is an important task left for future work.

3.3 Nucleation from the disordered phase

In Section 3.1.1 it was demonstrated that a generic model with long-range repulsive interactions (viz., Eq. (3.10)) exhibits disorder at high temperatures. At lower temperatures (and away from the critical point) the disordered phase becomes metastable and eventually

unstable. The topic of this section is nucleation near the disordered phase spinodal.

It has previously been suggested that nucleating droplets near the spinodal have a core with hexagonal symmetry in two dimensions and either body centered cubic (BCC) or icosahedral symmetry in three dimensions [47, 3, 41]. This class of droplets has a *lattice-structure* (LS). Such droplets are modulated by an envelope with well defined scaling behavior near the spinodal: the amplitude and radius scale as ε and $\varepsilon^{-1/2}$ respectively where ε is the reduced temperature (i.e., the distance from the spinodal). The free energy cost of LS droplets scales $\varepsilon^{3-d/2}$ [3]. These scaling results are valid in the asymptotic limit $\varepsilon \ll 1$.

I introduce the *onion-structure* (OS) droplet – an alternative to LS droplets. The OS droplet is spherically symmetric about its center, and is so named because it resembles the layers of skin in an onion. I will show that, near the spinodal, the OS droplet has an amplitude that scales as $\varepsilon^{1/2}$. Within the relevant length scales, the OS droplet amplitude decays algebraically (rather than exponentially) with distance. The free energy cost of the OS droplet scales as $\varepsilon^{3/2}$, which is surprisingly independent of the dimension d .

The difference between LS and OS droplets is most striking in Fourier space: as the spinodal is approached LS droplets tend to a discrete set of δ -function peaks (viz. Eq. (3.76)) while the OS droplet tends to a single spherical δ -function shell (viz. Eq. (3.86)). Slightly away from the spinodal the δ -functions become sharply peaked, but non-singular, regions.

A comparison of the LS and OS droplet free energy scaling formulas indicates that, near the spinodal, the former are preferred when $d = 2$ while the latter are preferred when $d > 3$. A more refined argument suggests that OS droplets are also preferred at the critical dimension, $d = 3$.

3.3.1 Preliminaries

Assume a generic free energy functional F with repulsive long-range interactions, as given in Eq. (3.10). An expansion in powers of ψ yields

$$\tilde{R}^{-d}F = \tilde{F} = \tilde{F}_2 + \tilde{F}_3 + O(\psi^4) \quad (3.63)$$

where

$$\tilde{F}_2 = \frac{1}{2} \int d\vec{q}_1 d\vec{q}_2 A(\vec{q}_1) \psi_{\vec{q}_1} \psi_{\vec{q}_2} \delta(\vec{q}_1 + \vec{q}_2) \quad (3.64)$$

$$\tilde{F}_3 = -\frac{1}{3} B \int d\vec{q}_1 d\vec{q}_2 d\vec{q}_3 \psi_{\vec{q}_1} \psi_{\vec{q}_2} \psi_{\vec{q}_3} \delta(\vec{q}_1 + \vec{q}_2 + \vec{q}_3) \quad (3.65)$$

and

$$\tilde{R}^d = \frac{R^d}{(2\pi)^d} \quad (3.66)$$

$$B = -\frac{1}{2(2\pi)^d} \beta^{-1} f^{(3)}(m). \quad (3.67)$$

Recall that the total magnetization is fixed,

$$\psi(\vec{q} = 0) = 0. \quad (3.68)$$

The quantity $F[\psi]$ represents the free energy cost for deviations $\psi(\vec{q})$ from the disordered phase. As before, expand the spherically symmetric function $A(\vec{q})$ about its minimum,

$$A(\vec{q}) = \varepsilon + \sigma^2 (|\vec{q}| - q_0)^2 + O((|\vec{q}| - q_0)^3) \quad (3.69)$$

where $q_0 \neq 0$ and

$$\varepsilon = \Lambda(q_0) + \beta^{-1} f^{(2)}(m) \quad (3.70)$$

$$\sigma^2 = \frac{1}{2} \Lambda''(q_0). \quad (3.71)$$

The reduced temperature ε denotes the distance from the spinodal (cf. Section 3.1.1).

The nucleating droplet is a saddle point of the free energy functional (cf. Section 1.5.1) and is obtained by solving the Euler-Lagrange equation,

$$\frac{\delta F}{\delta \psi(\vec{q})} = 0. \quad (3.72)$$

Insertion of the free energy functional, Eq. (3.63), yields

$$\begin{aligned} A(\vec{q})\psi(\vec{q}) &= B \int d\vec{q}' \psi(\vec{q}')\psi(\vec{q} - \vec{q}') + O(\psi^3) \\ &= B \times (\psi * \psi)(\vec{q}) + O(\psi^3). \end{aligned} \quad (3.73)$$

I will seek both LS and OS type droplet solutions using the following strategy. Ansatz functional forms are proposed (cf. Eqs. (3.75), (3.84)) and are inserted into the Euler-Lagrange equation, which is solved near the spinodal limit

$$0 < \varepsilon \ll 1; \quad (3.74)$$

terms that do not contribute to the leading order free energy cost are dropped. If no inconsistencies arise, the method of dominant balance [48] indicates that the droplet solutions that are found are valid near the spinodal.

Note that, upon truncation of the expansions in Eqs. (3.63) and (3.69), there is only a small set of relevant parameters (viz., ε, σ, q_0 , and B). Because of this fact, predictions for nucleation near the spinodal are universal.

3.3.2 Lattice-structure droplets

Following Klein and Leyvraz [3], consider lattice-structure (LS) droplets of the form

$$\psi_{\text{LS}} = \frac{\varepsilon}{B} \sum_{\vec{e} \in \mathcal{Q}} \left(\frac{\sigma}{\varepsilon^{1/2}} \right)^d f_{\vec{e}} \left(\frac{\sigma}{\varepsilon^{1/2}} (\vec{q} - q_0 \vec{e}) \right). \quad (3.75)$$

The set of unit vectors \mathcal{Q} determines the lattice symmetry of the droplet and is, for the moment, unspecified. A general argument, originally due to Alexander and McTague [47], restricts the possible sets \mathcal{Q} that must be considered.

The functions $f_{\vec{e}}$, indexed by the unit vectors $\vec{e} \in \mathcal{Q}$, are to be determined. It is, however, assumed each $f_{\vec{e}}$ is localized, implying that

$$\lim_{\varepsilon \rightarrow 0} \psi_{\text{LS}} \propto \sum_{\vec{e} \in \mathcal{Q}} \delta^d(\vec{q} - q_0 \vec{e}). \quad (3.76)$$

From Eq. (3.76) it follows that, for ε sufficiently small, the overlap between the terms in the sum of Eq. (3.75) is negligible. It is also assumed that the $f_{\vec{e}}$ inherit the rotational symmetries of \mathcal{Q} , i.e.,

$$f_{\vec{e}}(\vec{v}) = f_{\mathcal{R}(\vec{e})}(\mathcal{R}(\vec{v})), \quad (3.77)$$

for all $\vec{e} \in \mathcal{Q}$ and all rotations \mathcal{R} under which the set \mathcal{Q} is invariant. This assumption is natural because the Euler-Lagrange equation, Eq. (3.73), is isotropic.

For arbitrary functions g, h , the following is an identity

$$\begin{aligned} g(\vec{r} - \vec{r}_0) * h(\vec{r} - \vec{r}_1) &= \int d\vec{r}' g(\vec{r}' - \vec{r}_0) h((\vec{r} - \vec{r}') - \vec{r}_1) \\ &= \int d\vec{r}' g(\vec{r}') h((\vec{r} - \vec{r}_0 - \vec{r}_1) - \vec{r}') \\ &= (g * h)(\vec{r} - \vec{r}_0 - \vec{r}_1). \end{aligned} \quad (3.78)$$

We apply Eq. (3.78) to the expansion of ψ in Eqs. (3.73) using the ansatz of Eq. (3.75), and work at leading order in ε . The result is,²

$$A(\vec{q}) f_{\vec{e}} \left(\frac{\sigma}{\varepsilon^{1/2}} (\vec{q} - q_0 \vec{e}) \right) = \varepsilon \sum_{\vec{e}_2 + \vec{e}_3 = \vec{e}} \left(\frac{\sigma}{\varepsilon^{1/2}} \right)^d (f_{\vec{e}_2} * f_{\vec{e}_3}) \left(\frac{\sigma}{\varepsilon^{1/2}} (\vec{q} - q_0 \vec{e}) \right), \quad (3.79)$$

where the choice of $\vec{e} \in \mathcal{Q}$ is inconsequential due to rotational symmetry, Eq. (3.77). The sum in Eq. (3.79) is over all vectors $\vec{e}_2, \vec{e}_3 \in \mathcal{Q}$ which add to \vec{e} . Equation (3.79) can be satisfied only if triples of vectors from \mathcal{Q} form equilateral triangles – a result due to Alexander and McTague[47]. In two dimensions, a natural choice of \mathcal{Q} is the set of reciprocal lattice vectors for the hexagonal crystal (cf. $\mathcal{Q}_b \cup \mathcal{Q}_c$ from Eqs. (3.26) and (3.27)). In three dimensions, the three main options are the sets of reciprocal lattice vectors for (a) hexagonally packed cylinders, (b) the icosahedral quasicrystal and (c) the BCC crystal. Other choices of \mathcal{Q} are possible but energetically unfavorable (e.g., superpositions of the above sets of lattice vectors).

Both the left-hand and right-hand sides of Eq. (3.79) represent functions that are sharply

²Expansion of Eqs. (3.73) and (3.75) also yields terms $(f_{e_j} * f_{e_k})$ for which $|e_j + e_k| \neq 1$. These can be balanced with extra contributions to ρ which are higher order in ε , and therefore are neglected in our calculation.

peaked about $\vec{q} = q_0 \vec{e}_1$.

Define the scaled wave vector

$$\vec{v} = \frac{\sigma}{\varepsilon^{1/2}}(\vec{q} - q_0 \vec{e}_1), \quad (3.80)$$

At leading order in ε , the left-hand side of Eq. (3.79) can be simplified using Eq. (3.69),

$$\begin{aligned} A(\vec{q})f_{\vec{e}}(\vec{v}) &= (\varepsilon + \sigma^2(|\vec{q}| - q_0)^2 + O((|\vec{q}| - q_0)^3))f_{\vec{e}}(\vec{v}) \\ &= \varepsilon(1 + (\vec{v} \cdot \vec{e})^2)f_{\vec{e}}(\vec{v}). \end{aligned} \quad (3.81)$$

The approximation $|\vec{q}| \approx \vec{q} \cdot \vec{e}$ is valid for \vec{q} near $q_0 \vec{e}$; its application to Eq. (3.81) is exact at leading order in ε .

The full Euler-Lagrange equation, Eq. (3.79), becomes

$$\begin{aligned} (1 + (\vec{v} \cdot \vec{e})^2)f_{\vec{e}}(\vec{v}) &= \sum_{\vec{e}_2 + \vec{e}_3 = \vec{e}} \int d\vec{v}' f_{\vec{e}_2}(\vec{v}') f_{\vec{e}_3}(\vec{v} - \vec{v}') \\ &= \sum_{\vec{e}_2 + \vec{e}_3 = \vec{e}} (f_{\vec{e}_2} * f_{\vec{e}_3})(\vec{v}). \end{aligned} \quad (3.82)$$

The convolution operation appearing on the right-hand side of Eq. (3.82) is with respect to the new variable, \vec{v} .

Equation (3.82) admits multiple solutions. The trivial solution $f_{\vec{e}} = 0$ represents the metastable disordered phase. A second, somewhat less trivial solution of Eq. (3.82) is $f_{\vec{e}}(\vec{v}) \propto \delta(\vec{v})$. This solution was first thought to describe a stable phase [47], but was later shown to be unstable [41]. Although this solution is a saddle point of the free energy, it is not a localized nucleating droplet; the free energy cost of this solution is proportional to the system volume.

Nontrivial solutions to Eq. (3.82), if they exist, would be smooth functions $f_{\vec{e}}(\vec{v})$. The expression $(\vec{v} \cdot \vec{e})$ which appears on the left-hand side of Eq. (3.82) indicates that $f_{\vec{e}}(v)$ is anisotropic. In two dimensions, I have obtained numerical solutions to Eq. (3.82). In three dimensions, the same method fails to find LS solutions (OS droplets are found instead, see

Section 3.3.3).

The replacement $(\vec{v} \cdot \vec{e}_i)^2 \rightarrow v^2$ brings rotational invariance to Eq. (3.82),

$$(1 + \vec{v}^2)f(\vec{v}) \approx^? (f * f)(\vec{v}), \quad (3.83)$$

and reproduces the equations describing spinodal nucleation in the ferromagnet [2] (cf. Section 2.2 and Ref. [2]). Solutions for the envelope function $f(\vec{v})$ of Eq. (3.83) are spherically symmetric and exist when $d < 6$ [34]. It is emphasized, however, that Eq. (3.83) is an uncontrolled approximation to Eq. (3.82), even in the spinodal limit $\varepsilon \rightarrow 0$.

3.3.3 Onion-structure droplets

Droplets with a real-space onion-structure (OS) have the Fourier space scaling form

$$\psi_{\text{OS}} = a \frac{\sigma}{\varepsilon^{1/2}} g \left(\frac{\sigma}{\varepsilon^{1/2}} (|\vec{q}| - q_0) \right), \quad (3.84)$$

which is different than that of LS droplets, Eq. (3.75). The parameters q_0 , σ , and ε are as before. The constant a and the function g will be determined exactly at leading order in $\varepsilon \ll 1$. The function g is normalized such that

$$\int du g(u) = 1, \quad (3.85)$$

and is sufficiently peaked about the origin such that

$$\lim_{\varepsilon \rightarrow 0} \psi_{\text{OS}} = a \delta(|\vec{q}| - q_0). \quad (3.86)$$

In real space OS droplets have spherically symmetric density oscillations resembling the layers of an onion.

The first task is to determine a and g in Eq. (3.84). I begin with the Euler-Lagrange equation, Eq. (3.73), again truncating the $O(\psi^3)$ terms (which are self-consistently negligible at leading order in ε). Application of Eqs. (3.69) and (3.84) to the left-hand side of

Eq. (3.73) yields, at leading order in ε ,

$$A(|\vec{q}|)\rho = \varepsilon(1 + u^2)a\frac{\sigma}{\varepsilon^{1/2}}g(u), \quad (3.87)$$

where

$$u = \frac{\sigma}{\varepsilon^{1/2}}(|\vec{q}| - q_0). \quad (3.88)$$

Now consider the right-hand side of Eq. (3.73) and apply Eq. (3.86), which is justified at leading order in ε . The result is

$$\begin{aligned} B \times (\rho * \rho)(\vec{q}) &= Ba^2 \int d\vec{q}' \delta(|\vec{q}'| - q_0) * \delta(|\vec{q} - \vec{q}'| - q_0) \\ &= Ba^2 \left(\sqrt{q_0^2 - \vec{q}^2/4} \right)^{d-2} S_{d-2} \\ &= Ba^2 \left(\sqrt{3}q_0/2 \right)^{d-2} S_{d-2} + O(|\vec{q}| - q_0), \end{aligned} \quad (3.89)$$

where S_n is the surface area of the n -sphere,

$$S_n = \frac{2\pi^{(n+1)/2}}{\Gamma[(n+1)/2]} = \begin{cases} 2 & n = 0 \\ 2\pi & n = 1 \\ 4\pi & n = 2 \end{cases} \quad (3.90)$$

The second step in Eq. (3.89) uses the fact that the convolution of $(d-1)$ -sphere δ -function shells is the surface area of overlap, a $(d-2)$ -sphere. After some algebra, Eqs. (3.73), (3.87), and (3.89) give $g(u)$ at leading order in ε ,

$$g(u) = \frac{1}{\pi(1 + u^2)}. \quad (3.91)$$

The constant

$$a = \frac{\varepsilon^{1/2}\sigma}{B\pi \left(\sqrt{3}q_0/2 \right)^{d-2} S_{d-2}} \quad (3.92)$$

is determined by the normalization of g given in Eq. (3.85). Collecting Eqs. (3.84), (3.91),

and (3.92) yields a final expression for the onion-structure droplets in Fourier space,

$$\psi_{\text{OS}} = \frac{\sigma^2}{B\pi^2 (\sqrt{3}q_0/2)^{d-2} S_{d-2}} (1 + u^2)^{-1}, \quad (3.93)$$

where u is defined in Eq. (3.88).

The OS droplets can be transformed to real space,

$$\begin{aligned} \psi_{\text{OS}}(|\vec{r}|) &= (2\pi)^{-d} \int d\vec{q} e^{-i\vec{q}\cdot\vec{r}} \psi_{\text{OS}}(|\vec{q}|) \\ &= \frac{S_{d-2}}{(2\pi)^d} \int_0^\pi d\theta (\sin\theta)^{d-2} \int_0^\infty dq q^{d-1} e^{-iq|\vec{r}|\cos\theta} \psi_{\text{OS}}(q), \end{aligned} \quad (3.94)$$

where θ is the zenith angle. The shorthand notation $r = |\vec{r}|$ is used in the following steps.

Because $\psi_{\text{OS}}(q)$ is sharply peaked at $q = q_0$, it is justified to extend the bounds of the radial integral in Eq. (3.94) to the entire real line. Application of Eqs. (3.84) and (3.91) yields

$$\begin{aligned} \int_0^\infty dq q^{d-1} e^{-iqr \cos\theta} \psi_{\text{OS}}(q) &= q_0^{d-1} \int du \exp[-i(q_0 + \varepsilon^{1/2}\sigma^{-1}u)r \cos\theta] ag(u) \\ &= aq_0^{d-1} \exp[-iq_0 r \cos\theta] \exp[-\varepsilon^{1/2}\sigma^{-1}r|\cos\theta|], \end{aligned} \quad (3.95)$$

which is valid at leading order in ε . Terms of the order $\varepsilon^{1/2}r$ have been retained in anticipation of large r . The second step in Eq. (3.95) uses the identity

$$\int_{-\infty}^{+\infty} du \frac{e^{ibu}}{\pi(1+u^2)} = e^{-|bu|}. \quad (3.96)$$

For $d = 3$, Eqs. (3.94) and (3.95) can be integrated, with the result

$$\psi_{\text{OS},3d}(r) = \exp[-\varepsilon^{1/2}\sigma^{-1}r] \frac{\varepsilon^{1/2}\sigma q_0}{B2\sqrt{3}\pi^4} \left(\frac{\sin q_0 r}{q_0 r} \right). \quad (3.97)$$

For general d we set $\varepsilon = 0$ and integrate Eqs. (3.94) and (3.95),

$$\psi_{\text{OS}}(r) = \frac{\varepsilon^{1/2}\sigma q_0 (8/3)^{d/2-1}}{B\pi^{1/2}(2\pi)^d} \Gamma[(d-1)/2] \frac{J_{d/2-1}(q_0 r)}{(q_0 r)^{d/2-1}}. \quad (3.98)$$

Both Eqs. (3.97) and (3.98) are valid at leading order in ε for fixed r . When $d = 3$ and r is large (e.g., $r \lesssim \varepsilon^{-1/2}$), then Eq. (3.97) is more precise. Equations (3.97) and (3.98) are obtained using Eq. (3.92) and an integral representation of the Bessel function [49],

$$J_\nu(r) = \frac{1}{\pi^{1/2}\Gamma(\nu + 1/2)} \left(\frac{r}{2}\right)^\nu \int_0^\pi e^{-ir \cos \theta} \sin^{2\nu} \theta d\theta. \quad (3.99)$$

3.3.4 Droplet free energy costs

Both LS and OS solutions are candidate descriptions of nucleating droplets. In the mean-field, large R , limit the droplet with the smallest free energy cost, \tilde{F} , dominates nucleation (cf. Section 1.5.1). In this section the free energy costs of LS and OS droplets are evaluated and compared.

When $\varepsilon \ll 1$, the $O(\psi^4)$ terms in the free energy functional (Eqs. (3.63), (3.64), and (3.65)) are negligible for both LS and OS droplets (Eqs. (3.75) and (3.84)). The evaluation of the free energy cost for LS and OS droplets can be simplified through the identity

$$\begin{aligned} \tilde{F} &= \tilde{F}_2 + \tilde{F}_3 & (3.100) \\ &= \tilde{F}_2 - \frac{B}{3} \int d\vec{q}_1 d\vec{q}_2 \psi(\vec{q}_1) \psi(\vec{q}_2) \psi(-\vec{q}_1 - \vec{q}_2) \\ &= \tilde{F}_2 - \frac{1}{3} \int d\vec{q}_1 \psi(\vec{q}_1) [B(\psi * \psi)(-\vec{q}_1)] \\ &= \tilde{F}_2 - \frac{2}{3} \times \frac{1}{2} \int d\vec{q}_1 \psi(\vec{q}_1) [A(\vec{q}_1) \psi(-\vec{q}_1)] \\ &= \frac{1}{6} \int d\vec{q} A(\vec{q}) |\psi(\vec{q})|^2 \\ &= \frac{1}{3} \tilde{F}_2, \end{aligned}$$

where Eqs. (3.65), (3.73), and (3.64) were applied in steps 2, 4, and 5 respectively.

We apply Eq. (3.100) to calculate the free energy cost of the OS droplets at leading

order in ε ,

$$\begin{aligned}
\tilde{F}[\psi_{\text{OS}}] &= \frac{1}{6} \int d\vec{q} A(|\vec{q}|) \psi_{\text{OS}}(|\vec{q}|)^2 \\
&= \frac{1}{6} S_{d-1} \int dq q^{d-1} \varepsilon (1+u^2) \psi_{\text{OS}}^2 \\
&= \frac{\varepsilon^{3/2} \sigma^3}{B^2 q_0^{d-3}} \left[6\pi^3 (3/4)^{d-2} \right]^{-1} \frac{S_{d-1}}{S_{d-2}^2},
\end{aligned} \tag{3.101}$$

where substitutions from Eqs. (3.69), (3.88), and (3.93) have been made. Extension of the bounds of integration in step 2 is justified because $\psi_{\text{OS}}(q)$ is sharply peaked about $q = q_0$.

Similarly, the free energy cost of LS droplets is,

$$\begin{aligned}
\tilde{F}[\psi_{\text{LS}}] &= \frac{1}{6} \int d\vec{q} A(|\vec{q}|) \psi_{\text{LS}}(\vec{q})^2 \\
&= \frac{1}{6} n \int d\vec{q} \varepsilon (1 + (\vec{v} \cdot \vec{e})^2) \left(\frac{\varepsilon}{B} \right)^2 \left(\frac{\sigma}{\varepsilon^{1/2}} \right)^d f_{\vec{e}}(\vec{v})^2 \\
&= \frac{\varepsilon^{3-d/2} \sigma^d}{B^2} \left[\frac{n}{6} \int d\vec{v} (1 + (\vec{v} \cdot \vec{e})^2) f_{\vec{e}}(\vec{v})^2 \right] \\
&= \frac{\varepsilon^{3-d/2} \sigma^d}{B^2} \left[\frac{cn}{6m^2} \right]
\end{aligned} \tag{3.102}$$

where substitutions from Eqs. (3.75), (3.81), and (3.80) have been made, and

$$c = \int d\vec{v} (1 + (\vec{v} \cdot \vec{e})^2) (m f_{\vec{e}}(\vec{v}))^2 \approx^? 1. \tag{3.103}$$

Equation (3.102) is independent of the choice $\vec{e} \in \mathcal{Q}$ because of rotational symmetry, Eq. (3.77). The symbol n represents the number of reciprocal lattice vectors,

$$n = |\mathcal{Q}| = \begin{cases} 6 & \text{hexagonal} \\ 12 & \text{BCC} \\ 30 & \text{icosahedral(quasicrystal)}. \end{cases} \tag{3.104}$$

and m represents the number of pairs $\vec{e}', \vec{e}'' \in \mathcal{Q}$ which sum to a specific $\vec{e} \in \mathcal{Q}$,

$$m = \begin{cases} 2 & \text{hexagonal} \\ 4 & \text{icosahedral, BCC}. \end{cases} \tag{3.105}$$

Although f_ε is not known analytically, Eq. (3.82) indicates that f_ε scales like m^{-1} and is otherwise dimensionless. It is therefore natural, but not rigorously justified, to assume that $c \approx 1$, as in Eq. (3.103).

3.3.5 Droplets categorized by spatial dimension

Equations (3.101) and (3.102) are exact scaling forms for the OS and LS droplet free energy costs in the limit $\varepsilon \ll 1$, and imply the following:

- In $d = 1$ both the OS and LS droplets are ill-defined (OS because S_{d-2} diverges, LS because wave vectors cannot form equilateral triangles so $m = 0$). The absence of nucleating droplets is consistent with the mean-field prediction of a continuous phase transition (no metastability) [46, 43].
- In $d = 2$ the OS and LS free energies scale as $\varepsilon^{3/2}$ and ε^2 respectively. LS droplets are therefore preferred for $\varepsilon \ll 1$. The reciprocal vectors \mathcal{Q} represent the hexagonal lattice, which is verified by numerical solution of the Euler-Lagrange equation, Eq. (3.72).
- In $d = 3$ the OS and LS free energies scale identically in all physically relevant parameters $(\varepsilon, \sigma, D, q_0)$ and the universal dimensionless constants in Eqs. (3.101), (3.102) determine the preferred droplet structure. In the following we assume that $c \approx 1$. Among LS droplets, BCC symmetry is preferable to hexagonal and icosahedral symmetries because of the smaller value of n/m^2 . More significantly, OS droplets have a free energy which is approximately 50 times smaller than that of BCC droplets! The numerical solution of the Euler-Lagrange equation, Eq. (3.72), is consistent with the conclusion that OS droplets are preferred.
- In $d \geq 4$ the OS and LS free energies scale as $\varepsilon^{3/2}$ and $\varepsilon^{3-d/2}$, and OS droplets are therefore preferred for $\varepsilon \ll 1$. Unlike nucleation in ferromagnetic models (Section 2.2), there is no singularity in OS droplets at $d = 6$.

3.4 Spatial symmetry breaking and the emergent CHC theory

The subject of this section is the early time dynamics of a system quenched into an unstable state, when the initial and final phases differ in *spatial symmetry*. For example, if a two-dimensional system in the disordered phase is quenched below the spinodal, how does it acquire the spatial oscillations associated with the stripe or clump phases?³ As usual, long-range Kac-type interactions are assumed.

I will show that the CHC theory, originally developed to describe continuous ordering and spinodal decomposition processes (cf. Sections 2.4.1 and 2.4.4, [11, 12]) can be generalized to describe order-to-order transitions. The main prediction of the CHC theory, initial exponential growth of Fourier modes, is generalized in two ways: (1) the modes which grow exponentially are linear combinations of Fourier modes and (2) exponential growth does not begin immediately after the quench. This section largely follows the presentation of Barros et al. [50].

The CHC theory applies only when the system configuration is *stationary* following the quench. That is, in the absence of noise the system would not evolve at all.⁴ The CHC theory therefore fails to describe continuous ordering following an off-critical, $h \neq 0$, quench [51] and most solid-to-solid phase transitions. For solid-to-solid transitions, however, a generalized theory, analogous to CHC, applies.

For large interaction range R , the effective noise scales like $R^{-d/2}$. The dynamical order parameter can be expanded in powers of $R^{-d/2}$ [23], separating the noise independent *background* (of order $R^0 = 1$) from the noise dependent *fluctuations* (of order $R^{-d/2}$). Roughly speaking, the background represents the overall shape of the system configuration and the fluctuations represent typically small deviations from the background. The CHC theory requires the background to be stationary and describes the evolution of the fluctuations at leading order in $R^{-d/2}$ (cf. Section 2.4.1).

³The disorder, stripe, and clump phases are discussed in Sections 3.1.1 and 3.2.1.

⁴The generic term *noise* refers to both noise in the initial conditions and dynamical noise. Note that noise in the initial conditions reflects dynamical noise prior to the quench.

A phase transition involves spatial *symmetry breaking* if the initial phase contains a rotational or translational symmetry not present in the final phase.⁵ The noiseless evolution of the background preserves these spatial symmetries. Thus, when spatial symmetry breaking is present, the background evolves toward a configuration that minimizes the free energy functional subject to spatial symmetry constraints. This configuration is a stationary point of the free energy functional and is unstable to symmetry breaking fluctuations.

It is possible to distinguish between two stages of early time evolution: *stage 1*, in which the background is evolving, and *stage 2*, in which the background has nearly converged to the constrained free energy minimum. For R sufficiently large, it is predicted that the growth of symmetry breaking fluctuations changes from non-exponential (stage 1) to exponential (stage 2).⁶ Stage 2 evolution in many ways resembles the CHC theory.

Assume the generic free energy functional given in Eq. (3.1) and apply NGF dynamics (Section 1.4)

$$\frac{\partial \phi(\vec{x}, t)}{\partial t} = -M \frac{\delta F[\phi]}{\delta \phi(\vec{x}, t)} + \sqrt{M} \eta(\vec{x}, t). \quad (3.106)$$

$F[\phi]$ is the free energy of the configuration ϕ at time t . The Gaussian white noise $\eta(\vec{x}, t)$ has zero mean and second moment $\langle \eta(\vec{x}, t) \eta(\vec{x}', t') \rangle = 2\beta^{-1} \delta(t - t') \delta(\vec{x} - \vec{x}')$. Set $M = 1$ corresponding to the rescaling of time, $t \rightarrow t' = t/M$. The drift term is given by

$$\begin{aligned} \frac{\delta F[\phi]}{\delta \phi(\vec{x})} &= \int d\vec{x}' \Lambda_R(\vec{x}') \phi(\vec{x} - \vec{x}') + \beta^{-1} \frac{df(\phi(\vec{x}))}{d\phi} - h \\ &= (\Lambda_R * \phi)(\vec{x}) + g'(\phi(\vec{x})) - h, \end{aligned} \quad (3.107)$$

where Λ_R is a Kac potential of the form $\Lambda_R(\vec{x}) = R^{-d} \Lambda(\vec{x}/R)$. The function $g' = \beta^{-1} df/d\phi$ represents entropic forces deriving from the degeneracy in coarse-graining ϕ . Without loss of generality, set $g(\phi)|_{\phi=0} = 0$. The symbol h either represents an external field or chemical potential.

⁵In ferromagnetic systems with spontaneous magnetization, all stable phases exhibit the same uniform spatial symmetry.

⁶Corberi et al. have also reported a rich structure in early stage phase ordering kinetics which, notably, is not associated with an evolving background [52]

Scale all lengths by R so that Eq. (3.106) simplifies to

$$\frac{\partial u(\vec{r}, t)}{\partial t} = -\frac{\delta \tilde{F}[u]}{\delta u(\vec{r}, t)} + R^{-d/2} \tilde{\eta}(\vec{r}, t), \quad (3.108)$$

where $\vec{r} = \vec{x}/R$, $\tilde{F}[\phi] = R^{-d}F[u]$, and

$$u(\vec{r}, t) = \phi(\vec{x}, t) \quad (3.109)$$

$$\frac{\delta \tilde{F}[u]}{\delta u(\vec{r})} = (\Lambda * u)(\vec{r}) + g'(u(\vec{r})) - h. \quad (3.110)$$

The parameter R in Eq. (3.106) appears solely as a prefactor to the noise term. The term $\tilde{\eta}(\vec{r}, t) = R^{d/2}\eta(\vec{x}, t)$ represents Gaussian white noise with zero mean and second moment $\langle \tilde{\eta}(\vec{r}, t) \tilde{\eta}(\vec{r}', t') \rangle = 2\beta^{-1} \delta(t - t') \delta(\vec{r} - \vec{r}')$, which follows from the identity $a^{-d} \delta(\vec{x}/a) = \delta(\vec{x})$.

The form of Eq. (3.108) suggests expanding u in the small parameter $R^{-d/2}$:

$$u = u^{(0)} + R^{-d/2} u^{(1)} + R^{-d} u^{(2)} + \dots \quad (3.111)$$

We substitute Eq. (3.111) into Eq. (3.108) and obtain the dynamical equations

$$\frac{\partial u^{(0)}}{\partial t} = -\frac{\delta \tilde{F}[u^{(0)}]}{\delta u} = -\Lambda * u^{(0)} - g'(u^{(0)}) + h \quad (3.112)$$

$$\frac{\partial u^{(1)}}{\partial t} = \mathcal{L}u^{(1)} + \tilde{\eta}, \quad (3.113)$$

where

$$\mathcal{L}u^{(1)} = -\Lambda * u^{(1)} - g''(u^{(0)})u^{(1)}, \quad (3.114)$$

and $g''(u) = d^2g/du^2$. Note that the nonlinear dynamics of $u^{(0)}$ in Eq. (3.112) is deterministic and decoupled from higher orders. The dynamics of $u^{(1)}$ is stochastic, linear, and depends on $u^{(0)}$ through \mathcal{L} .

As mentioned, the CHC theory emerges as the evolution of $u^{(1)}$ when $u^{(0)}$ is a stationary point of the free energy. Let us see how this works for a disordered-order transition occurring after a rapid quench from infinite to finite temperature and $h = 0$ (recall that $g(0) = 0$). At $t = 0$ the system is initially disordered so Eq. (3.112) has the trivial solution $u^{(0)} = 0$

for all time. With this solution, Eq. (3.113) can be solved in Fourier space,

$$u^{(1)}(\vec{q}, t) = u^{(1)}(\vec{q}, 0)e^{\tilde{D}(\vec{q})t} + \int_0^t dt' e^{\tilde{D}(\vec{q})(t-t')} \tilde{\eta}(\vec{q}, t'), \quad (3.115)$$

where $\tilde{D}(\vec{q}) = -\Lambda(\vec{q}) - g''(u^{(0)} = 0)$. The structure factor $S(k, t) = \langle |\phi|^2 \rangle / V$ can be calculated using Eq. (3.109), thus reproducing the CHC theory. For spin systems the volume V equals the total number of spins because the lattice spacing is taken to be unity.

Let us determine the time scale for which the CHC theory is applicable. Equation (3.111) is meaningful when the neglected $O(R^{-d})$ terms are small. One requirement is that $R^{-d/2}u^{(1)} \ll u^{(0)} \simeq 1$. The exponential growth of $u^{(1)}$ from Eq. (3.115) suggests that the linear theory breaks down at a time $t \sim \ln R$ [7, 14].

For many phase transitions (such as solid-to-solid) we must consider the evolution of both $u^{(0)}$ and $u^{(1)}$. Equation (3.113) predicts exponential growth of $u^{(1)}(t)$ whenever \mathcal{L} is time independent, which from Eq. (3.112) occurs when $\delta\tilde{F}/\delta u^{(0)}(x, t) = 0$. In general, the initial configuration $u^{(0)}(t=0)$ will not be such a stationary point. I will show that, due to symmetry breaking, $u^{(0)}$ converges to an unstable stationary configuration u^* . Correspondingly, \mathcal{L} will converge to a time independent operator. This instability of u^* means that \mathcal{L} will have positive eigenvalues, corresponding to the unstable symmetry breaking growth modes.

Let \mathcal{G} be the symmetry group containing rotations under which both $u^{(0)}(\vec{r}, 0)$ and $\Lambda(\vec{r})$ are invariant, and containing translations under which $u^{(0)}(\vec{r}, 0)$ is invariant. To show that Eq. (3.112) preserves these symmetries, we discretize

$$u_{t+\Delta t}^{(0)} = u_t^{(0)} + \Delta t(-\Lambda * u_t^{(0)} - g'(u_t^{(0)}) + h). \quad (3.116)$$

A short calculation establishes that if $u_t^{(0)}$ is invariant under \mathcal{G} , then so is $u_{t+\Delta t}^{(0)}$. By induction, $u^{(0)}(\vec{r}, t)$ is therefore invariant under \mathcal{G} for all t .⁷

How does $u^{(0)}$ evolve for a phase transition with symmetry breaking? It is determined

⁷Note that $u^{(0)}$ is a meaningful approximation to u only when the $R^{-d/2}$ expansion is valid, i.e., $t \lesssim \ln R$.

from Eq. (3.112) that $\tilde{F}[u^{(0)}]$ is non-increasing. Physically, \tilde{F} must be bounded from below, so $u^{(0)}$ converges to some configuration u^* . This convergence occurs on a time scale independent of R because R does not appear in Eq. (3.112). It is known that u^* is not the stable phase for a symmetry breaking transition because Eq. (3.112) preserves the spatial symmetries of the initial configuration. Therefore we expect that u^* is an unstable free energy stationary point. Parallel to the evolution of $u^{(0)}$, symmetry breaking fluctuations $R^{-d/2}u^{(1)}$ evolve according to Eq. (3.113). These fluctuations are unstable, and if $u^{(0)}$ has sufficiently converged to u^* , will grow exponentially for a time proportional to $\ln R$, analogous to the predictions of CHC.

The conclusion is that spatial symmetry breaking phase transition kinetics can be decomposed into two stages:

1. $t \lesssim t_0$: Nonlinear evolution of $u^{(0)}$ toward u^* , a configuration of minimum free energy subject to symmetry constraints. The configuration u^* is not the stable phase. The dynamical equation for $u^{(1)}$ is linear but has an explicit time dependence. Note that t_0 is independent of R .
2. $t_0 \lesssim t \lesssim \ln R$: To a good approximation $u^{(0)}$ has converged to u^* . The linear theory of $u^{(1)}$ becomes analogous to the CHC theory, and describes exponential growth of the unstable symmetry breaking modes.

These two stages are illustrated in Fig. 3-5(b). In contrast, there is no stage 1 process in the CHC theory, as illustrated in Fig. 3-5(a).

Phase transition kinetics *without* spatial symmetry breaking, such as solid-to-fluid, are qualitatively different. Here $u^{(0)}$ will evolve toward u^* but, unlike the symmetry breaking case, u^* is the stable phase because no spatial symmetries are lost in the transition from initial to final configuration (symmetry breaking does not occur). Note that all the interesting dynamics in this transition occurs through $u^{(0)}$, which is independent of the noise. This process is illustrated in Fig. 3-5(c).

Let us see how exponential growth arises in the second stage of a symmetry breaking

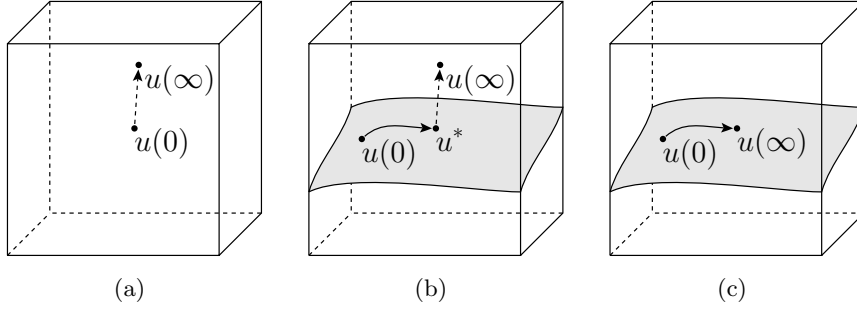


Figure 3-5: (a) The CHC theory is applicable if the initial configuration $u(0)$ is a free energy stationary point. CHC describes the immediate exponential growth of Fourier modes, lasting a time $t \sim \ln R$. (b) For symmetry breaking transitions (e.g., solid-to-solid) the early time kinetics of $u(t)$ has two stages. In the first stage the leading order contribution to u evolves deterministically and non-linearly toward a symmetry-constrained (shaded plane) free energy minimum u^* over a time scale $t \sim 1$. In the second stage, symmetry breaking modes grow exponentially for a time $t \sim \ln R$. (c) Without symmetry breaking (e.g., solid-to-fluid) the leading order contribution to u evolves deterministically toward the stable phase $u(\infty)$ over a time scale $t \sim 1$.

transition by considering Eq. (3.112). Because \mathcal{L} is a real and symmetric linear operator, it has a complete orthonormal eigenbasis and real eigenvalues.⁸ The eigenvectors of \mathcal{L} are Fourier modes only if $u^{(0)}$ is uniform. The dynamics of $u^{(1)}$ can be expressed in the eigenbasis of \mathcal{L} :

$$\frac{\partial u_v^{(1)}}{\partial t} = \sum_{v'} \mathcal{L}_{vv'} u_{v'}^{(1)} + \tilde{\eta}_v = \lambda_v u_v^{(1)} + \tilde{\eta}_v, \quad (3.117)$$

where v and λ_v represent the corresponding eigenvectors and eigenvalues of \mathcal{L} . The subscripts indicate eigenbasis components, for example $u_v = \int d\vec{r} v(\vec{r}) u(\vec{r})$ and $\mathcal{L}_{vv'} = \int d\vec{r} v(\vec{r}) \mathcal{L} v'(\vec{r}) = \lambda_v \delta_{vv'}$. The eigenvectors are normalized and satisfy $\langle \tilde{\eta}_v(t) \tilde{\eta}_{v'}(t') \rangle = \delta_{vv'} \delta(t - t')$.

For times $t \gtrsim t_0$ the operator \mathcal{L} is time independent and Eq. (3.117) can be solved directly:

$$u_v^{(1)}(t) = u_v^{(1)}(t_0) e^{\lambda_v(t-t_0)} + \int_{t_0}^t dt' e^{\lambda_v(t-t')} \tilde{\eta}_v(t'). \quad (3.118)$$

⁸It is assumed that \mathcal{L} is a finite matrix, corresponding to a finite system volume discretized in space.

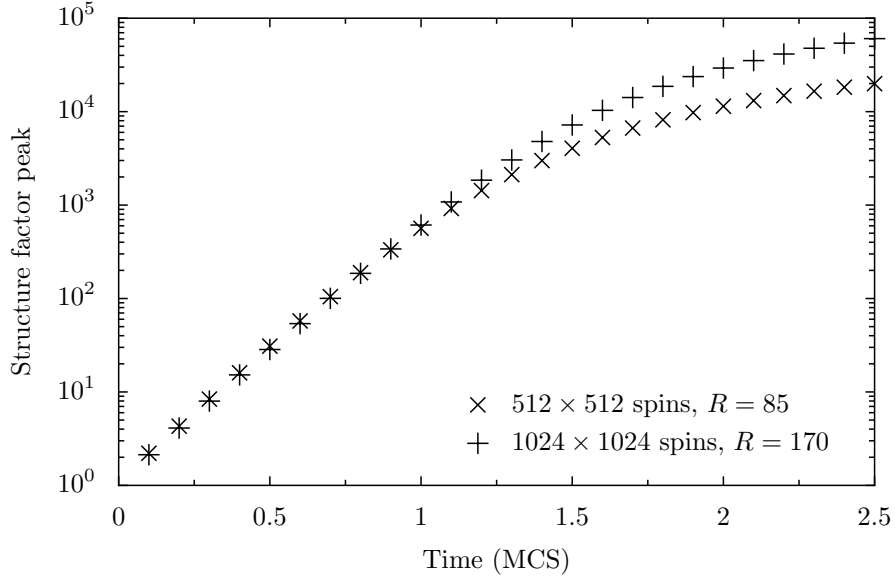


Figure 3-6: Evolution of the structure factor peak ($\langle |\phi_{\max}|^2 \rangle / V$) for the fluid-stripe transition following a critical ($h = 0$) quench. The CHC theory correctly predicts exponential growth, beginning immediately after the quench for this transition.

The exponential growth of $u^{(1)}$ is apparent. In the Fourier basis $u^{(1)}$ becomes

$$u^{(1)}(\vec{q}, t) = \sum_v v(\vec{q}) u_v^{(1)}(t), \quad (3.119)$$

where $v(\vec{q})$ is the Fourier representation of the eigenvector v . If R is sufficiently large and there is a single largest eigenvalue λ_v , then a single eigenvector v will grow exponentially faster than all others. In this case, and at sufficiently large times, we can approximate

$$u^{(1)}(\vec{q}, t) \approx v(\vec{q}) \left[u_v^{(1)}(t_0) e^{\lambda_v(t-t_0)} + \int_{t_0}^t dt' e^{\lambda_v(t-t')} \tilde{\eta}_v(t') \right]. \quad (3.120)$$

Thus, the exponential growth of the eigenvector v implies exponential growth of all the Fourier modes of $u^{(1)}$, $\langle |u^{(1)}(\vec{q}, t)|^2 \rangle \propto e^{2\lambda_v t}$. These Fourier modes eventually dominate all other contributions to the structure factor $S = \langle |\phi(\vec{k}, t)|^2 \rangle / V$, provided that the linear theory is valid ($t \lesssim \ln R$).

To test the generalized CHC theory, consider the two-dimensional antiferromagnetic Ising model with a long-range square interaction. This model contains a disordered *fluid*

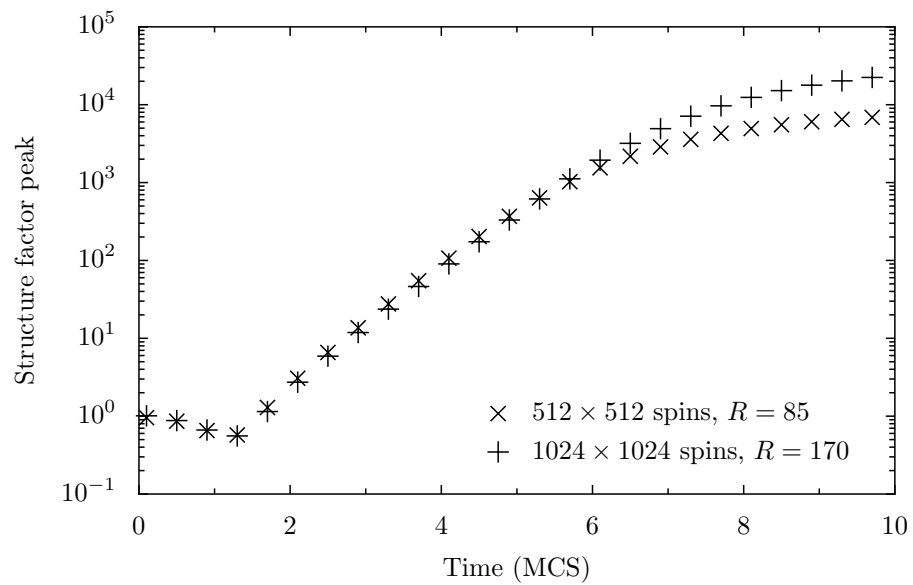


Figure 3.7: Evolution of the structure factor peak ($\langle |\phi_{\max}|^2 \rangle / V$) for the fluid-clump transition following an off-critical ($h \neq 0$) quench. The initial growth has two stages, confirming the prediction the theoretical predictions. The first stage is non-exponential and is independent of R . The second stage is exponential growth of the symmetry breaking modes (in this case Fourier modes) in analogy to the CHC theory.

phase, as well as *clump* and *stripe* solid phases (cf. Section 3.2.1). In the clump phase localized regions of enhanced magnetization are arranged on a square lattice. In the stripe phase regions of enhanced magnetization are arranged in periodic stripes. All fluid-to-solid phase transitions involve symmetry breaking, as do the transitions between clump and stripe phases. In contrast, solid-to-fluid transitions do not involve symmetry breaking because the uniform fluid phase contains all possible spatial symmetries.

I simulated the antiferromagnetic Ising model using SFG dynamics (cf. Section 2.3.1). Figures 3-6 and 3-7 display the peak of the structure factor, $S(\vec{k}, t) = \langle \phi(\vec{k}, t)^2 \rangle / V$, for fluid-to-solid phase transitions following critical ($h = 0$) and off-critical ($h = 0.8$) quenches. The final phases are stripes and clumps respectively. In both cases the temperature is reduced from $T = \infty$ to 0.05. The critical and off-critical transitions are described, respectively, by the CHC theory and its generalization. As predicted, the off-critical dynamics can be separated into two stages: initial non-exponential growth followed by an extended period of exponential growth. The growth modes are Fourier modes for both types of quenches considered because the initial phase is disordered. In the case of the stripe-to-clump transition, however, the growth modes are not Fourier modes [53].

To summarize, the CHC theory can be generalized to describe solid-to-solid transitions. The key ingredient of this generalization is spatial symmetry breaking. The predictions of the generalized theory differ from those of the CHC theory in two fundamental ways: (1) the exponential growth of the symmetry breaking modes does not immediately follow the quench, and (2) these symmetry breaking modes are not generally Fourier modes. I have presented simulations of the long-range antiferromagnetic Ising model for the off-critical fluid-to-solid transition which confirm the existence of a transient stage preceding exponential growth of the structure factor. An important limitation of this theory is that it assumes defect free initial conditions.

Chapter 4

Closing remarks

4.1 Closing remarks

Phase transition kinetics, including both nucleation and unstable growth, have been investigated in models with effective long-range, Kac-type interactions. Two categories of interactions have been considered: ferromagnetic (attractive), and antiferromagnetic (repulsive).

It is known that the long-range ferromagnet undergoes non-classical nucleation near the spinodal, and that the corresponding nucleation rate scales in a universal way [2]. This prediction, spinodal-aided nucleation, is applicable to real systems, at least in principle. The concept of spinodal-aided nucleation also applies to antiferromagnetic systems with modulated phases [3]. By doing a careful asymptotic analysis, I have shown that disorder-to-solid nucleation near the spinodal occurs through onion-structure nucleating droplets above two dimensions. This mathematical result is dependent on certain assumptions, viz., a scalar order parameter, metastable equilibrium, homogeneity, and pairwise interactions that are spherically symmetric and sufficiently long-range. In reality, all of these assumptions are questionable; more realistic studies of nucleation often involve non-trivial order parameters, complex interactions, heterogeneities, and limited equilibration times [54, 55]. Nonetheless, the value of simple models is their potential to reveal the essence of universal mechanisms. In fact, there is experimental evidence that onion-structure droplets appear in a lyotropic liquid crystal within the context of nucleation [56] (the connection to spinodal-aided nucleation is, admittedly, uncertain).

One difficulty faced by non-equilibrium statistical mechanics is the enormous variety of

dynamical behaviors that are consistent with a single equilibrium model. An example is the equilibrium Ising model and its dynamical extensions. The process of continuous ordering can be studied in the Ising model using spin-flip Glauber (SFG), spin-flip Metropolis (SFM), or some other dynamics. When the model is endowed with long-range interactions, the Cahn-Hilliard-Cook (CHC) linear theory provides an excellent, universal description of the early time ordering process. Immediately after the CHC theory fails, however, the process is surprisingly sensitive to the choice of dynamics. Indeed, nonlinear corrections to the CHC theory are $O(R^{-d})$ and $O(R^{-d/2})$ for SFG and SFM dynamics, respectively. This sensitivity is an important *negative* result regarding the universality of intermediate stage unstable ordering kinetics. Interestingly, universality is restored in the late stage of continuous ordering dynamics, which is well described by curvature driven domain growth [16, 57]. Another example of emergent dynamic universality occurs in early stages of unstable order-to-order transitions, where a CHC-like theory appears following initial transients [50].

Appendix A

Mathematical tools

A.1 The Fourier transform

The Fourier transform of a function $f(\vec{x})$ is defined to be

$$\hat{f}(\vec{k}) = \int d\vec{x} e^{i\vec{k}\cdot\vec{x}} f(\vec{x}). \quad (\text{A.1})$$

When there is no risk of confusion I will often recycle notation, $\hat{f}(\vec{k}) \rightarrow f(\vec{k})$.

The inverse Fourier transform is given by

$$f(\vec{x}) = \frac{1}{(2\pi)^d} \int d\vec{x} e^{-i\vec{k}\cdot\vec{x}} \hat{f}(\vec{k}), \quad (\text{A.2})$$

which follows directly from the Dirac δ -function identity

$$\delta(\vec{x}) = \frac{1}{(2\pi)^d} \int d\vec{x} e^{i\vec{k}\cdot\vec{x}} \quad (\text{A.3})$$

It is sometimes convenient to express Fourier and inverse Fourier transforms using operator notation:

$$\hat{f}(\vec{k}) = \mathcal{F}[f(\vec{x})] \quad (\text{A.4})$$

$$f(\vec{x}) = \mathcal{F}^{-1}[\hat{f}(\vec{k})]. \quad (\text{A.5})$$

The Fourier transform of a product of functions is

$$\mathcal{F}[f_1(\vec{x}) \dots f_n(\vec{x})] = (2\pi)^{-(n-1)d} (\hat{f}_1 * \hat{f}_2 * \dots * \hat{f}_n)(\vec{k}) \quad (\text{A.6})$$

and the inverse transformation is

$$\mathcal{F}^{-1}[\hat{f}_1(\vec{k}) \dots \hat{f}_n(\vec{k})] = (f_1 * f_2 * \dots * f_n)(x). \quad (\text{A.7})$$

The symbol $(*)$ denotes the convolution operation, defined by

$$(f_1 * f_2 * \dots * f_n)(\vec{x}) = \int d\vec{x}_1 \dots d\vec{x}_n f_1(\vec{x}_1) \dots f_n(\vec{x}_n) \delta(\vec{x} - \vec{x}_1 - \dots - \vec{x}_n), \quad (\text{A.8})$$

An “exponent” notation to indicate a series of convolutions is occasionally useful, e.g.,

$$\mathcal{F}[f(\vec{x})^n] = (2\pi)^{-(n-1)d} \hat{f}(\vec{k})^{n*} \quad (\text{A.9})$$

$$\mathcal{F}^{-1}[\hat{f}(\vec{k})^n] = f(\vec{x})^{n*}. \quad (\text{A.10})$$

A special case of the Fourier transformation identities is Parseval’s theorem,

$$\int d\vec{x} f(\vec{x}) g(\vec{x})^* = \mathcal{F}[f g^*](\vec{k} = 0) = (2\pi)^{-d} \int d\vec{k} \hat{f}(\vec{k}) \hat{g}(\vec{k})^*, \quad (\text{A.11})$$

where g^* indicates the complex conjugate of g .

The asymmetric appearance of 2π factors is admittedly annoying; these factors usually cancel at the end of a calculation. Alternate Fourier transform conventions, such as

$$\tilde{f}(\vec{\xi}) = \int d^d x e^{i2\pi\vec{\xi}\cdot\vec{x}} f(\vec{x}) \quad (\text{A.12})$$

$$f(\vec{x}) = \int d^d x e^{-i2\pi\vec{\xi}\cdot\vec{x}} \tilde{f}(\vec{\xi}), \quad (\text{A.13})$$

have advantages, but are nonstandard in physics.

A.2 Functionals and functional derivatives

A mathematical object F which takes a function, ϕ , and produces a single number, $F[\phi]$, is called a *functional*. Three examples are

$$F_1[\phi] = \int d\vec{x}' (\phi(\vec{x}'))^m \quad (\text{A.14a})$$

$$F_2[\phi] = \int d\vec{x}' \delta(\vec{x}' - \vec{x}_0) \phi(\vec{x}') = \phi(\vec{x}_0) \quad (\text{A.14b})$$

$$F_3[\phi] = \int d\vec{x}' (\nabla \phi(\vec{x}'))^2. \quad (\text{A.14c})$$

To emphasize that ϕ is a function it is conventional to write $\phi = \phi(\vec{x})$, but ambiguities can sometimes arise in the context of functionals. An alternative notation, $\phi = \phi(\bullet)$, indicates that ϕ expects an argument. One should interpret \bullet as “hole” to be filled by function application.

The *functional derivative* is defined as

$$\frac{\delta F[\phi]}{\delta \phi(\vec{x})} = \lim_{h \rightarrow 0} \frac{F[\phi(\bullet) + h\delta(\bullet - \vec{x})] - F[\phi(\bullet)]}{h}, \quad (\text{A.15})$$

where we have used the Dirac- δ function (note that, e.g., $\delta(\bullet - x)$ evaluated at \vec{x}' yields $\delta(\vec{x}' - x)$).

The derivatives of the functionals in Eqs. (A.14) are

$$\frac{\delta F_1}{\delta \phi(\vec{x})} = m\phi(\vec{x})^{m-1} \quad (\text{A.16a})$$

$$\frac{\delta F_2}{\delta \phi(\vec{x})} = \delta(\vec{x} - \vec{x}_0) \quad (\text{A.16b})$$

$$\frac{\delta F_3}{\delta \phi(\vec{x})} = -2\nabla^2 \phi(\vec{x}). \quad (\text{A.16c})$$

The minus sign in the third derivative follows from integration by parts.

Functional derivatives inherit many properties of ordinary derivatives; they are linear,

$$\frac{\delta(aF[\phi] + bG[\phi])}{\delta \phi(\vec{x})} = a \frac{\delta F}{\delta \phi(\vec{x})} + b \frac{\delta G}{\delta \phi(\vec{x})}, \quad (\text{A.17})$$

and satisfy multiple forms of the chain rule, e.g.,

$$\frac{\delta f(F[\phi])}{\delta \phi(\vec{x})} = \frac{df(F[\phi])}{dF} \frac{\delta F}{\delta \phi(\vec{x})} \quad (\text{A.18})$$

$$\frac{\delta F[f(\phi)]}{\delta \phi(\vec{x})} = \frac{\delta F}{\delta f(\phi(\vec{x}))} \frac{df(\phi(\vec{x}))}{d\phi}. \quad (\text{A.19})$$

A special case of Eq. (A.19) is

$$\frac{\delta}{\delta \phi(\vec{x})} \int d\vec{x}' g(\vec{x}') f(\phi(\vec{x}')) = g(\vec{x}) \frac{df(\phi(\vec{x}))}{d\phi}. \quad (\text{A.20})$$

Functionals can be Taylor expanded using functional derivatives:

$$F[\phi + \psi] = F[\phi] + \int d\vec{x} \frac{\delta F[\phi]}{\delta \phi(\vec{x})} \psi(\vec{y}) + \frac{1}{2} \int d\vec{x} d\vec{y} \frac{\delta^2 F[\phi]}{\delta \phi(\vec{x}) \delta \phi(\vec{y})} \psi(\vec{x}) \psi(\vec{y}) + \dots \quad (\text{A.21})$$

Functional identities such as this one are quite often easy to derive in discretized form. Let us see how it works. An ordinary, “well behaved” function can be discretized by sampling values on a regularly spaced lattice

$$\phi(\vec{x}) \rightarrow (\tilde{\phi}_1, \tilde{\phi}_2, \dots, \tilde{\phi}_n). \quad (\text{A.22})$$

Here the system volume V has been divided into n unique discretization cells, each with volume $\Delta x^d = V/n$. When Δx is sufficiently small, $\phi(\vec{x})$ is roughly constant over the entire discretization cell, and the sampling procedure is unambiguous. The continuum limit is recovered by taking $n \rightarrow \infty$ and $\Delta x \rightarrow 0$ while fixing the system volume $V = n\Delta x^d$.

The discretization of a functional is an ordinary function which takes n arguments:

$$F[\phi] \rightarrow \tilde{F}(\tilde{\phi}_1, \tilde{\phi}_2, \dots, \tilde{\phi}_n). \quad (\text{A.23})$$

Integrals naturally discretize to sums,

$$\int d\vec{x} \rightarrow \sum_{i=1}^n \Delta x^d. \quad (\text{A.24})$$

Discretized functional derivatives are simply partial derivatives with a Δx^{-d} “amplification

factor”,

$$\frac{\delta F[\phi]}{\delta \phi(\vec{x})} \rightarrow \frac{1}{\Delta x^d} \frac{\partial}{\partial \tilde{\phi}_i} \tilde{F}(\tilde{\phi}_1, \tilde{\phi}_2, \dots, \tilde{\phi}_n). \quad (\text{A.25})$$

This recipe derives from the relationship between the Dirac δ -function and the Kronecker δ symbol,

$$\delta(\vec{x}) \rightarrow \frac{1}{\Delta x^d} \delta_i. \quad (\text{A.26})$$

As an example, discretize the functional F_1 of Eq.(A.14a) and take the partial derivative,

$$\tilde{F}_1 = \sum_{i=1}^n \Delta x \tilde{\phi}_i^m \quad (\text{A.27})$$

$$\frac{1}{\Delta x^d} \frac{\partial \tilde{F}_1}{\partial \tilde{\phi}_i} = m \tilde{\phi}_i^{m-1}. \quad (\text{A.28})$$

Comparison of Eqs. (A.16a) and (A.28) confirms the discretization recipe. Notice that, unlike the partial derivative $\partial \tilde{F}_1 / \partial \tilde{\phi}_i$, the functional derivative remains finite in the continuum limit.

Discretization is a powerful tool – the functional Taylor expansion of Eq. (A.21), when discretized using Eqs. (A.22)-(A.25), reduces to the ordinary Taylor expansion of multivariate calculus. This identification *establishes* the correctness of the functional Taylor expansion, Eq. (A.21).

When ϕ depends on multiple variables, multiple types of functional derivatives arise. For example, consider $\phi(\vec{x}, t)$ which depends on both position \vec{x} and time t . Furthermore, consider two functionals with different types,

$$F_s[\phi] = F_s[\phi(\bullet, s)] \quad (\text{A.29a})$$

$$G[\phi] = G[\phi(\bullet, \diamond)]; \quad (\text{A.29b})$$

the argument to F_s is a function of position only, whereas the argument to G is a function

of both position and time. The most *natural* functional derivatives of F_s and G are

$$\frac{\delta F_s[\phi]}{\delta \phi(\vec{x})} = \lim_{h \rightarrow 0} \frac{F_s[\phi(\bullet, s) + h\delta(\bullet - \vec{x})] - F_s[\phi(\bullet, s)]}{h} \quad (\text{A.30a})$$

$$\frac{\delta G[\phi]}{\delta \phi(\vec{x}, t)} = \lim_{h \rightarrow 0} \frac{G[\phi(\bullet, \diamond) + h\delta(\bullet - \vec{x})\delta(\diamond - t)] - G[\phi(\bullet, \diamond)]}{h}. \quad (\text{A.30b})$$

Note, however, that the functional derivative $\delta/\delta\phi(\vec{x}, t)$ *can also* operate on $F_s[\phi]$,

$$\frac{\delta F_s[\phi]}{\delta \phi(\vec{x}, t)} = \frac{\delta F_s[\phi(\bullet, \diamond)_{\diamond=s}]}{\delta \phi(\vec{x}, t)} \quad (\text{A.31})$$

$$= \lim_{h \rightarrow 0} \frac{F_s[\phi(\bullet, s) + h\delta(\bullet - \vec{x})\delta(s - t)] - F_s[\phi(\bullet, s)]}{h} \quad (\text{A.32})$$

$$= \delta(s - t) \frac{\delta F_s[\phi]}{\phi(\vec{x})}. \quad (\text{A.33})$$

Thus, care must be taken to distinguish between the operators $\delta/\delta\phi(\vec{x})$ and $\delta/\delta\phi(\vec{x}, t)$.

A.3 White Gaussian noise

White Gaussian noise $\eta(t)$ is defined by its probability distribution,

$$\mathcal{P}[\eta] \propto \exp \left[-\frac{1}{2\sigma^2} \int dt \eta(t)^2 \right]. \quad (\text{A.34})$$

The mean and two-point correlation function completely characterize η ,

$$\langle \eta(t) \rangle = 0 \quad (\text{A.35})$$

$$\langle \eta(t)\eta(t') \rangle = \sigma^2 \delta(t - t'). \quad (\text{A.36})$$

Higher order correlations are reducible to the sum of all two-point correlations (Wick's theorem). For example,

$$\langle \eta_1 \eta_2 \eta_3 \eta_4 \rangle = \langle \eta_1 \eta_2 \rangle \langle \eta_3 \eta_4 \rangle + \langle \eta_1 \eta_3 \rangle \langle \eta_2 \eta_4 \rangle + \langle \eta_1 \eta_4 \rangle \langle \eta_2 \eta_3 \rangle, \quad (\text{A.37})$$

where $\eta_i = \eta(t_i)$. Note that $\eta(t)$ and $\eta(t')$ are uncorrelated for $t \neq t'$.

Discretization of $\eta(t)$ yields the sequence $(\tilde{\eta}_1, \tilde{\eta}_2, \tilde{\eta}_3 \dots)$ where $\tilde{\eta}_i = \tilde{\eta}(i\Delta t)$ for some small discretization length Δt . The $\tilde{\eta}_i$ are chosen to be independent Gaussian variables

with

$$\langle \tilde{\eta}_i \rangle = 0 \quad (\text{A.38})$$

$$\langle \tilde{\eta}_i \tilde{\eta}_j \rangle = \frac{\sigma^2}{\Delta t} \delta_{ij}, \quad (\text{A.39})$$

so that their joint probability distribution

$$\mathcal{P}(\tilde{\eta}_1, \tilde{\eta}_2, \dots) \propto \exp \left[-\frac{1}{2\sigma^2} \sum_i \Delta t \tilde{\eta}_i^2 \right] \quad (\text{A.40})$$

matches Eq. (A.34). An equivalent construction of $\tilde{\eta}_i$ is

$$\tilde{\eta}_i = \frac{1}{\Delta t} \int_{i\Delta t}^{(i+1)\Delta t} \eta(t) dt; \quad (\text{A.41})$$

$\tilde{\eta}_i$ can be thought of as a “coarse grained” $\eta(t)$. In the limit that $\Delta t \rightarrow 0$, integrals and discretized sums are equivalent for all “well behaved” test functions f ,

$$\int_{t_0}^{t_1} dt \eta(t) f(t) = \sum_{i=t_0/\Delta t}^{t_1/\Delta t} \Delta t \tilde{\eta}_i f(i\Delta t). \quad (\text{A.42})$$

The continuum limits of Eqs. (A.40), (A.42) can serve as the *definition* of $\eta(t)$.

Application of Parseval’s theorem to the argument of the exponential in Eq. (A.34) indicates that the Fourier transform of the noise, $\hat{\eta}(\omega) = \mathcal{F}[\eta(t)]$, is again white noise with zero mean and is characterized by

$$\langle \hat{\eta}(\omega) \hat{\eta}(\omega')^* \rangle = (2\pi)^{-1} \sigma^2 \delta(\omega - \omega'). \quad (\text{A.43})$$

Note that $\hat{\eta}(\omega)^* = \hat{\eta}(-\omega)$ since $\eta(t)$ is real.

White Gaussian noise is readily generalized to take multiple parameters. For example, if $\eta(\vec{x}, t)$ has zero mean then it is completely characterized by

$$\langle \eta(\vec{x}, t) \eta(\vec{x}', t') \rangle = \sigma^2 \delta(\vec{x} - \vec{x}') \delta(t - t'). \quad (\text{A.44})$$

A.4 Langevin equations

The Langevin equation (a stochastic differential equation) takes the form

$$\frac{\partial}{\partial t}\phi(\vec{x}, t) = \theta[\phi(\vec{x}, t)] + \sqrt{2B[\phi(\vec{x}, t)]}\eta(\vec{x}, t). \quad (\text{A.45})$$

The stochasticity of this equation results from the white Gaussian noise $\eta(\vec{x}, t)$, which is distributed with probability

$$\mathcal{P}[\eta] = \exp\left[-\frac{1}{2}\int d\vec{x}dt\eta(\vec{x}, t)^2\right]. \quad (\text{A.46})$$

The singular character of η forces a careful interpretation of Eq. (A.45). I will discretize, making the replacements

$$\phi(i\Delta x, j\Delta t) \rightarrow \phi_{ij} \quad (\text{A.47})$$

$$\frac{\partial}{\partial t}\phi(i\Delta x, j\Delta t) \rightarrow \frac{\phi_{i,j+1} - \phi_{i,j}}{\Delta t} \quad (\text{A.48})$$

$$\eta(i\Delta x, j\Delta t) \rightarrow (\Delta^d x \Delta t)^{-1/2}\xi_{i,j}, \quad (\text{A.49})$$

where $\xi_{i,j}$ is a Gaussian random variable with zero mean and unit variance (for more discussion on the discretization of η , see Section A.3). Thus, Eq. (A.45) is actually defined by

$$\phi_{i,j+1} = \phi_{i,j} - \Delta t\theta[\phi_{i,j}] + \sqrt{\frac{\Delta t}{\Delta x^d}2B[\phi_{i,j}]\xi_{i,j}}, \quad (\text{A.50})$$

in the continuum limit that $\Delta t \rightarrow 0$ first, and $\Delta x \rightarrow 0$ second [58].

Equation (A.50) represents the Ito interpretation of the Langevin equation. If $B[\phi_{i,j+\frac{1}{2}}]$ rather than $B[\phi_{i,j}]$ is chosen to appear on the RHS of Eq. (A.50), the Stratonovich interpretation results (where, by definition, $\phi_{i,j+\frac{1}{2}} = \frac{1}{2}(\phi_{i,j} + \phi_{i,j+1})$). Remarkably, the Ito and Stratonovich interpretations differ in the continuum limit [59]. For systems with long-range interactions, however, the noise is effectively small and the distinction is often irrelevant.

The Langevin equation, Eq. (A.45), has an equivalent Fokker-Planck description. Under

the Ito interpretation, the probability distribution $\mathcal{P}[\phi]$ evolves according to

$$\frac{\partial \mathcal{P}}{\partial t} = \int d^d x \left[-\frac{\delta}{\delta \phi} \theta \mathcal{P} + \frac{\delta}{\delta \phi} B \frac{\delta}{\delta \phi} \mathcal{P} \right]. \quad (\text{A.51})$$

The equilibrium distribution \mathcal{P}_{eq} is stationary under Fokker-Planck evolution,

$$\frac{\partial \mathcal{P}_{\text{eq}}}{\partial t} = 0. \quad (\text{A.52})$$

A.5 The radial step function

A simple choice of Kac potential is the radial step function

$$\Theta_R(\vec{x}) = R^{-d} \Theta(\vec{x}/R) \quad (\text{A.53})$$

where

$$\Theta(\vec{r}) = \begin{cases} \frac{\Gamma[\frac{d}{2}]d}{2\pi^{d/2}} & \text{if } |r| < 1 \\ 0 & \text{otherwise} \end{cases}. \quad (\text{A.54})$$

The normalization is chosen to satisfy

$$\int d\vec{x} \Theta_R(\vec{x}) = \int d\vec{r} \Theta(\vec{r}) = 1. \quad (\text{A.55})$$

The Fourier transform of the radial step function is

$$\hat{\Theta}_R(\vec{k}) = \int d\vec{x} e^{i\vec{k}\cdot\vec{x}} \Theta_R(\vec{x}) = \hat{\Theta}(|\vec{k}|R), \quad (\text{A.56})$$

where

$$\hat{\Theta}(q) = \left(\frac{2}{q}\right)^{d/2} \Gamma(d/2 + 1) J_{d/2}(q), \quad (\text{A.57})$$

and J_ν is the Bessel function of the first kind [49]. An interesting property of the radial step function is that

$$\frac{d^2 \hat{\Theta}(q_0)}{dq^2} = -\hat{\Theta}(q_0) \quad (\text{A.58})$$

whenever $\frac{d}{dq}\hat{\Theta}(q_0) = 0$, which follows from the Bessel function identities [49]

$$k (J_{m-1}(k) + J_{m+1}(k)) = 2mJ_m(k) \quad (\text{A.59})$$

$$\frac{d}{dk} (k^m J_m(k)) = k^m J_{m-1}(k). \quad (\text{A.60})$$

The maximum of $\hat{\Theta}(q)$ occurs at $\hat{\Theta}(q_0 = 0) = 1$. The minimum of $\hat{\Theta}(q)$ occurs at

$$q_0 \approx \begin{cases} 5.1356 & d = 2 \\ 5.7635 & d = 3 \end{cases}, \quad (\text{A.61})$$

for which

$$\hat{\Theta}(q_0) \approx \begin{cases} -0.13228 & d = 2 \\ -0.08617 & d = 3 \end{cases}. \quad (\text{A.62})$$

List of Journal Abbreviations

Acta Metall.	Acta Metallurgica
Adv. Phys.	Advances in Physics
Ann. Phys.	Annals of Physics
J. Chem. Phys.	Journal of Chemical Physics
J. Math. Phys.	Journal of Mathematical Physics
J. Phys.	Journal of Physics
J. Stat. Phys.	Journal of Statistical Physics
Mdl. Simul. Mat. Sci. Eng.	Modelling and Simulation in Materials Science and En- gineering
Phys. Rev.	Physical Review
Phys. Rev. Lett.	Physical Review Letters
Prog. Theor. Phys.	Progress of Theoretical Physics
Rev. Mod. Phys.	Reviews of Modern Physics
Sov. Phys. JETP	Soviet Physics JETP
Z. Phys.	Zeitschrift für Physik
Z. Phys. Chem.	Zeitschrift für Physikalische Chemie

References

- [1] J. D. Gunton, *Homogeneous Nucleation*, *J. Stat. Phys.* **95** (1999) 903.
- [2] C. Unger and W. Klein, *Nucleation theory near the classical spinodal*, *Phys. Rev. B* **29** (1984) 2698.
- [3] W. Klein and F. Leyvraz, *Crystalline Nucleation in Deeply Quenched Liquids*, *Phys. Rev. Lett.* **57** (1986) 2845.
- [4] Y. C. Shen and D. W. Oxtoby, *bcc Symmetry in the Crystal-Melt Interface of Lennard-Jones Fluids Examined through Density Functional Theory*, *Phys. Rev. Lett.* **77** (1996) 3585.
- [5] W. Ostwald, *Studien über die Bildung und Umwandlung fester Körper*, *Z. Phys. Chem.* **22** (1897) 289.
- [6] M. Kac, G. E. Uhlenbeck, and P. C. Hemmer, *On the van der Waals Theory of the Vapor-Liquid Equilibrium. I. Discussion of a One-Dimensional Model*, *J. Math. Phys.* **4** (1963) 216.
- [7] K. Binder, *Nucleation barriers, spinodals, and the Ginzburg criterion*, *Phys. Rev. A* **29** (1984) 341.
- [8] F. J. Cherne, M. I. Baskes, R. B. Schwarz, S. G. Srinivasan, and W. Klein, *Non-classical nucleation in supercooled nickel*, *Modelling Simul. Mater. Sci. Eng.* **12** (2004) 1063.
- [9] M. Seul and D. Andelman, *Domain Shapes and Patterns: The Phenomenology of Modulated Phases*, *Science* **267** (1995) 476.
- [10] D. Chowdhury and D. Stauffer, *Principles of Equilibrium Statistical Mechanics*. Wiley-VCH, 1 ed., 2000.
- [11] J. W. Cahn and J. E. Hilliard, *Free Energy of a Nonuniform System. III. Nucleation in a Two-Component Incompressible Fluid*, *J. Chem. Phys.* **31** (1959) 688.
- [12] H. E. Cook, *Brownian Motion in Spinodal Decomposition*, *Acta Metall.* **18** (1970) 297.
- [13] J. Marro, A. B. Bortz, M. H. Kalos, and J. L. Lebowitz, *Time evolution of a quenched binary alloy. II. Computer simulation of a three-dimensional model system*, *Phys. Rev. B* **12** (1975) 2000.

- [14] D. W. Heermann, *Test of the Validity of the Classical Theory of Spinodal Decomposition*, *Phys. Rev. Lett.* **52** (1984) 1126.
- [15] J. D. Gunton, M. S. Miguel, and P. S. Sahni, *The Dynamics of First Order Phase Transitions*, in *Phase Transitions and Critical Phenomena* (C. Domb and J. L. Lebowitz, eds.), vol. 8. Academic, New York, 1983.
- [16] A. J. Bray, *Theory of phase-ordering kinetics*, *Adv. Phys.* **43** (1994) 357.
- [17] J. Langer, M. Bar-On, and H. Miller, *New computational method in the theory of spinodal decomposition*, *Phys. Rev. A* **11** (1975) 1417.
- [18] K. Kawasaki, M. C. Yalabik, and J. D. Gunton, *Growth of fluctuations in quenched time-dependent Ginzburg-Landau model systems*, *Phys. Rev. A* **17** (1978) 455.
- [19] C. Billotet and K. Binder, *Nonlinear relaxation at first-order phase transitions: A Ginzburg-Landau theory including fluctuations*, *Z. Phys. B* **32** (1979) 195.
- [20] K. R. Elder and R. C. Desai, *Role of nonlinearities in off-critical quenches as described by the Cahn-Hilliard model of phase separation*, *Phys. Rev. B* **40** (1989) 243.
- [21] J. M. Hyde, A. P. Sutton, J. R. G. Harris, A. Cerezo, and A. Gardiner, *Modelling spinodal decomposition at the atomic scale: beyond the Cahn - Hilliard model*, *Modelling Simul. Mater. Sci. Eng.* **4** (1996) 33.
- [22] J. Mainville, Y. S. Yang, K. R. Elder, M. Sutton, K. L. Ludwig, and G. B. Stephenson, *X-ray Scattering Study of Early Stage Spinodal Decomposition in $Al_{0.62}Zn_{0.38}$* , *Phys. Rev. Lett.* **78** (1997) 2787.
- [23] M. Grant, M. S. Miguel, J. Vinnals, and J. D. Gunton, *Theory for the early stages of phase separation: The long-range-force limit*, *Phys. Rev. B* **31** (1985) 3027.
- [24] M. E. Peskin and D. V. Schroeder, *An Introduction To Quantum Field Theory*. Westview Press, 1995.
- [25] A. D. Masi, E. Orlandi, E. Presutti, and L. Triolo, *Glauber evolution with Kac potentials. I. Mesoscopic and macroscopic limits, interface dynamics*, *Nonlinearity* **7** (1994) 633.
- [26] P. C. Hohenberg and B. I. Halperin, *Theory of dynamic critical phenomena*, *Rev. Mod. Phys.* **49** (1977) 435.
- [27] J. Cardy, *Field Theory and Nonequilibrium Statistical Mechanics, Notes: Troisieme cycle de la Physique en Suisse Romande* (1998).
- [28] J. S. Langer, *Theory of the condensation point*, *Ann. Phys.* **41** (1967) 108.
- [29] J. W. Gibbs, *The Collected Works of J. Willard Gibbs*. Yale University Press, 1948.

- [30] D. Stauffer, A. Coniglio, and D. W. Heermann, *Monte Carlo Experiment for Nucleation Rate in the Three-Dimensional Ising Model*, *Phys. Rev. Lett.* **49** (1982) 1299.
- [31] J. G. Kirkwood and E. Monroe, *Statistical Mechanics of Fusion*, *J. Chem. Phys.* **9** (1941) 514.
- [32] N. Grewe and W. Klein, *The Kirkwood-Salsburg equations for a bounded stable Kac potential. II. Instability and phase transitions*, *J. Math. Phys.* **18** (1977) 1735.
- [33] M. Struwe, *Variational Methods*. Springer, 2008.
- [34] C. B. Muratov and E. Vanden-Eijnden, *Breakup of Universality in the Generalized Spinodal Nucleation Theory*, *J. Stat. Phys.* **114** (2004) 605.
- [35] V. I. Manousiouthakis and M. W. Deem, *Strict detailed balance is unnecessary in Monte Carlo simulation*, *J. Chem. Phys.* **110** (1999) 2753.
- [36] A. D. Masi, E. Orlandi, E. Presutti, and L. Triolo, *Glauber evolution with Kac potentials: II. Fluctuations, Nonlinearity* **9** (1996) 27.
- [37] W. Paul, D. W. Heermann, and K. Binder, *Relaxation of metastable states in finite mean-field kinetic Ising systems*, *J. Phys. A* **22** (1989) 3325.
- [38] J. J. Binney, N. J. Dowrick, A. J. Fisher, and M. E. J. Newman, *The Theory of Critical Phenomena: An Introduction to the Renormalization Group*. Oxford University Press, 1992.
- [39] K. Kawasaki, *Dynamics of Fluctuations in Unstable Systems. II : Evolution Equation of Long Wavelength Fluctuation Spectra*, *Prog. Theor. Phys.* **58** (1977) 175.
- [40] K. Kawasaki, *Dynamics of Fluctuations in Unstable Systems. I*, *Prog. Theor. Phys.* **57** (1977) 410.
- [41] W. Klein, *Instability of Alexander-McTague crystals and its implication for nucleation*, *Phys. Rev. E* **64** (2001) 056110.
- [42] T. Garel and S. Doniach, *Phase transitions with spontaneous modulation-the dipolar Ising ferromagnet*, *Phys. Rev. B* **26** (1982) 325.
- [43] K. R. Elder and M. Grant, *Modeling elastic and plastic deformations in nonequilibrium processing using phase field crystals*, *Phys. Rev. E* **70** (2004) 051605.
- [44] S. A. Brazovskii, *Phase transition of an isotropic system to a nonuniform state*, *Sov. Phys. JETP* **41** (1975) 85.
- [45] G. H. Fredrickson and K. Binder, *Kinetics of metastable states in block copolymer melts*, *J. Chem. Phys.* **91** (1989) 7265.

- [46] L. D. Landau and E. M. Lifshitz, *Statistical Physics*. Butterworth-Heinemann, 3rd ed., 1984.
- [47] S. Alexander and J. McTague, *Should All Crystals Be bcc? Landau Theory of Solidification and Crystal Nucleation*, *Phys. Rev. Lett.* **41** (1978) 702.
- [48] C. M. Bender and S. A. Orszag, *Advanced Mathematical Methods for Scientists and Engineers*. Springer, 1 ed., 1999.
- [49] G. B. Arfken and H. J. Weber, *Mathematical Methods for Physicists*. Academic Press, 5 ed., 2000.
- [50] K. Barros, R. Dominguez, and W. Klein, *Beyond Cahn-Hilliard-Cook ordering theory: Early time behavior of spatial-symmetry-breaking phase transition kinetics*, *Phys. Rev. E* **79** (2009) 042104.
- [51] B. Morin, K. R. Elder, and M. Grant, *Theory for quenches from ordered states in nonconserved systems*, *Phys. Rev. B* **47** (1993) 2487.
- [52] F. Corberi, A. Coniglio, and M. Zannetti, *Early stage scaling in phase ordering kinetics*, *Phys. Rev. E* **51** (1995) 5469.
- [53] R. Dominguez, K. Barros, and W. Klein, *Early time kinetics of systems with spatial symmetry breaking*, *Phys. Rev. E* **79** (2009) 041121.
- [54] J. A. Warren, T. Pusztai, L. Kornyei, and L. Granasy, *Phase field approach to heterogeneous crystal nucleation in alloys*, *Phys. Rev. B* **79** (2009) 014204.
- [55] A. O. Schweiger, K. Barros, and W. Klein, *Transient nucleation near the mean-field spinodal*, *Phys. Rev. E* **75** (2007) 031102.
- [56] Y. Iwashita and H. Tanaka, *Spontaneous Onion-Structure Formation from Planar Lamellar Nuclei*, *Phys. Rev. Lett.* **98** (2007) 145703.
- [57] K. Barros, P. L. Krapivsky, and S. Redner, *Freezing into Stripe States in Two-Dimensional Ferromagnets and Crossing Probabilities in Critical Percolation*, *arXiv:0905.3521* (2009).
- [58] J. G. Gaines, *Numerical experiments with S(P)DE's*, in *Stochastic Partial Differential Equations* (A. M. Etheridge, ed.), vol. 216 of *London Mathematical Society Lecture Note Series*, p. 55. Cambridge Univ. Press., 1995.
- [59] N. V. Kampen, *Stochastic Processes in Physics and Chemistry, Third Edition*. North Holland, 3 ed., 2007.

Curriculum Vitae

Kipton Marcos Barros

Contact information:

Department of Physics
Boston University
590 Commonwealth avenue
Boston, MA 02215, USA

Email: kbarros@bu.edu
Phone: (+1) 617 358-5333
Fax: (+1) 617 353-9393

Date & Place of birth:

Jul. 31st 1979, State College, PA

Education:

Ph.D., Physics, Boston University (2005-2010)

B.S., Computer Science, Carnegie Mellon University (1997-2001)

Experience:

2004–2005, Visitor, Clark University

2003–2004, Software Engineer, NeuroPhysics Corporation, Shirley, MA

2001–2002, Software Engineer, Green Hills Software, Santa Barbara, CA

Fall 1999 and Summer 2000, Student Researcher,
Biophysics Group, Los Alamos National Laboratory, Los Alamos, NM

Awards:

Graduate Book Prize, 2009, Boston University

GSNP Student Speaker Award, \$1000 prize, 2009, APS March Meeting

IGERT Fellowship, 2006–2008, Center for Computational Science,
Boston University

Chairman's Book Prize, 2007, Boston University

Dean's Fellow, 2005–2006, Boston University

Presidential Scholarship, 1997–2001, Carnegie Mellon University

Invited talks:

3. *Massively parallel computing with graphics processors and CUDA*
Seminar at the Center for Computational Science, Boston University, Jan. 30th, 2009.
2. *Graphics cards for high performance computational physics*
Guest lecture, Course 6.963, Massachusetts Institute of Technology, Jan. 26th, 2009.
1. *Blasting through lattice calculations using CUDA*
Seminar at the Lattice QCD group, Massachusetts Institute of Technology, Oct. 7th, 2008.

Conferences & Presentations:

5. *Liquid to solid nucleation through onion-structure droplets*
Contributed talks at the APS March 2009 Meeting, Pittsburgh, PA. Mar. 16th and 19th, 2009.
4. *Generalizing Alexander-McTague: A new form of crystalline nucleation*
Contributed talk at the 10th Greater Boston Area Statistical Mechanics Meeting, Brandeis University, Oct. 18th, 2008.
3. *Nucleation in a long-range repulsive model*
Contributed talk at the APS March 2008 Meeting, New Orleans, LA. Mar. 14th, 2008.
2. *Nucleation in the long-range repulsive "clump" model*
Contributed talk at the 9th Greater Boston Area Statistical Mechanics Meeting, Brandeis University, Oct. 13th, 2007.
1. *Langevin dynamics for the long-range Ising model*
Contributed talk at the 8th Greater Boston Area Statistical Mechanics Meeting, Brandeis University, Oct. 21th, 2006.

Research papers:

6. *Freezing into Stripe States in Two-Dimensional Ferromagnets and Crossing Probabilities in Critical Percolation*
K. Barros, P. L. Krapivsky, S. Redner
Submitted to Phys. Rev. Lett. [arXiv:0905.3521].

5. *Early stage kinetics of systems with spatial symmetry breaking*
R. Dominguez, K. Barros, and W. Klein
Phys. Rev. E **79** 41121 (2009) [arXiv:0812.3889].
4. *Beyond Cahn-Hilliard-Cook: Early time behavior of symmetry breaking phase transition kinetics*
K. Barros, R. Dominguez, and W. Klein
Phys. Rev. E **79** 42104 (2009) [arXiv:0810.3949].
3. *Blasting through lattice calculations using CUDA*
K. Barros, R. Babich, R. Brower, M. A. Clark, and C. Rebbi
PoS (Lattice 2008) **045** [arXiv:0810.5365].
2. *Approaching equilibrium and the distribution of clusters*
H. Wang, K. Barros, H. Gould, and W. Klein
Phys. Rev. E **76**, 041116 (2007) [arXiv:0704.0938].
1. *Transient nucleation near the mean-field spinodal*
A. O. Schweiger, K. Barros, and W. Klein
Phys. Rev. E **75**, 039902 (2007) [arXiv:cond-mat/0609406].